Study of Carbon Fibre Reinforced PA6/PP Blend Based Composites: Processing and Characterization

THESIS

Submitted in partial fulfillment

of the requirements for the degree of

DOCTOR OF PHILOSOPHY

By

APARNA S

ID. No. 2015PHXF0003H

Under the Supervision of

Dr. D. Purnima

&

Under the Co-Supervision of

Prof. Ramesh Babu Adusumalli

BITS Pilani

Pilani | Dubai | Goa | Hyderabad
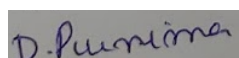
BIRLA INSTITUTE OF TECHNOLOGY & SCIENCE, PILANI

Hyderabad Campus

2021

CERTIFICATE

This is to certify that the thesis entitled "**Study of Carbon Fibre Reinforced PA6/PP Blend Based Composites: Processing and Characterization"** submitted by **APARNA S,** ID. No. **2015PHXF0003H** for award of Ph.D. of the institute embodies original work done by her under my supervision.

Signature of the Supervisor:

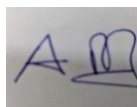Name in capital letters: **Dr. D. PURNIMA**

Designation: Assistant Professor,

Department of Chemical Engineering

Date: 12th April 2021

Signature of the Co-Supervisor:

Name in capital letters: **Prof. RAMESH BABU ADUSUMALLI**

Designation: Associate Professor,

Department of Chemical Engineering

Date: 12th April 2021

ACKNOWLEDGEMENT

ABSTRACT

Carbon fibre composites are widely used in automotive and aerospace applications due to their high specific modulus, specific strength and corrosion resistance and these are primarily made with thermoset matrices such as epoxy resin. Considering the growing environmental issues, research over thermoplastic matrix based composites for high end applications has been of growing interest. Thermoplastic matrices are preferred due to their processing flexibility and partial recyclability. This thesis is aimed at studying the novel thermoplastic blend as matrix material for carbon fibre reinforced composites. Polyamide 6 (PA6) has been chosen as major matrix component due to its high impact strength. PA6 has been modified with Polypropylene (PP) and PP grafted with maleic anhydride (PP-g-MA) for improving the water resistance. PA6/PP/PP-g-MA blend is used as matrix and Short carbon fibres (SCF) and Unidirectional Carbon fibre (UDCF) mats are used as reinforcements. This thesis focuses on processing, structure and mechanical properties (dry, wet) of SCF and UDCF thermoplastic composites.

The first objective was to prepare the new thermoplastic matrix material by optimizing the PA6, PP and PP-g-MA content. Various studies had chosen 70/30 or 80/20 weight ratio of PA6/PP as matrix material with different PP-g-MA (compatibilizer) contents. To choose the right amount of PP content which would result the blend with comparable tensile properties to that of the PA6 (dry, wet), better impact strength and lower water absorption, the PA6/PP blends with 5, 10, 20, 30 and 50 wt% PP and PA6/PP/PP-g-MA matrix blends with 5, 10, 20, 30 and 50 wt% PP (4phr PP-g-MA) were studied. These blends were compounded using twin screw extruder. To understand the dispersion and domain size of PP in blends, morphology of blend samples after "selectively etching PP" was studied. It was found that PA6/PP had poor interfacial adhesion leading to lower retention of yield strength post water absorption, whereas the PA6/PP/PP-g-MA blend had better interfacial adhesion due to better dispersion of PP and its lower domain size (0.3-0.8 μm) in the presence of compatibilizer. It was also found that the 30 wt% PP content is optimum for PA6/PP/PP-g-MA blends. Later, PP-g-MA compatibilizer was also optimized between 3, 4, and 5 phr using the studies carried out on SCF composites (PA6/PP 70/30 wt % with 5 wt% SCF content). The composite was extruded and injection molded in similar procedure as that of blends. From experimental and Grey relational

analysis, it was found that 3 phr PP-g-MA is the optimum content for achieving better tensile strength before and after water absorption, comparable impact strength to that of PA6 and ductile fracture (matrix pull out) indicating the good interfacial adhesion within the matrix (blend) and also between matrix and fibre. Hence, the matrix blend was fixed as 70/30/3 wt/wt/phr of PA6/PP/PP-g-MA for both SCF and UDCF composites.

Secondly, the novel thermoplastic blend was used as matrix to make SCF reinforced composites with varying SCF contents (3, 6, 9 and 15 wt%) and its mechanical, thermal and morphological properties were studied. These composites were also extruded and injection molded. The tensile strength and modulus of the composites increases with increase in SCF content. It was found that the water absorption reduces by ~72% and the tensile strength reduction post water absorption was only 15% (compared to dry composite) for 15 wt% SCF composite indicating the good interfacial adhesion for wet composites. Residual fibre length of 50-100 μm was found in all injection molded composite specimens.

Thirdly, the novel thermoplastic blend pellets were used to process the matrix sheets (~900 μm) and long carbon fibre (UDCF of 12K rovings) composites, and its mechanical, thermal and morphological properties were studied. The laminate composite was made by placing alternative layers of matrix sheets and UDCF fabric (thickness of ~120 μm) and processed by film stacking (compression molding). The obtained UDCF laminate composite had six times higher strength than pure PA6. The impact strength and thermal conductivity of the composite was also higher than pure PA6. Since the matrix sheet thickness and viscosity was higher, the wettability of the fibres in the middle layers especially core region of the rovings was poor, but the interaction between the fibre-matrix was good in the top and bottom layers as revealed by X-Ray CT and SEM images. Thereby 24.5% reduction in tensile strength and 64% increase in impact strength was found for wet composites compared to dry composites.

Finally, properties before and after water absorption between PA6, PA6/PP/PP-g-MA (matrix), PA6/PP/PP-g-MA/SCF (15 wt%) and PA6/PP/PP-g-MA/UDCF (30 wt%) were compared. It is found that SCF composite modulus is "3 times" and UDCF composite modulus is "17 times" higher than "matrix blend" indicating the effect of

short and long carbon fibres. From the above results it can be recommended to use SCF composites in humid conditions because of less reduction in modulus/strength (~15 %) due to water absorption. UDCF composites should be made of thin matrix sheets (<400 μm) and thin carbon fabric of 3K rovings to overcome the poor wetting in the middle layers of the composite.

Table of Contents

List of Tables

List of Figures

Abbreviations, Units & Symbols

ABS	Acrylonitrile butadiene styrene
ABS-g-MA	Acrylonitrile butadiene styrene grafted with Maleic anhydride
ASTM	American Society for Testing and Material
BDCF	Bidirectional carbon fabric
CB	**Compatibilized blend**
CF	**Carbon fibre**
CFRP	Carbon fibre reinforced plastic
CTE	Coefficient of thermal expansion
DGEBA	Bisphenol A diglycidyl ether
DSC	**Differential scanning calorimetry**
EAG	Ethylene–ethyl acrylate–glycidyl methacrylate
EBA	Ethylene butyl acrylate
EBA-g-MA	Ethylene butyl acrylate grafted with Maleic anhydride
ECO	poly (epichlorohydrin-co-ethylene oxide)
EEA	Ethylene–ethyl acrylate copolymer
EMA-GMA	Ethylene-methyl acrylate-glycidyl methacrylate
EMG	Ethene–maleic anhydride–glycidyl methacrylate
EPDM	Ethylene propylene diene monomer
EPDM-g-MA	Ethylene propylene diene monomer grafted with Maleic anhydride
EPR	Ethylene propylene rubber
EPR-g-MA	Ethylene propylene rubber grafted with Maleic anhydride
EVA	Ethylene vinyl acetate
EVA-g-MA	Ethylene vinyl acetate grafted with Maleic anhydride
FTIR	Fourier transform infra-red spectroscopy
g/10min	gram per ten minutes
GF	glass fibre
GPa	Giga pascals
GRA	**Grey relational analysis**
GRG	**Grey relational grade**
H_2	Hydrogen
HCN	Hydrogen cyanide
HDPE	High density polyethylene
HDPE-g-MA	High density polyethylene grafted with Maleic anhydride
hrs	Hours
IFSS	Interfacial shear strength
IITRI	The Illinois Institute of Technology Research Institute
ILSS	**Interlaminar shear strength**
J	Joules
J/g	Joules/gram
J/m	Joules/metre
kg	Kilogram
kgf/cm^2	kilogram force per centimetre square

kJ/m^2	kilo joules per metre square
kN	kilo Newton
KT	kilo ton
LCF	Long carbon fibre
LDPE	Low density polyethylene
LDPE-g-MA	Low density polyethylene grafted with Maleic anhydride
LVI	**Low velocity impact**
MA	**Maleic anhydride**
MFI	Melt flow index
min	Minutes
mm	Millimetre
MPa	Megapascal
mPaS	Millipascal-seconds
N$_2$	Nitrogen
NBBSA	N-Butylbenzenesulfonamide
OM	Optical microscopy
PA	**Polyamide**
PA10	Polyamide 10
PA11	Polyamide 11
PA12	Polyamide 12
PA6	**Polyamide 6 or Nylon 6**
PA612	Polyamide 6, 12
PA66	Polyamide 6,6 or Nylon 6,6
PA6B	**Polyamide 6 blend (PA6/PP/PP-g-MA)**
PAN	Polyacrylonitrile
PB-g-MA	Polybutadiene grafted with maleic anhydride
PEEK	Poly ether ether ketone
PES	Poly ether sulphone
PET	Polyethyleneterephthalate
phr	**Parts per hundred parts of resin (Parts per hundred parts of PA6/PP)**
POE-g-MA	Poly(octane-co-ethylene) grafted with Maleic anhydride
PP	Polypropylene
PP-B	Block Polypropylene
PP-g-AcA	Polypropylene grafted with acrylic acid
PP-g-MA	**Polypropylene grafted with maleic anhydride**
PP-H	Homopolymer polypropylene
PPO	Poly(2,6-dimethyl-1,4-phenylene oxide)
PP-R	Random polypropylene
SAMA	Styrene acrylonitrile maleic anhydride
SCF	**Short carbon fibre**
SEBS	Styrene ethylene butylene styrene
SEBS-g-MA	Styrene ethylene butylene styrene grafted with Maleic anhydride
SEM	Scanning electron microscopy

SGF	Short glass fibre
T_g	Glass transition temperature
T_m	Melting point
TPU	Thermoplastic polyurethane
TPV	Thermoplastic vulcanizates
UB	Uncompatibilized blend
UD	Unidirectional
UDCF	**Unidirectional carbon fabric**
UTM	**Universal testing machine**
UV	Ultraviolet
vol%	Volume percentage
W/m-K	Watt per metre Kelvin
wt%	Weight percentage
X-Ray CT	**X-Ray Computed tomography**
α-PA6	Alpha polyamide 6
γ-PA6	Gamma polyamide 6
%χ_c	% Crystallinity
ΔH_M	Melting enthalpy
%	Percentage
°C	Degree celcius
µm	Micrometre
12k	**Twelve thousand (carbon fibres in a single roving)**
3D-Printing	Three dimensional printing
3k	Three thousand (carbon fibres in a single roving)
6k	Six thousand (carbon fibres in a single roving)

CHAPTER 1

Introduction to PA6, PA6 blend and blend based composites

1. Introduction

Properties such as corrosion resistance, light weight, high specific mechanical properties, ease of moldability, and tailoring of properties are some of the reasons for the success of plastic composites in this era. Starting from the umbrella shaft to aerospace parts, plastics composites have replaced conventional materials like wood and metals. Both thermoplastics and theromsets are used widely as matrix materials in making these polymer composites. In India around 15000 kT of thermoplastics, 1000 kT of thermosets and 200 kT of elastomers are produced. Thermoplastics are the linear chain polymers (Figure 1.1a) which can be reused or reprocessed by heating or melt blending. Elastomers (Figure 1.1b) can be thermoplastic or thermosets and can be partially reprocessed. Thermosets are cross-linked polymers (Figure 1.1c) which cannot be reprocessed post curing.

Thermosets such as epoxy, polyester are used in several high end applications as matrices, due to their better thermal stability (250-300°C) and low viscosity (800 mPas) which makes it easier for making composites. Generally thermoset matrix based composites are manufactured using compression molding, pultrusion, filament winding or resin transfer molding. In case of composite prepregs, autoclave technique is used for curing the matrix material which could take several hrs depending on the type of matrix used. Large amount of energy is required to produce thermoset composites and they are not recyclable after usage.
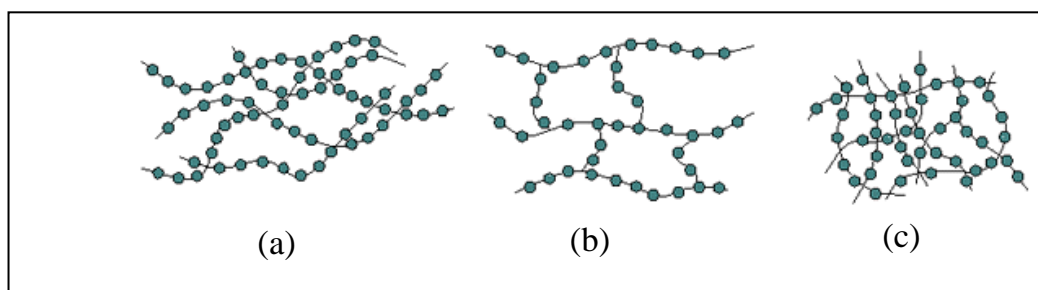
Figure 1.1: Chain structures of a) thermoplastics, b) elastomers and c) thermosets

Thermoplastic matrix based composite are manufactured using injection molding and compression molding. In both the processes, the processing time is very low from minutes to less than an hr as curing is not necessary for thermoplastic matrices. Hence thermoplastics are more favored for making commodity goods and automobile parts. It has the added advantage of recyclability which is important criteria for the recent regulations such as "End of life vehicle regulation" and "European composite recycling concept" which need to be followed by automobile manufactures. Due to these reasons, research is being done in the recent years on replacing thermoset matrices with thermoplastic matrices such as PEEK (Polyether ether ketone), Polyamides (PA), Polypropylene (PP) and thermoplastic polyurethanes (TPU) because of their better service temperature, recyclability and toughness.

Plastics that can withstand temperatures above 100°C without losing its dimensional stability and can bear tensile stresses of 40-160 MPa are called as engineering plastics. Some of the thermoplastics which are engineering plastics are PA [Tensile strength ~ 81-83 MPa], PET [Tensile strength ~ 154 MPa], ABS [Tensile strength ~ 41 MPa] and so on (*Campbell, 2012*). PA has been considered as potential thermoplastic matrix because of its high fatigue resistance, optimum service temperature and high toughness (*Bahadur, 1995*). Commonly and commercially polyamides (PA) are known as Nylons. PA having the functional group -[CONH]- are the class of engineering plastics that have been used from past 70 years (*Viswanathan, 2010*). They are widely used in automobile, electrical, electronic, and packaging industry.

Figure 1.2: Formation of a) PA6,6 and b) PA6 (polycaprolactam) polymer.
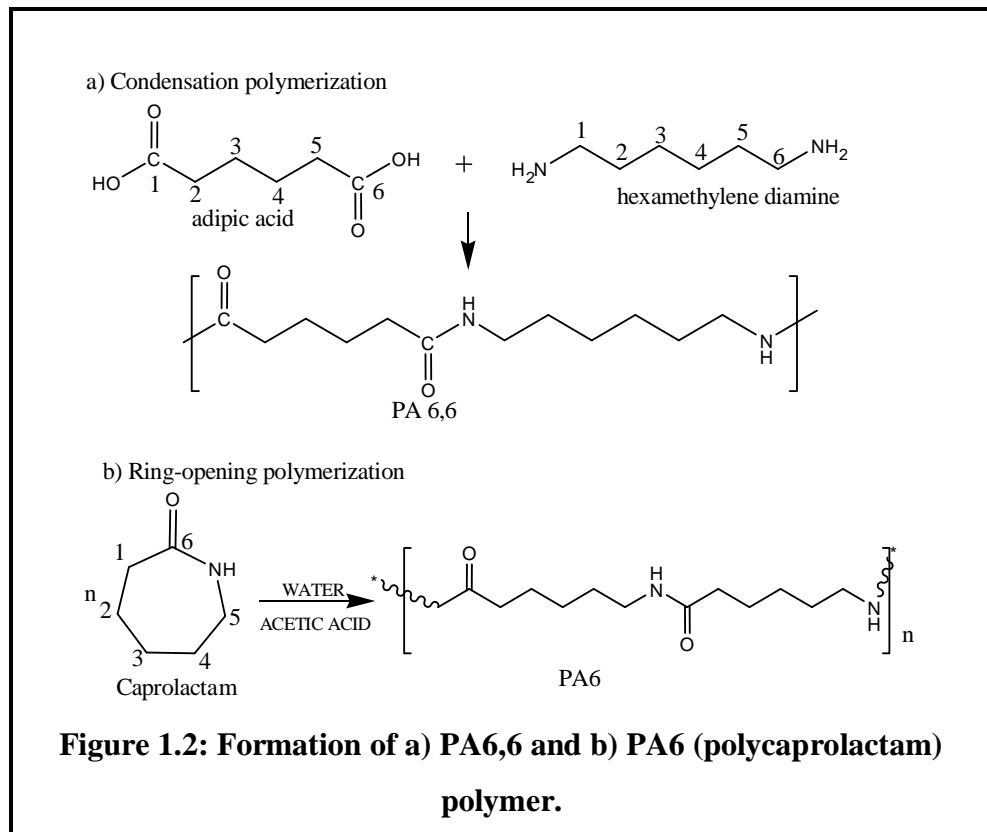
PA's are processed by two mechanisms, first being the condensation reaction between a dibasic acid and diamine which leads to the formation of amides. Consider PA6,6 (Figure 1.2a) wherein first digit represents the number of carbon atoms in the dibasic acid and the second digit represent the number of carbon atoms in the diamine. Second method is ring-opening polymerization of amino acid or lactam to form PA6 (Figure 1.2b) where the number represents the number of carbon atoms in the monomer. The various types of existing PA's are PA6; PA10; PA11; PA12; PA6,6; PA6,10 and PA6,12(*Gilbert, 2016*). Both PA6 and PA6,6 are linear chain polymers, but PA6,6 melts 40-45°C higher than PA6. Due to this, PA6,6 is harder and rigid than PA6, but in this study, PA6 is considered due to its low melting point and low viscosity at the given temperature.

1.1. Polyamide 6 (PA6)

PA6 is a semicrystalline polymer obtained through ring opening polymerization of caprolactum (Figure 1.2b). Its T_g (Glass transition temperature) is between 47-52°C and T_m (Melting point) is around 220°C. PA6 has high toughness, wear resistance,

chemical resistance, high un-notched impact resistance (*Kudva, 2000b*; *Sun, 2008*), low density, low dielectric constant, high tensile strength and high thermal stability (*Karsli, 2013*; *Luo, 2014*). But, use of PA6 has been restricted due to its moisture absorption, notch sensitivity and poor room temperature impact strength (*Navid, 2011*; *Taghizadeh, 2011*). Its applications include automobile parts, electrical, electronic appliances, packaging, textile industries, house wares, radiator fans and air-intake manifolds of automobiles (*Chow, Abu Bakar, 2005*; *Geier, 2013*; *Liao, 2011*).

1.1.1. *Structure - property relationship of PA6*

The repeat unit of PA6 is illustrated in Figure 1.3a. There are two forms of PA6 depending on the molecular arrangement of the polymeric chain. They are α and γ forms of PA6. In a polymer, it is understood that the base chain tries to maximize the hydrogen bonding with the neighboring polymer chains which forms the crystalline zones in the polymer. In α-PA6 (Figure 1.3b), the hydrogen bonds are satisfied by linear cross linking of the polymer chain, whereas in γ-PA6 (Figure 1.3c), the hydrogen bonds are formed due to twisting of polymers by 60°. However, γ-PA6 is thermodynamically less stable. The molecular structure formation is dependent on various factors viz., type of cooling during processing, presence of moisture, and rate of cooling (*Fornes, 2003*). Faster cooling and quenching of PA6 leads to more of γ-PA6 especially in case of injection molding and extrusion. In case of compression molding, the cooling technique determines the formation of the PA6 phases. Faster cooling through water/coolant leads to more of γ-PA6, whereas air cooling leads to formation of α-PA6. The α-PA6 gives strength and γ-PA6 gives toughness to the PA6. For obtaining tougher PA6 film with greater ductility, the γ-PA6 is induced by addition of nucleating agent or by stretching the film so as to convert the existing α-PA6 to γ-PA6. By annealing, γ-PA6 can be converted to α-PA6. Generally, both of these phases are present and the properties of the blend/composite depend upon the ratio of these phases. Addition of dispersed phase, reinforcement and compatibilizer also leads to conversion of α-PA6 to γ-PA6 (*Augustine, 2012*; *Bhattacharyya, 2005*).

Figure 1.3: Structure of a) PA6, b) α-PA6 and c)γ-PA6

The –NH- and –CO- groups of PA6 are bonded by strong intermolecular forces of attraction, which are the hydrogen bonds (Fig. 1.3). The H-bonds are present in both crystalline phase and amorphous phase, because of which PA6 has high impact strength. The amount of γ-PA6 also determines the impact strength of PA6. The α-PA6 contributes to strength due to their order in crystalline phase, whereas γ-PA6 contributes to impact strength as it has better mobility than α-PA6 structure. This difference in structure can be found through Differential scanning calorimetry (DSC), where the melting peak of PA6 shows twin peak at 220°C and 214°C corresponding to α-phase and γ-phase of PA6 respectively (*Augustine, 2012*; *Bhattacharyya, 2005*).

FTIR can also be used to analyze these fragments as both phases have distinct ⁻CH$_2$-bending vibrations (*Ogunsona, 2017*). The PA6 used in this study was obtained from Gujarat state fertilizer Corporation (Gujlon M28RC), Vadodara, Gujarat. Datasheet of this grade is not available; hence the properties of the material are taken from the existing literature (*Bhattacharyya, 2003*; *Dayma, 2013*; *Hemlata, 2012*; *Jogi, 2014*; *Prasath Balamurugan, 2008*).

Table 1.1: Characteristics of PA6					
Property	Value	Reference	Property	Value	Reference
Melt flow index (MFI)	28 g/10min	*(Bhattacharyya, 2003; Hemlata, 2012; Prasath Balamurugan, 2008)*	Notched impact strength	4-8 kJ/m^2	*(Feng, 2013)*(*Y. Chen, 2006*)(*Yin, 2013*)
Tensile strength	40-60 MPa	*(Bhattacharyya, 2002; Shashidhara, 2014)*(*Feng, 2013*)	Density	1.14 g/cm^3	*(Balamurugan, 2007; Prasath Balamurugan, 2008*)
Tensile modulus	1-3 GPa	*(Bhattacharyya, 2002)* (*Feng, 2013*)	Thermal conductivity	0.24 W/m-K	*(Minghui Li, 2013; Yan, 2014*)
Elongation at break (50 % RH)	100-300 %	*(Prasath Balamurugan, 2008;Bhattacharyya, 2002)*	Coefficient of thermal expansion	70-100 $10^{-6}/^{\circ}$C	*(Warlimont, 2005*)

1.1.2. Commercial components of PA6

Commercial PA6 products include household commodity goods to automobile, electrical, electronic and photovoltaic parts (Figure 1.4). Generally PA6 is used directly or as a blend or composite in commercial products. Among composites, PA6/GF (Glass fibre) is widely used. Currently filaments of PA6/GF and PA6/CF (Carbon fibre) are available which can be used for 3D-Printing applications.

Rope	Gears	Flexible conduit
Solar panel	Engine cover	3-D printing PA6/CF filament
Aquaculture net	Resonator	3-D printing PA6/GF filament
Figure 1.4: Commercial goods of PA6 used in various applications		

1.2. Polypropylene (PP)

Figure 1.5: Structure of PP
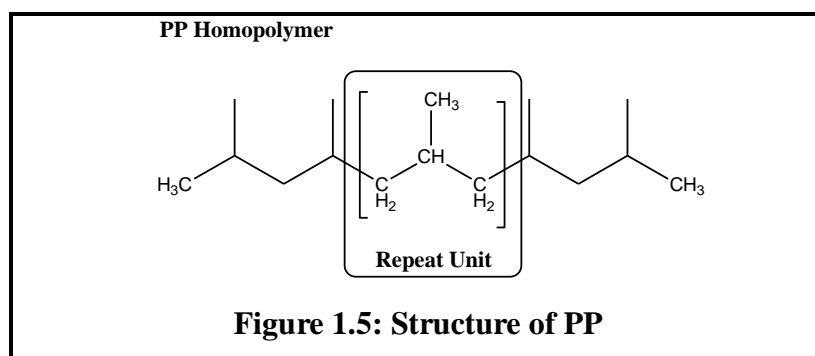
Polypropylene (PP) is a semicrystalline polymer that has become important due to its low density ($0.95 g/cm^3$) and good chemical inertness which makes it suitable in automobiles, appliances and other commercial products in which creep resistance, stiffness, toughness and cost savings are expected. Since it has only 'C' and 'H' in its polymeric back bone, PP is hydrophobic in nature. It is resistant to water because of

7

which it is used in making laboratory products. It comes under the category of commodity plastic with moderate stiffness and strength. PP is manufactured using Himont's Spheripol process where propylene monomer is converted to PP using $MgCl_2$ based Zieglar-Natta catalyst at 60-80°C temperature and 3.5-4 MPa pressure (*Gowariker, 1986*). PP can be homopolymer (PP-H) (Figure 1.5), random copolymer (PP-R) and block copolymer (PP-B) based on the structure of PP. In this study, homopolymer from Reliance Polymer (Repol H030SG) has been used. The property of the polymer from its datasheet is given in Table 1.2. PP has been used as dispersed phase, copolymer, and matrix phase in filler/fibre reinforced composites and also as dispersed phase in hybrid composite. PP is generally available as pellets of 3-5 mm diameter and also available as sheets of 1-10 mm thickness.

Table 1.2: Characteristics of PP			
Property	**Value**	**Property**	**Value**
MFI	3.4 g/10 min	Notched impact strength	40 J/m
Tensile strength	34 MPa	Thermal conductivity	0.12 W/m-K
Elongation at break	40-50%	Coefficient of thermal expansion	146-180 $10^{-6}/°C$
Density	0.905 g/cm^3		
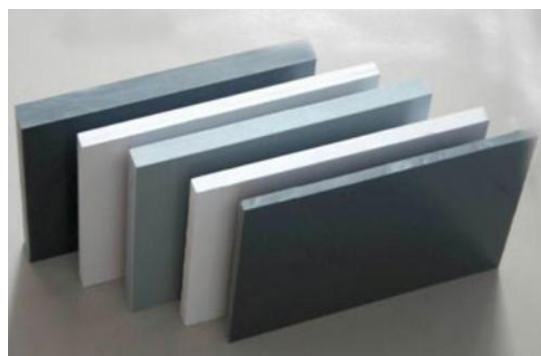
(a)   (b)

Figure 1.6: Pellets of PP (a) and Sheets of PP (b)

1.3. PP grafted with Maleic Anhydride (PP-g-MA)

PP-g-MA (Figure 1.7) is used as compatibilizer in polymer blend, as adhesion promoter in fibre reinforced composite and as processing aid for recycling of plastics.

Maleic anhydride (MA) is grafted to PP in the presence of organic peroxide during extrusion, or as solution or using ultrasonic initiation. Post grafting, the crystallinity, stiffness and strength of PP-g-MA is usually lesser than that of the PP, especially if a homopolymer is used.

Figure 1.7: PP-g-MA pellets

PP-g-MA has been used widely because it can be produced readily and economically and it forms a bridge between polar and non-polar groups in blends. The peroxide grafting of the MA occurs at the tertiary carbons of the polymer chain or at the terminal unsaturation of the chain. Structural studies (*Ranganathan, 1999*) suggest that the grafting utilizes the carbon–carbon unsaturation of the maleic anhydride group to form the bond to the polymer chain thus leaving the anhydride group free to react as an anhydride in the newly formed polymer. The presence of polar anhydride group in PP chain makes it viable to use in making natural fibre based PP composites. Unlike acrylic or methacrylic acid, maleic anhydride does not readily react with itself under typical industrial grafting conditions. The decreased tendency to participate in side reactions and the versatility of the anhydride group over an acid group makes maleic anhydride the graft moiety of choice when grafting a reactive polar group on to PP. As the polymer is grafted with MA, the viscosity is lowered; hence the molecular weight reduces due to chain degradation via beta-scission reaction.

Figure 1.8: Grafting of MA to PP
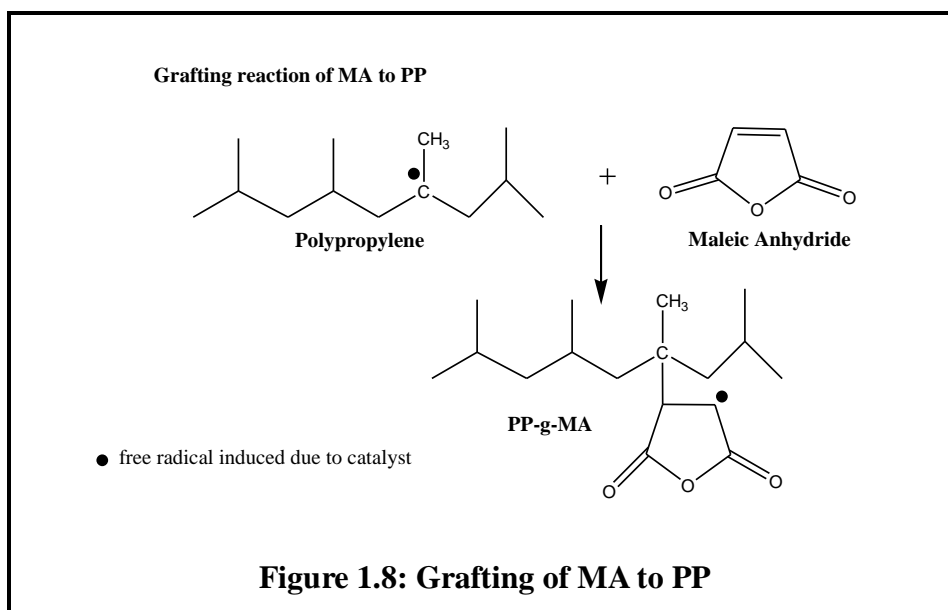
The reaction mechanism and structure of PP-g-MA (*Oromiehie, 2014*)is shown in Figure 1.8. The PP-g-MA used in this study was obtained from Pluss Polymers (OPTIM-408), Haryana. It has very high grafted MA content, which was found to be 1.375%. The properties of material are given from the datasheet (Table 1.3).

Table 1.3: Characteristics of PP-g-MA	
Property	**Value**
MFI	50 g/10 min
Tensile strength	34 MPa
Elongation at break	9 %
Tensile modulus	0.75 GPa

1.4.Carbon fibre

Carbon fibres are made from organic precursor fibres such as polyacrylonitrile (PAN) or rayon fibres, by carbonization followed by graphitization at high temperatures. Fabrication processes involves the following steps (*Chawla, 1998*):

1. Precursor fibre is produced from raw material through wet-spinning, dry-spinning, or melt-spinning followed by drawing or stretching of fibre.

2. A stabilization treatment is done by keeping the fibre at tension in presence of oxygen by slowly increasing the temperature to 250°C which prevents the

fibre from melting during further treatment and the fibre color changes to black.

3. A thermal treatment called carbonization involving heating of the fibre at elevated temperatures is done, which removes most of the non-carbon elements in the form of H_2, N_2, HCN, etc.

4. An optional thermal treatment called graphitization is done, which improves the tensile modulus of carbon fibre obtained in the previous step (step 3).

Figure 1.9: Schematic conversion of PAN fibre to Carbon fibre
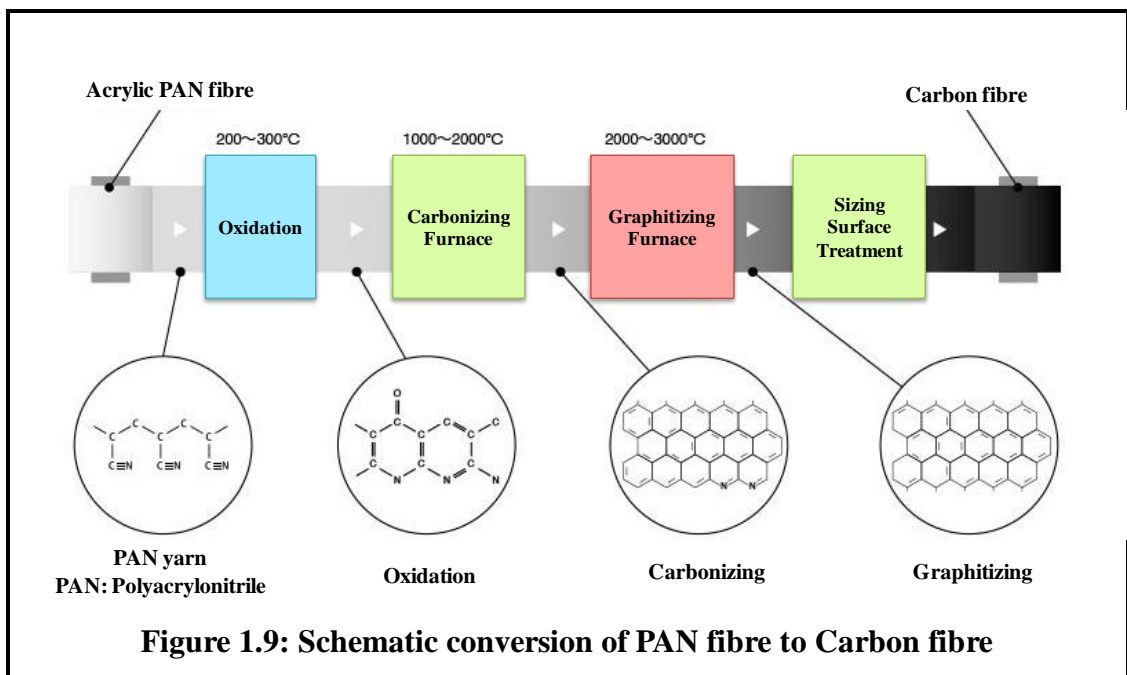
Carbon fibres made from PAN (Figure 1.9) are called ex-PAN carbon fibres. The PAN fibres are stabilized in air (a few hrs at 250°C) to prevent melting during further processing. The fibres are kept under tension to prevent from contraction during the oxidation treatment. The black fibres obtained after this treatment are heated slowly in an inert atmosphere to 1,000–1500°C where carbonization occurs. Slow heating allows higher degree of order in the fibre. The rate of temperature increase should be low so as not to destroy the molecular order in the fibres. The final optional heat treatment consists of holding the fibres for very short duration at temperatures up to 3000°C for graphitization to occur. This improves the fibre texture, i.e. the orientation of the basal planes and thus increases the elastic modulus of the fibre but it reduces the tensile strength of the fibres.

Carbon fibres thus made can exists in several forms such as short carbon fibre (SCF), roving, unidirectional carbon fabric (UDCF) and bidirectional carbon fabric (BDCF) (Figure 1.10). Diameter of individual carbon fibres can vary between 7-10 μm. The SCF are made by chopping the long carbon fibres (filaments) to 1-12mm in length. Mostly SCF are used as reinforcement for thermoplastic composite, where the composites are made using extrusion followed by injection molding. SCF are used for applications where minimal improvement in tensile strength is required along with the improvement in impact strength of thermoplastics. Widely, SCF reinforcements are used in making gears, cams, sports goods and small structures in sports vehicles. The advantage of SCF is the random distribution of fibres in the matrix, which induces isotropic properties in the composites. PA6, PP, PET, and PEEK are few matrices used with SCF reinforcement. If the fibre length reduces to less than critical fibre length, then these fibres act as fillers instead of reinforcement. The critical fibre length also varies with type of matrix used. With thermosets as matrices, SCF (nonwoven) mat is generally used for prepreg preparation for sheet moulding composite. The SCF used in this study was obtained from Sun young industries, South Korea. The properties of the carbon fibres used for making SCF are as follows (Table 1.4).

(a) (b) (c) (d)

Figure 1.10: Different forms of carbon fibre, a) Short carbon fibre (1 mm length) b) Carbon fibre roving (untwisted 3000 fibres-3K), c) UDCF fabric (untwisted 12000 fibres-12K, woven fabric) and d) BDCF fabric (untwisted 6000 fibres-6K, plain weave)
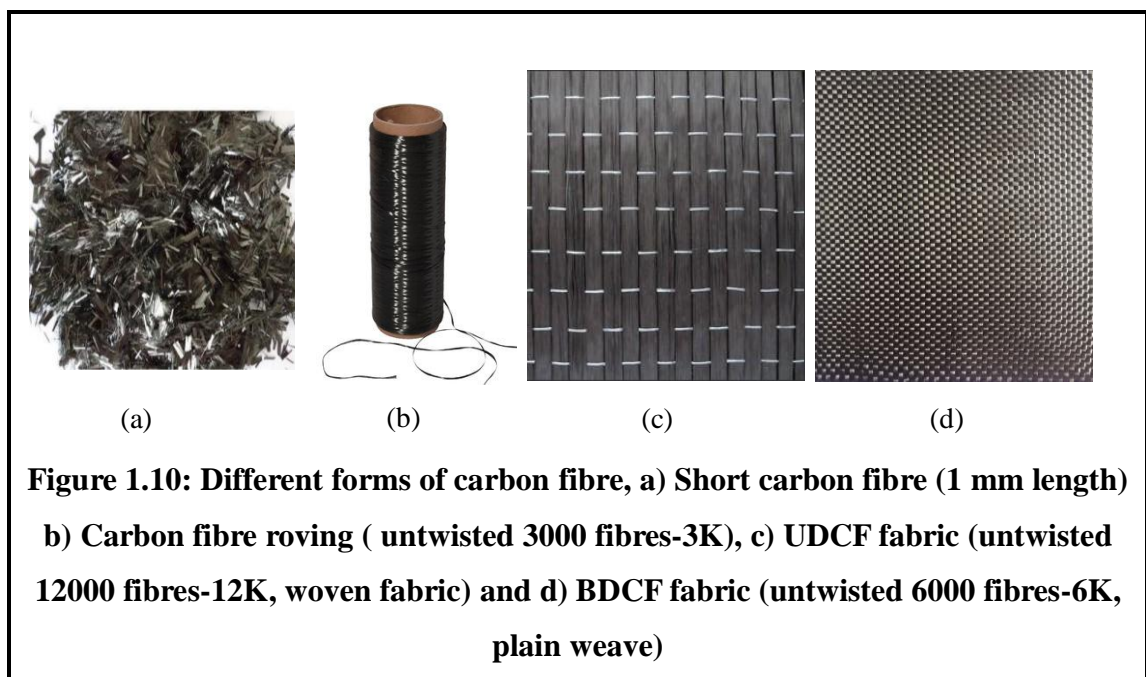
Table 1.4: Characteristics of Carbon fibres			
Property	**Value**	**Property**	**Value**
Tensile strength	2200-2700 MPa	Thermal conductivity (longitudinal)	11-15 W/m-K
Elongation at break	1.5 %	Coefficient of thermal expansion (longitudinal)	$-0.6\ 10^{-6}/^{\circ}C$
Tensile modulus	200-225 GPa	Sizing	1% oligomeric epoxy
Density	1.78 g/cm^3		

UDCF used in this study is a woven UDCF fabric with 12k roving in warp direction and fine white thread in weft direction. Each roving can have 3000-12000 individual fibres. Rovings in fabric can be chosen depending on the process and product. The generally available UDCF/BDCF fabrics are made using 3k, 6k, and 12k rovings. But while using thermoplastic matrix, owing to high matrix viscosity, it is difficult to coat the entire fibres with matrix material and 3k roving based UDCF would be suitable. But, the availability of 3k UDCF is very scarce in India, hence widely available 12k UDCF fabric has been used in this study. The strength of the composite also depends on the roving type i.e. with increase in fibre quantity, the strength of the composite increases but possess issues related to impregnation with matrix.

Rovings are used as reinforcement with thermoset matrix in pultrusion technique and filament winding technique. In case of thermoplastic matrices, CF rovings are used directly for making 3D-printing filaments along with PA. Here the roving is coated with PA using modified extrusion technique. UDCF mat is widely used with epoxy and phenolic matrices for making most of the aerospace, aircraft parts and sports vehicles. As discussed before, these UDCF mats are made from 12k roving and mostly UDCF prepregs (partially cured composite) are used to make UDCF composite used in high end applications.

In case of thermoplastic composite, the ratio of fibre modulus to matrix modulus can lie between 50-200, so the load sharing becomes saturated between 20-40 vol % of fibres fraction in a composite. With thermoplastic as matrices, due to their higher melt viscosity, carbon fibre prepregs are made by embedding the UDCF mat on thermoplastic films and then compression molded to form the final structure. Widely,

film stacking technique, polymerization of thermoplastics after coating on UDCF is used for making composite structure. UD fabric/BD fabric based epoxy prepreg are widely available. But in case of thermoplastic composite only PA6/UDCF prepregs are currently available. UDCF composites have higher strength and stiffness in fibre direction (Table 1.4). For obtaining isotropic properties, different orientations of UDCF (0, +90, -90, +45, -45, 0) or BDCF (0, 90, +45, -45) is used as reinforcement. In this study, 12k fibre UDCF was procured from CHN tech., China. The tensile strength and tensile modulus of carbon fibre used for making the UDCF sheet are 2500 MPa and 200-225 GPa respectively.

1.4.1. *Sizing on carbon fibre*

All commercially available carbon fibres are sized before being converted to roving/fabric as per the end user requirement. The widely used sizing is epoxy, as generally UDCF fabric and rovings are used as reinforcement for epoxy based composite. The sizing is applied on the fibres for providing ease of working with the fibre and also to make it compatible with matrix. Currently due to the vast variety of matrix material being used, the sizing agent is chosen such that it can be used along with thermosets (epoxy, phenolics, polyester) and thermoplastic (PES, PEEK, PP, PA). The sizing content varies from 0-5%. Unsized fibres are also provided by the manufacturer if prepreg tapes have to be made. Along with matrix type, sizing can also be categorized based on the type of processing method involved. Different sizing agent is used for weaving and prepreg making. The sizing content is more if the fibre is being weaved and less when prepregs are made. The application of sizing improves the flexibility of the UDCF fabric. SCF have 0-3% polymer sizing. In some studies authors have varied the sizing agent and studied the effect of sizing on PA6/SCF composites (*Feng, 2013*; *Luo, 2014*).

1.5.Limitations of PA6

The major drawback of PA6 is moisture and water absorption. It is hygroscopic in nature due to the presence of polar groups in its chain. Initially, the amide groups bonds with water molecule forming a dimeric association through proton acceptance/donation, which pushes the PA6 chains apart, leading to swelling of the

sample (Figure 1.11a). As the water diffuses through the PA6 phase, it forms firmly and loosely bound bonds in the amide linkages by hydrogen bonding. The firmly bound molecules are the ones that directly form the bonds with the amide linkage and loosely formed molecules are the water molecules that cluster around the firmly bound molecules. These clusters lead to spacing of PA6 chains leading to swelling of the sample. This sliding of molecules and disruption in the packing of the PA6 molecules leads to lower tensile modulus, lower glass transition temperature and structural transition of α-PA6 to γ-PA6. At elevated temperature, above 85°C, and on prolonged exposure to wet environment, hydrolysis of PA6 chain occurs (Figure 1.11b) which leads to scissoring of PA6 chains leading to lower molecular weight as the water bonds at the amide linkages, breaking them into smaller molecules (*Ogunsona, 2017*). The voids left behind by the water acts as defects, which leads to slippage of PA6 chains which convert α-PA6 to γ-PA6. These structural changes in PA6 post water absorption can be analyzed through FTIR.
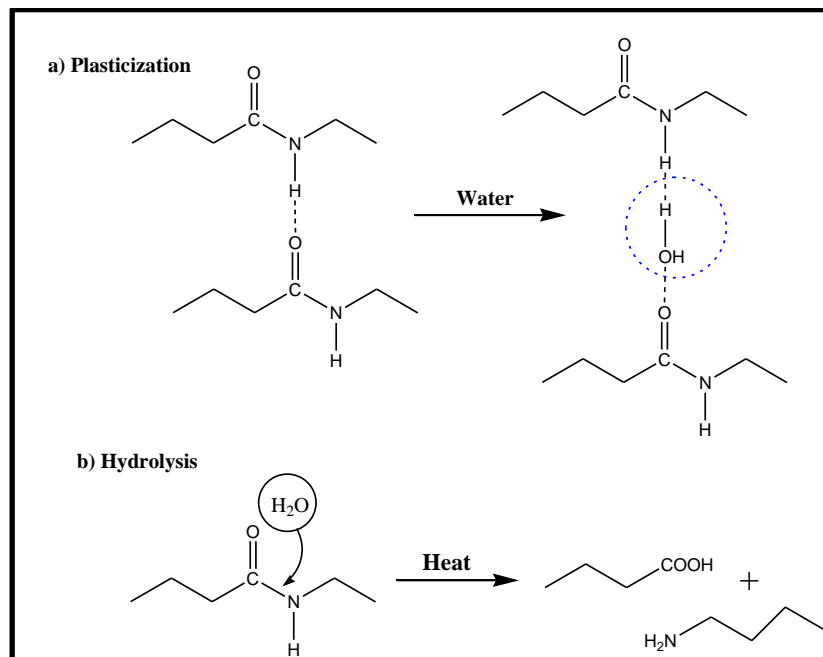
Figure 1.11: a) Plasticization of PA6 by water b) Hydrolysis reaction

Other drawback of PA6 is notch sensitivity and low temperature impact strength. Compared to other thermoplastics, PA6 has higher toughness, but in presence of notch, the impact resistance becomes low. In PA6, energy required for crack initiation is higher but crack propagation is lower. The low temperature impact strength is lower

for PA6 as its T_g is near room temperature. Hence PA6 has been blended with various polymers such as PP, HDPE and ABS to overcome the above drawbacks.

1.6. PA6 Blends and Compatibilizer

To increase the thermo-mechanical properties of the engineering plastics, two polymers are melt-blended to form blends or alloys, in order to increase properties such as stiffness, toughness, impact resistance, abrasion resistance or for ease of processing depending on the end use. Blends can either be miscible or immiscible. The immiscible blends form two phase morphology which is highly heterogeneous in nature, and possess lower thermo-mechanical property as they have poor interfacial adhesion. To enhance the adhesion between the immiscible blends, compatibilizers are used. Without compatibilizers, the physical, thermal and mechanical properties of blend yields very low value than the parent polymers in most cases. The importance of compatibilized blends and normal blends had been discussed by Koning et al. (*Koning, 1998*) and Litmanovich et al. (*Litmanovich, 2002*).

PA6 has been blended with various thermoplastics including PP, HDPE, LDPE, ABS and thermoplastic elastomers such as EPR, SEBS, TPV and EVA (Table 1.5). The aim of blending polyolefins is mainly to reduce the water absorption and for improving the processability of PA6, whereas blending with thermoplastic elastomers leads to better impact resistance of the blend i.e. increase in toughness with a decrease in stiffness. Since, the dispersed phase is immiscible with PA6, compatibilizers has been studied and successfully used in making blends.

Polyolefinic compatibilizers gave balanced stiffness and toughness depending on the compatibilizer type and content. The dispersion and adhesion characteristic is dependent on the processing technique and compatibility between the dispersed phase and compatibilizer used (*Geier, 2013*). Table 1.5 shows the literature data of blends studied along with compatibilizer

Table 1.5: Blends of PA6 along with its application				
Blend	**Purpose**	**Compatibilizer used**	**Application**	**Reference**
PA6/PP	Ease of processability and reduction of water absorption	PP-g-MA SEBS-g-MA EPR-g-MA EMA-GMA	Connectors, electrical/ electronic appliances, switches, pump housing, impellers, gears and bearing retainers	(*Agrawal, 2010*; *González-Montiel, 1995a*; *Huber, 2014*; *La Mantia, 1999*; *Ohlsson, 1998*)
PA6/ABS	Increased impact strength	ABS-g-MA POE-g-MA PP-g-MA SAMA	Sporting goods, consumer goods housing	(*J. Chen, 2013*; *Y. Fu, 2013*; *Jime, 2011*; *Kudva, 1999, 2000a, 2000b*)
PA6/HDPE PA6/LDPE	Superior barrier properties, Ease of processability	PP-g-MA HDPE-g-MA LDPE-g-MA	Packaging films Cables Mandrel Tubes and pipes	(*Hamid, 2014*; *Kudva, 1999*; *L. P. Li, 2012*)
PA6/EVA PA6/EBA PA6/ECO	Resistant to oil, fuel and ozone	EVA-g-MA EBA-g-MA EPR-g-MA	Fuel hose Sealant Cable	(*Balamurugan, 2007*; *Bhattacharyya, 2003*; *Taghizadeh, 2011*)
PA6/SEBS PA6/EPR PA6/EPDM PA6/TPV	Increased low temperature toughness	SEBS-g-MA EPDM-g-MA EPR-g-MA	Plugs Rollers Sports goods	(*Borggreve, 1989*; *L. F. Ma, 2012*; *Okada, 2001*; *Oshinski, 1992*; *Tang, 2007*)

For all blends, where compatibilizer is used, the dispersed phase is grafted with MA in its chain. MA is a reactive group which reacts with PA6 leading to better interfacial adhesion between the PA6 and dispersed phase. In most of polyolefinic blends, compatibilizer are used in lower quantity, as with increase in compatibilizer, it plasticizes the matrix leading to lower stiffness. Compatibilizer, when used in higher quantity or as dispersed phase (> 15 wt %) is called as impact modifiers. In most of the elastomer based blends it was found that the compatibilizer was used as impact modifier to improve the low temperature toughness of the blends. Blends with ABS and SEBS as dispersed phase have very high impact resistance with reduced tensile

strength. For most of the blends the dispersed phase optimization and compatibilizer content optimization is found using the mechanical properties and domain size of the dispersed phase. Since the focus of this work was to reduce the water absorption of PA6, PP was used as dispersed phase along with PP-g-MA as compatibilizer.

1.6.1. PA6/PP blends

Table 1.6: Properties of the PA6/PP blends							
Author	Composition (wt/wt) PA6/PP	Compatibilizer	Parameter	Tensile strength (MPa)	%Elongation (%)	Impact Strength J/m or kJ/m^2	Type of Impact test
(González -Montiel, 1995a)	PA6/PP 64/16	PP-g-MA (20 wt %)	Increase in temperature	NA	NA	40-85 J/m	RT, Izod notched
	PA6/PP 64/16	SEBS and SEBS-g-MA (20 wt %)		NA	NA	200-1000 J/m	-25 to 25°C, Izod -notched
	PA6/PP 52.8/27.2	EPR-g-MA (20 wt %)				200-1100 J/m	-25 to 25°C, Izod -notched
(Ohlsson, 1998)	PA6/PP (50 to 73.9)/ (50 to 0)	SEBS (0 to 26.1 wt %)	Increase in compatibilizer content	~38-15 (TS)	50-400	NA	NA
	PA6/PP (42.5-37.5) /(42.5-37.5)	SEBS-g-MA (15to 25 wt %)		~25 (TS)	~80 to 200	NA	
(La Mantia, 1999)	PA6 100			26 (TS)	12	NA	NA
	PA6/PP 80/20	NA	Mixing time (0, 20 mins and 60 mins)	30-21(TS)	72-7		
	PA6 80	PP-g-AcA (20 wt %)		33-30(TS)	47-12		
	PA6 80	PP-g-MA (20 wt %)		34-27(TS)	38-16		
(Huber, 2014)	PA6/PP (100-75/0-25 wt/wt)	PP-g-MA 5 wt%	Type of compatibilizer	71-57 65-56 Reduction of TS	NA	30-60 J/m	RT, Izod notched

Since PA6 and PP form immiscible blends, due to their difference in polarity, the domain size of the PP in the blend is higher, leading to brittle fracture of the specimens. Hence many authors have worked to find the suitable compatibilizer, and suitable amount of compatibilizer that should be added to blends to obtain balanced mechanical properties. From the earlier reports, it has been deduced that MA (Maleic anhydride) is the most suitable functional group for compatibilization of PA6/PP

blend as MA reactively compatibilizes the blend by reacting with the -NH_2- end group of PA6. *SEBS-g-MA, EPR-g-MA* and *PP-g-MA* has been used as compatibilizers for PA6/PP blends (*Agrawal, 2010*; *González-Montiel, 1995a*; *Huber, 2014*; *La Mantia, 1999*; *Ohlsson, 1998*).

Addition of *SEBS-g-MA* and *EPR-g-MA* led to increase in impact strength but reduction in tensile strength of PA6/PP blend. Hence *PP-g-MA* was studied as compatibilizer to minimize the loss of tensile strength. Properties of the PA6/PP blends are summarized in Table 1.6. It is seen that with judicious use of MA with rubber phase such as SEBS, high impact strength of PA6/PP blends can be achieved, also if PP-g-MA are used with process where high pressure is involved in making the blends, then high tensile strength and tensile modulus can also be achieved (*D. Fu, 2015*). The amount of maleation also plays a key role in reduction of interfacial tension, but higher maleation can also lead to decrease in impact strength (*Huber, 2014*).

Huber et al. (*Huber, 2014*) studied two types of 5 wt% of PP-g-MA (~6.71% and 1.95% MA content) as compatibilizer and reported that compatibilizer with higher MA content effectively improved the interfacial adhesion with increment in tensile strength, but reduced the impact strength. Montiel et al. (*González-Montiel, 1995a*) stated that the degree of grafting of MA to PP determines the morphology and properties of PA6/PP blends. With increase in the MA content, the heterogeneity of the blend increases, therefore the amount of MA should be optimum for obtaining homogeneous morphology.

Overall, using optimum amount of PP-g-MA as compatibilizer for PA6/PP blends, balanced stiffness and toughness can be anticipated. However, with blending of PA6/PP/PP-g-MA, the compatibilized blend has properties intermediate to that of PA6 and PP. To improve the strength and stiffness of the blends, reinforcements such as nano-clay(*Chow, Abu Bakar, 2005*; *Isik-Gulsac, 2012*; *Kelnar, 2009*; *Scaffaro, 2008*; *Taghizadeh, 2011*) and short glass fibres (SGF) were used (*Andreeva, 2000*; *Arsad, 2010*; *Cho, 2001*; *Y. Li, 2014*). Very few studies (*Do, 2016*; *Y. Li, 2014*; *H. Zhou, 2007*; *S. Zhou, 2013*) were found for PA6 blend based short carbon fibres (SCF) composites.

1.7. Thermoplastic composites

Thermoplastics were mostly invented and processed in large scale during early 1950's. It gained popularity very easily, and was manufactured along with fillers. Initially, PP and PS were used widely. The laminate composite of rubber modified polystyrene sheet with glass fibre mat was reported by Frazier et al. *(Frazier, 1957)* from Union Carbide. The concept of injection molded glass fibre reinforced composite was first patented by *Rexford, 1959*. Following which short glass fibre was widely used with various thermoplastic matrices including various polystyrenes as reported by Lee et al. *(Lee, 1969)*. The commercial use of carbon fibres (CF) begun in 1960's and was widely used with phenolic and styrene matrices. Later CF was used as reinforcement with PA6, PP, and ABS (*Hollingsworth, 1969*). Later the use of thermoplastic composite in aircrafts started by 1970's and also graphite based composites were widely studied. The PP-g-MA was introduced as reactive compatibilizer in 1974 for PA6/PP blend (*Hasegawa, 1974*). However, the use of thermoplastic composite in construction, automobile, sports materials began by 1990. The powder coating of glass fibre roving with thermoplastic was also introduced (*Iyer, 1990*). The research on carbon fibre, wood fibre and natural fibre mat were established by 2000. Post 2000, the study of thermoplastic and thermoplastic blend based nano-composites came into play and it was widely researched area with nano-clay, CNT, and nano-talc (*Chow, 2003*; *Prasath Balamurugan, 2010*; *Z. Shen, 2009*). Currently the use of thermoplastic matrices for carbon fabric prepreg, 3D-printing and electrospinning are the key areas of research. In this study PA6 blend based SCF and UDCF composites has been studied.

1.8. PA6 based fibre composites

PA6 based CFRP (*An, 2014*; *Feng, 2013*; *Karsli, 2013*; *Luo, 2014*; *Molnár, 1999*) has been of interest due to superior mechanical properties of carbon fibre and high toughness of PA6. PA6/CF has been studied by different researchers by varying composite processing parameters. Both SCF and LCF (short and long CF) has been used as reinforcement in these composites. Karsli et al. (*Karsli, 2013*) studied the effect of 6mm and 12mm length SCF's on the properties of PA6/SCF composite and reported an average residual fibre length of 50 µm. Molnar et al. (*Molnár, 1999*)

studied various processing parameters of injection molding and found that increased fibre content and higher injection rate led to composite with higher stiffness and fracture toughness. Feng et al. (*Feng, 2013*) used recycled CF and modified the surface with DGEBA (epoxy) to improve the properties of PA6/SCF composites. Luo et al. (*Luo, 2014*) made core-shell PA6/LCF composite by coating LCF with PA6 during melt extrusion. They varied the silane based sizing amount and found that at 22 wt% of sizing, composites with high strength and stiffness can be obtained. Commonly it is seen that the strength and stiffness increases and "elongation at break" decreases with increase in fibre content due to restriction of mobility of polymer chains and brittleness of fibres (*An, 2014*; *Feng, 2013*; *Karsli, 2013*; *Luo, 2014*; *Molnár, 1999*). On the contrary, impact strength of the composites was higher than pure PA6 as seen by few authors (*Feng, 2013*; *Luo, 2014*) and it could be due to the surface modification of SCF which in turn leads to crack arresting. The processing technique for composites is as same as blends, where extrusion (single or twin screw) is used for mixing followed by injection/compression molding. It has to be noted that the fibre length reduces due to these processes and hence the properties of the composite vary with processing technique.

1.8.1. *PA6 based long fibre based (laminate) composites*

PA6 based laminate composites are being studied recently due to the increasing interest in replacing thermoset matrix by thermoplastic matrix. The general processing technique for making laminate composites is compression molding, but the initial stages vary. Either anionic PA6 is coated on CF (Figure 1.12a), PA6/CFprepreg is made (Figure 1.12b) or thin films of PA6 made and then compressed along with CF. Yan Ma et al, have done a series of study on PA6/UDCF, PA6/BDCF and compared with Epoxy/UDCF composite (*Y. Ma, 2016, 2018*; *Y. Ma, Ueda, 2017*; *Y. Ma, Yokozeki, 2017*; *Zhao, 2019*).

Figure 1.12: a) Anionic PA6 composite preparation b) PA6/CF prepreg preparation (*Park, 2015*)
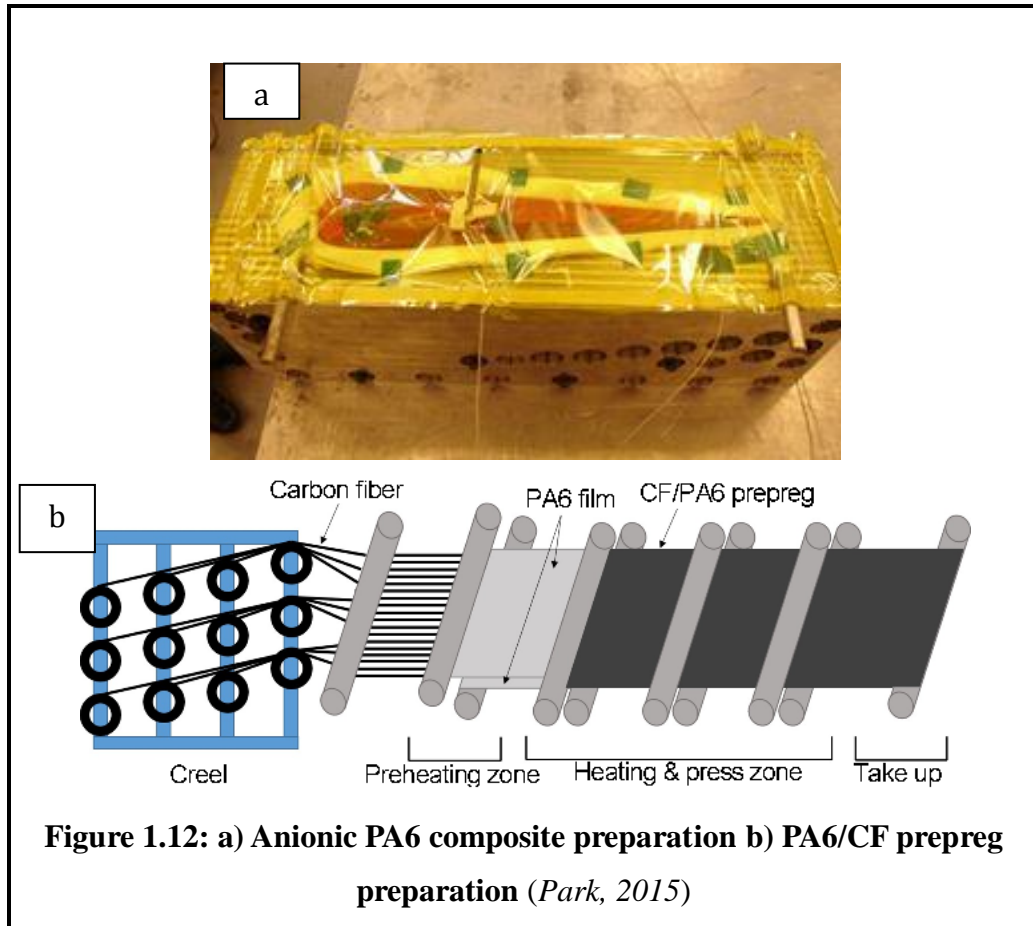
In their study while comparing PA6/UDCF and Epoxy/UDCF it was found that the fibre wetting was better in epoxy composites in comparison to PA6 composites. Dry spots were found in PA6 composites, where the interfacial adhesion was very poor. In well wetted areas, PA6 composites had better interfacial adhesion than epoxy composites. Arhant et al. (*Arhant, 2016*)studied the effect of sea water on tensile properties of PA6/UDCF laminate, whereas Pillay et al. (*Pillay, 2009*)studied the effect of UV-radiation. Botelho et al. (*Botelho, 2010*) studied the effect of free vibration in PA6/BDCF composite. However, use of blend based matrix system for laminate composite was not found in the literature. It could be understood from above literature that, with UDCF as reinforcement, the composite had very high tensile strength. But on exposure to water and UV, the tensile strength reduced by >50%.
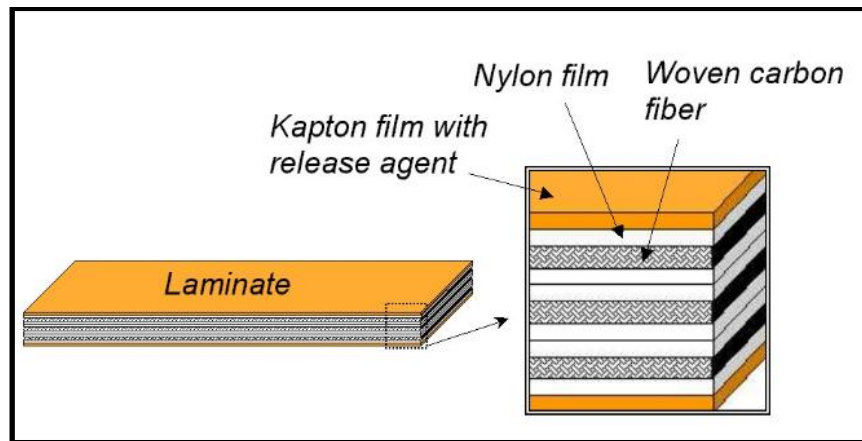
Figure 1.13: Film stacking technique for PA6/CF composite (*Bengtsson, 2006*)

However, Arhant et al. (*Arhant, 2016*) stated that, if PA6 is dried after water saturation, then 90% of the tensile strength could be recovered, but only on complete drying of the composite. Also, the dry spots in composites had occurred for both UDCF and BDCF, because of which matrix and fibre could be distinctly seen. The wettability of the composite ensures uniform interfacial adhesion, but in thermoplastic composites, always dry-spots are observed due to very high viscosity of the matrix material. The processing technique for making the laminate composite had been the film stacking technique for thermoplastic matrix (Figure 1.13). The other techniques include commingled yarns and powder coating of the fibres with the thermoplastic matrix and then compression molding it to form the laminate composite. In film stacking technique, the matrix film (100-200 µm thickness) is placed along with the fibre fabric as alternating layers. The stacked laminate is compression molded, where the thermoplastic matrix melts and impregnates into the fibre layers. Here the three processing parameters are temperature, pressure and time for consolidation of the composite. The temperature is always 30°C or more than the melting temperature of the matrix, to ensure the matrix is in liquid state and eases the impregnation of fibres. The pressure should be high enough to press the matrix into fibre layers, but not as much that the misalignment of fibre would take place. Similarly sufficient time has to be given for melting and penetration of matrix into the fibre layers, otherwise dry spots would appear in the composite.

1.9. PA6 blend based short fibre composites

To improve the impact strength, reduce water absorption and to obtain the balance between stiffness and toughness, dispersed phase was added in few hybrid composites of PA6. Zhou et al. (*H. Zhou, 2007*) added organically modified montmorillonite clay to PA6/SCF composite and found that the clay acted as lubricant and aided in reducing the fibre breakage during processing. Polymer was added as additional dispersed phase along with CF by few authors. Zo et al. (*Zo, 2014*) added TPU as dispersed phase to PA6, and LCF as reinforcement which led to tough composite. Further, Rashkovan et al. (*Rashkovan, 2014*) used PA6,6 as dispersed phase and found that better properties were achieved at 70/30 ratio of PA6/PA6,6. Other than SCF/LCF, biocarbon has also been studied (*Ogunsona, 2017*) where epoxidised natural rubber was added as impact modifier and considerable improvement in impact strength at the expense of tensile strength was found.

The use of PA6 ternary hybrid composites with a dispersed phase and compatibilizer along with reinforcement has been studied by few authors (*Arsad, 2010*; *Do, 2016*; *B. Li, 2009*; *S. Li, 2018*; *Y. Li, 2014*). As stated earlier, the widely used synthetic fibre reinforcement is SGF (short glass fibre). As mentioned above many literatures are available for PA6/SCF composite, but very few articles are available for PA6 blend based SCF reinforced composite. Do et al. (*Do, 2015*) studied the effect of PP content in PA6/PP/PP-g-MA/SCF composites and found that at 30 wt% PP content, better retention of strength and stiffness post water absorption was observed. However, the tensile strength and modulus decreased with increase in PP content and it was also confirmed that PP reduces the water absorption effectively. The objectives of the few studies related to blend based composite system are given in Table 1.7.

Table 1.7: PA6 blend based fibre reinforced composite			
Composition	**Compatibilizer**	**Objective**	**Reference**
PA6/PET/SGF	EEA, EAG and EMG	Best compatibilizer that can modify PA6/PET blend along with improving the adhesion between blend and fibre	(*S. Li, 2018*)
PA6/PPO/SGF	PPO-g-MA	Effect of PPO-g-MA was studied. With addition of PPO-g-MA and 30 wt% SGF, improvement in tensile strength, impact strength and flexural modulus was observed	(*B. Li, 2009*)
PA6/ABS/SGF	ABS-g-MA	Effect of ABS-g-MA was studied. Tensile strength and modulus increased with SGF content whereas the impact strength decreased.	(*Arsad, 2010*)
PA6/ABS/SGF	EPR-g-MA	Effect of ABS and SGF content was studied. With 45% ABS and 15% SGF, improvement in tensile modulus and impact strength was achieved	(*Cho, 2001*)
PA6/ABS/SCF/ Nano-CaCO$_3$	NA	Effect of addition of 0-8 wt% nano-CaCO$_3$ to the blend based SCF composite	(*Malekzadeh, 2016*)
PA6/PP/SCF	PP-g-MA	Effect of increasing PP content on mechanical properties before and after water absorption was studied	(*Do, 2015*)

NOTE: SGF: Short glass fibre; SCF: Short Carbon fibre

1.10. Gaps in Existing Research

After the extensive literature review on PA6/PP blends and composites based on PA6/PP matrix blend following gaps were found.

1. To overcome the drawback of PA6 i.e. moisture intake, PA6/PP blends with 70/30 wt% was studied, but the addition of compatibilizer along with the effect of water absorption on tensile and impact properties were not reported. It is also found that morphology of PP in the blend was not fully understood after adding compatibilizer.

2. Few studies reported on processing of PA6/PP blend based SCF composites but no studies were focused on resulting composite morphology, impact strength and tensile properties before and after water absorption which is needed in

considering these composites for high humid applications. Critical fibre length of carbon fibre was also not reported.

3. It is also observed from literature that processing of PA6 based UDCF composites is reported using rovings, but processing using PA6 blend as matrix and UDCF mat as reinforcement, which is important in making structural composites is not reported because it is challenging due to the high melt viscosity of the matrix and unavailability of thin UDCF fabrics.

4. Tensile, impact (falling weight impact test) and thermal properties of UDCF reinforced PA6/PP laminate composite has not been reported.

5. No comparison of properties was reported between PA6, PA6/PP/PP-g-MA (matrix blend), injection molded SCF composite and compression molded UDCF composites.

1.11. Objectives of the Proposed Research

- To process the new thermoplastic matrix material which is a blend of (PA6, PP, and PP-g-MA) by optimizing the PP content (5, 10, 20, 30, 50 wt %) and PP-g-MA content (3, 4 and 5 phr).

- To determine the mechanical, thermal and morphological properties of short carbon fibre (SCF) reinforced PA6/PP/PP-g-MA composites before and after water saturation by optimizing the SCF content between 3, 6, 9 and 15 wt %.

- To process the matrix sheets and long carbon fibre (Unidirectional mat of 12K fibres) reinforced PA6/PP/PP-g-MA laminate composites and to characterize the composites using mechanical, thermal and morphological studies.

- To compare the tensile properties before and after water absorption between PA6, PA6/PP/PP-g-MA (matrix), composite with SCF and composite with UDCF. For dry samples, impact energy and thermal conductivity values were also compared

The graphical abstract in Figure 1.14 depicts the raw material used, combinations studied, type of processing used, and the techniques used to analyze the samples. This study mainly focused on study of blends and composite by focusing on processing

and testing. Initially matrix blend of PA6 (70 wt %) /PP (30 wt %) /PP-g-MA (4 phr) was optimized successfully and matrix pellets were made available using extrusion. Few dog-bone specimens of matrix were also made using injection molding. 1 mm length short carbon fibres (SCF fibres) were extruded along with newly developed matrix pellets and dog-bone specimens were made using injection molding. UDCF mat (roving of 12 K carbon fibres) was used as sheet and laminate composites were made using compression molding (film stacking of alternate layers of matrix sheet and UDCF sheet). A special focus was given in measuring the tensile strength in dry and wet conditions. Here the wet indicates samples are soaked in water up to saturation and these wet tests are performed to see the possibility of using these composites in high humid applications.
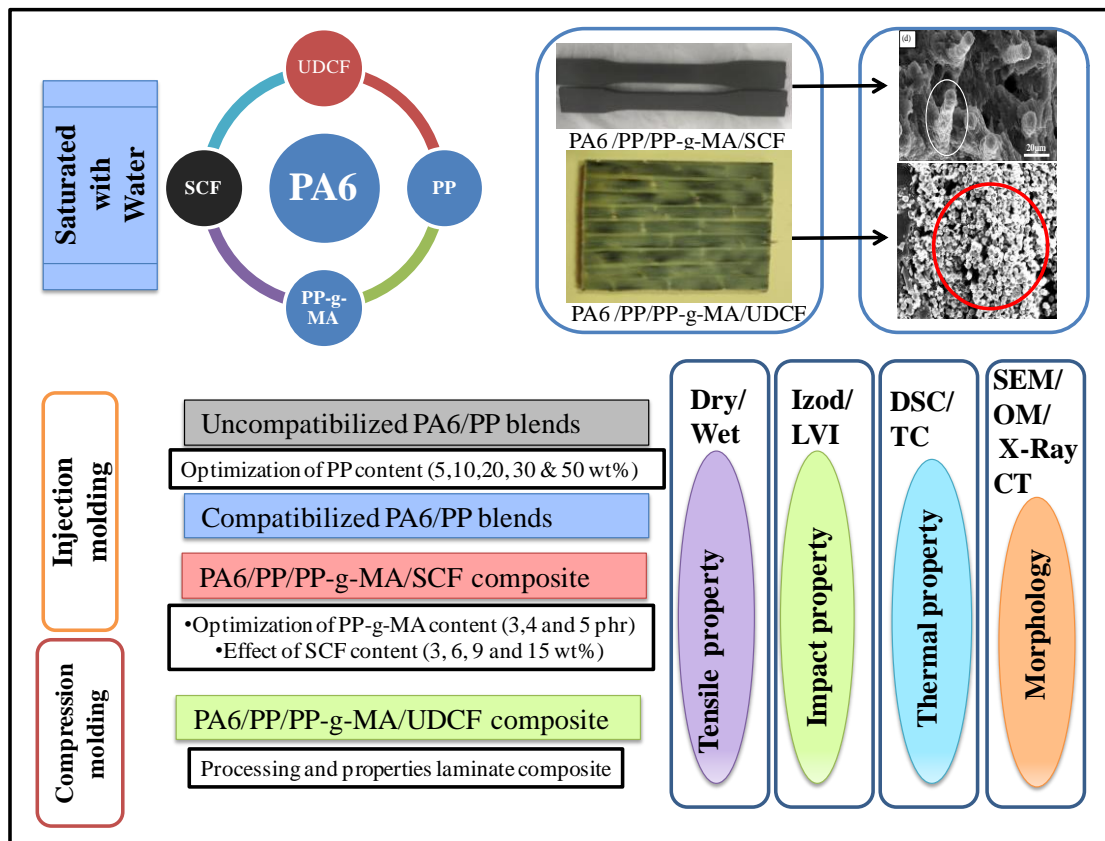
Figure 1.14: Graphical abstract of the thesis

Injection molded specimen were subjected to tensile testing according to ASTM D638 and compression molded specimen were subjected to tensile testing using ASTM D3039. Impact test of all injection molded specimens were done using notched izod test whereas the compression molded specimen (UDCF mat based laminates) was

tested using low velocity impact test technique. Thermal properties of the blends and composites were studied using DSC and thermal conductivity. Morphology of the blends and composites was studied using optical microscopy, SEM and X-Ray CT. Other than these studies, FTIR was used to understand the reaction mechanism occurring in the blend and composite. Residual fibre length of composites was determined to understand the fibre length distribution in the injection molded composite specimens.

As a part of the thesis work, the above mentioned objectives were executed experimentally and the findings were reported and published as papers.

1. Review on various compatibilizers and its effect on mechanical properties of compatibilized nylon blends, Polymer Plastic Technology and Engineering.
2. Influence of PP content on mechanical properties, water absorption, and morphology in PA6/PP blend, Journal of Applied Polymer Science.
3. Effect of Compatibilizer on the Properties of Polyamide 6 Blend Based Carbon Fibre Reinforced Composites, Fibres and Polymers.
4. Effect of carbon fibres and water absorption on mechanical properties and morphology of PA6/PP blend based composites, Polymer Composite.
5. Surface Modified Carbon Fibre Reinforced PA6 and its Blend-Based Composites, Advances in Interdisciplinary Engineering, Lecture Notes in Mechanical Engineering.

1.12. Structure of thesis

Chapter 2: In this chapter, mechanical, thermal and morphological properties of PA6/PP blends and PA6/PP/PP-g-MA blends with increasing PP content have been discussed. Wherein, the optimized PP content for PA6/PP blends would be found out by comparing the tensile properties of the blend before and after water absorption. DSC thermograms and PP size distribution in the blends were studied for both uncompatibilized and compatibilized blends. Impact strength along with fractography is discussed to understand the failure mechanism in the blends.

Chapter 3: This chapter has two parts. First part is optimization of PP-g-MA content for PA6/PP/SCF composite and second part is studying the effect of SCF content on properties of composite. Initially, the compatibilizer content was varied and the optimization was done experimentally and statistically (Grey relational analysis). Tensile properties before and after water absorption, impact strength and residual fibre length were studied. In the second part, with increase in SCF content, tensile properties before and after water absorption along with fractography, impact strength with fractography, PP size distribution and residual fibre length was studied.

Chapter 4: In this chapter, the processing of the PA6 blend based matrix/UDCF laminate using modified compression molding machine is discussed. Here, the bottlenecks faced and the solutions derived along with optimized parameters for making of PA6 blend sheet and PA6 blend/UDCF laminate composites has been elaborated. Further, tensile test, compression test, short beam shear test and low velocity impact test of the samples has been discussed. Water absorption of the samples was carried out and tensile test post water absorption was also studied.

Chapter 5: In this chapter, the overall tensile, impact, thermal and water absorption properties of PA6, PA6/PP/PP-g-MA (matrix), PA6 blend/SCF composite and PA6 blend/ UDCF laminate composite has been compared.

CHAPTER 2

Study on PA6/PP and PA6/PP/PP-g-MA blends: Optimization of PP content

2.0. Introduction

PA6/PP (uncompatibilized blends-UB) and PA6/PP/PP-g-MA (compatibilized blends-CB) blends were studied with an aim of optimizing the PP content in the blend. The effect of addition of compatibilizer as well as the PP content was studied. For uncompatibilized blends PP content was varied from 5 wt% to 50 wt% and comparison was made with the properties of PA6. Compatibilized blends were made with 4phr of PP-g-MA (fixed) and PP content was varied from 5 wt% to 50 wt% and compared with the properties of PA6 and PA6/PP blends. The properties of the blends were studied by measuring tensile strength and impact strength (Izod notched). Fractography of blends was studied post impact fracture to understand the nature of failure. Morphology of cryogenically broken samples was studied to understand the size distribution and dispersion of PP in PA6 phase in both uncompatibilized and compatibilized blend, as it is important to decide the optimum PP content and optimum domain size to obtain balance of stiffness and toughness in the resulting PA6/PP blend. Since the crystallization parameters affects the mechanical properties, thermal behavior of blends was studied using three-cycle DSC to understand the effect of crystallization on yield strength and impact strength. The effect of water absorption was studied by calculating the mass difference due to water absorption and by conducting tensile test of blends post water absorption.

2.1. Materials and methods
2.1.1. Compounding and Injection molding

PA6, PP and PP-g-MA were mixed manually and added to hopper directly. PA6 content was varied from 100 to 50 wt% while the PP content was varied from 0 to 50 wt%. PP-g-MA was added as 40 g per kg of PA6+PP mixture (4 Phr). Generally, in most of PA6 blend and blend based composites, compatibilizer was varied between 2-5 wt% (*Cheng, 2005*; *Chow, Bakar, 2005*; *Kim, 2003*; *Kitayama, 2001*). In PA6/ABS

(*Arsad, 2010*) and for PA6/HDPE (*Hamid, 2013*) blend it was found that 2 phr/wt% of compatibilizer resulted in better tensile strength. Hence in this study, an intermediate value, 4 phr of PP-g-MA was used. PA6 was preheated for 5 hrs at 80°C in a hot air oven, and then used for extrusion in a co-rotating twin screw extruder (ZE-25 , Berstorff Maschinenbau GmbH, Germany) with a temperature range in seven heater zones varying from 170°C to 235°C (Figure 2.1a, Figure 1.12). The extruded uncompatibilized and compatibilized blends were cooled using water bath, and then pelletized. The pelletized samples were further dried at 90°C for 5 hrs before injection molding. The composition used for this study is mentioned in Table 2.1. Injection molding of preheated extruded samples to tensile and impact specimens was carried out using Electronica Endura-90 (Figure 2.1b, Figure 1.13) at 49°C to 249°C temperature range and pressure of 800 kgf/cm^2. The cycle time for making two samples was 60 seconds. The tensile samples (dog bone) were made according to ASTM D638 and impact samples (cuboid) were made without notch as per ASTM D256.
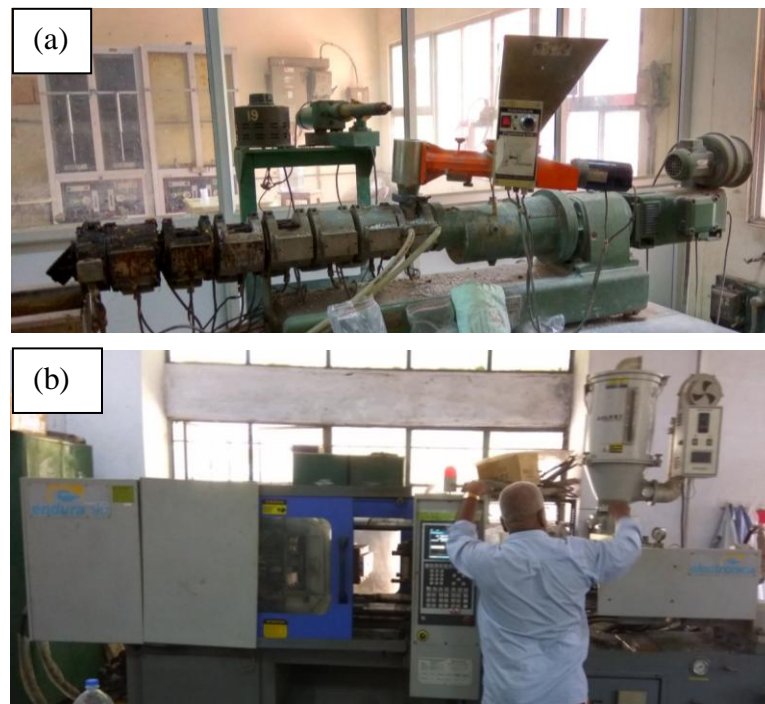
Figure 2.1: a) Twin screw extruder, b) Injection molding machine used to make PA6/PP blends

Table 2.1: Composition of blends				
Blend Type	Name	PA6 (wt%)	PP (wt%)	PP-g-MA (phr)
Nylon 6	PA6	100	0	0
Uncompatibilized blend (UB)	UB1	95	5	0
	UB2	90	10	0
	UB3	80	20	0
	UB4	70	30	0
	UB5	50	50	0
Compatibilized blend (CB)	CB1	95	5	4
	CB2	90	10	4
	CB3	80	20	4
	CB4	70	30	4
	CB5	50	50	4

2.1.2. Water absorption (saturation) test

Water absorption was carried out for tensile specimen according to ASTM D570-98 standard. The tensile specimens of PA6 and PA6 blends were immersed (80 % of the sample was dipped in water) in distilled water at room temperature and weighed every 24 hrs until saturation using electronic weighing balance (Sartorius BSA-423S-CW). Samples were removed from water bath and their weight was measured after surface drying using tissue paper. The level of water was maintained at same level to ensure proper saturation. The weight difference was found and the percentage increase in weight which is proportional to the amount of water absorbed was calculated using eqn. 2.1.

$$\%W = \frac{W_n - W_0}{W_0} \times 100 \qquad \text{(eqn. 2.1)}$$

Where, W_0 is the initial weight of the sample, W_n is the weight of the saturated sample, and $\%W$ gives the percentage increase in weight.

2.1.3. Mechanical properties

The tensile test was carried out using Universal Testing Machine (Micro-control

systems) at a crosshead speed of 5mm/min and a gauge length of 50mm as per ASTM D638 standard. Tensile properties of all dog bone specimens were studied before (dry) and after water absorption (wet). Wet samples were tested after 45 days of water saturation and tested immediately after surface drying. The notched-izod impact test was conducted as per ASTM D256 standard on pendulum type impact tester (CEAST 9050) for all compositions. Flat specimens of 3.2 mm thickness and 64 mm length obtained from injection molding were used for impact test (dry). The notch was made using the motorized notch cutter. The triangular notch dimension was 2.5 mm deep at an angle of 45°. Both tests were carried out at 23-25°C and 50-55 % relative humidity to avoid the influence of relative humidity on mechanical properties.

2.1.4. Differential Scanning Calorimetry (DSC)

Samples from injection molded specimen of constant weight (5mg) were used for DSC (Shimadzu DSC-60) analysis. Three cycles of DSC consisting of heating, cooling and re-heating cycle at 10°C/min scanning rate was conducted in nitrogen atmosphere (100ml/min flow rate). The initial heating cycle is used for removing the thermal histories, cooling cycle is used to study the crystallization behavior (enthalpy) and re-heating cycle gives the melting point of the blends in the temperature range of 25°C to 300°C. The % crystallinity was calculated using the following equation (eqn. 2.2) for PA6. Where, ΔH_m is the melting enthalpy and ΔH_m^0 is the melting enthalpy of 100% crystalline PA6. In this study ΔH_m^0 is 204.8 J/g (*Jogi, 2014*).

$$\% \chi_c = \frac{\Delta H_m}{\Delta H_m^0} \times 100 \qquad \text{(eqn. 2.2)}$$

Glass transition temperature (T_g) of blends were not studied as it is difficult to find the T_g of PP (-110 °C).

2.1.5. Morphological studies using SEM for PP size distribution and fractography

Injection molded specimens of blends were dipped in liquid nitrogen ~-170°C, where the plastics become brittle in nature and can be broken easily. Once the specimen is broken into two halves manually, a part from the fractured end is cut to a size of 5 x 12 x 3.2 mm^3 cuboids. These samples are then boiled in xylene solvent for 48 hrs at

138°C so as to remove the PP and PP-g-MA from the PA6 phase. This led to dissolution/etching of PP and PP-g-MA from PA6. The surface etched samples which have PA6 phase only were sputter coated with gold & palladium mixture and then analyzed using SEM (Thermo Fisher Scientific FEI ApreoS) to understand the dispersion of PP by locating voids created by etched PP. The diameter of etched PP was analyzed using imageJ2 software through measuring the diameter of the voids left behind by the dissolved PP/PP-g-MA phase. Fractography of impact fractured samples were studied by sputter coating the fractured ends with gold & palladium mixture and then analyzed using SEM to understand the fracture mechanism. Fractography of tensile samples were not carried out.

2.2. Tensile properties of PA6/PP and PA6/PP/PP-g-MA blends

From the conducted tensile test in UTM (Figure 2.2a), tensile strength and elongation at break were not calculated, as the PA6/PP blends did not break in wet condition (up to 20 wt% PP content) and PA6/PP/PP-g-MA blend did not break in both dry & wet condition (Figure 2.2b). The machine had an elongation limit of 300 mm. Most of the samples kept elongating and slipped out of the grip instead of breaking due to reduction in thickness during testing. Hence only yield strength is compared. Figure 2.3 depicts the tensile yield strength of PA6/PP (UB) and PA6/PP/PP-g-MA (CB) blends in dry and wet conditions (wet indicates after water saturation).
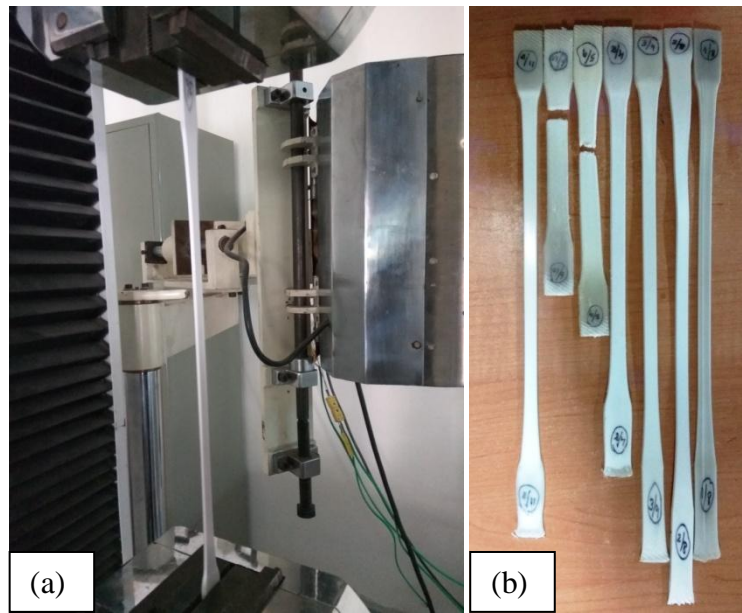
Figure 2.2: Testing of blends in a) UTM set-up, b) representative image of blend samples elongated without fracture (2 out of 7 samples were fractured)

2.2.1. *Effect of PP content on tensile properties of PA6/PP and PA6/PP/PP-g-MA blends*
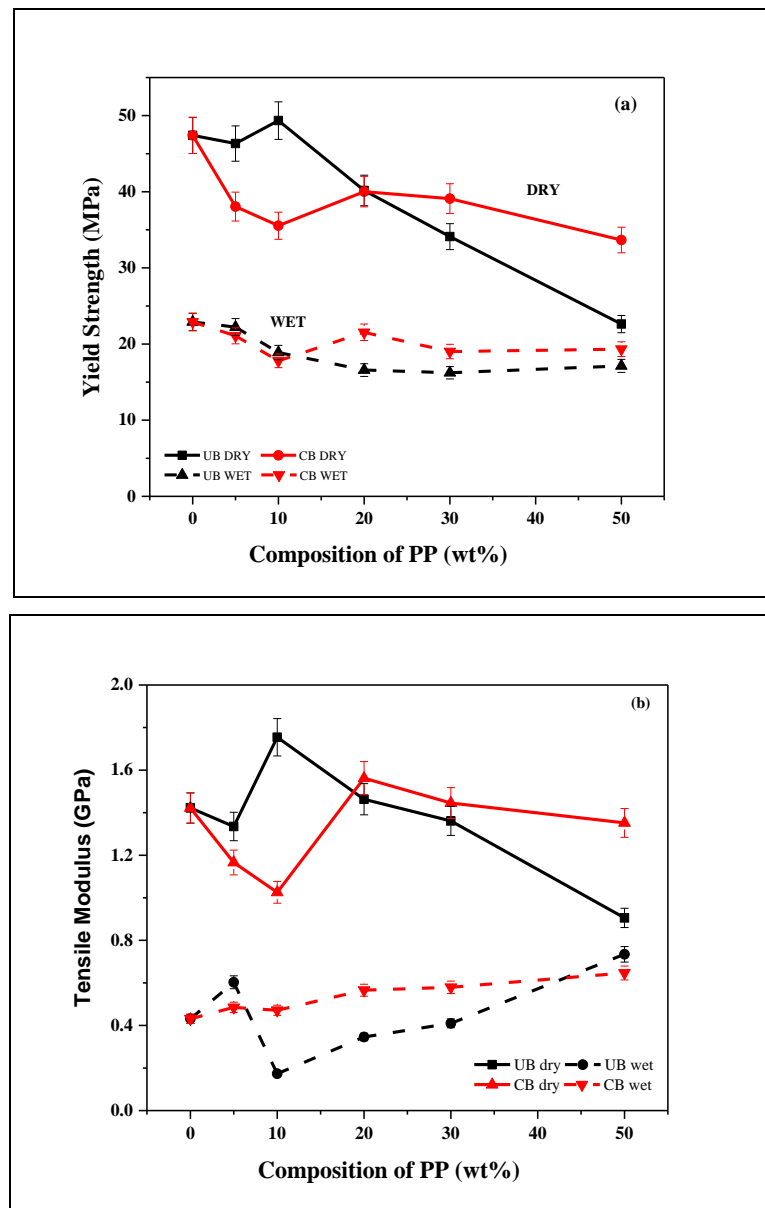
Figure 2.3: Variation of (a) tensile yield strength and (b) tensile modulus with increasing PP content. PA6/PP: UB and PA6/PP/PP-g-MA: CB

The yield strength of dry PA6/PP blends (Figure 2.3a) was equivalent to PA6 up to 10 wt% PP content and then decreases drastically due to lower strength of PP as also observed by others (*Huber, 2014*; *D. Li, 2009*). This might be due to better dispersion of PP at lower PP content (discussed in later section). When 20 wt% PP & 30 wt% PP was added, the yield strength reduced drastically by 15.2% and 28% respectively in

comparison to pure PA6. Hence, the variation of yield strength was lower when PP was increased in smaller weight fractions, but as larger amount of PP was added the yield strength reduces drastically as also observed by Huber et al. (*Huber, 2014*). Further when PP proportion was increased to 50 wt%; it was found that the yield strength reduces by 52.2%. It could be due to that the interfacial adhesion was better at lower PP content (*Huber, 2014*), but as the PP content increases above 10 wt%, the yield strength reduces drastically due to reduced interfacial adhesion.

Tensile modulus showed similar trend to that of the yield strength (Figure 2.3b). It is important to study the tensile modulus as it provides the dynamics of elastic, reversible and linear modes and provides structural information, predominantly intermolecular packing, degree and quality of order, defects and nature of interfaces in a material. For PA6/PP blend, with increase in PP content the tensile modulus increases initially and then decreases. It could be understood that at lower PP content (5 and 10 wt%), the interfacial adhesion between PA6 and PP is higher and as PP content is increased, coalescence of PP occurs, leading to lower tensile modulus. In comparison to PA6, 50 wt% PP + 50 wt % PA6, shows 36.3% reduction in tensile modulus.

For dry PA6/PP/PP-g-MA (compatibilized blend) as seen from Figure 2.3, as PP content increases, the yield strength decreases in comparison to pure PA6. With increase in the PP content, the PP-g-MA to PP ratio reduces, because the amount of PP-g-MA was kept constant (4 phr), while the PP content was varied from 5 to 50 wt%. For 5 wt% PP content yield strength reduces by 19.7% and 25% respectively in comparison to pure PA6 and its dry uncompatibilized counterpart which might be due to the higher PP-g-MA to PP ratio causing plasticization of blend due to compatibilization at this composition of blend, which is also seen by Arsad et al. (*Arsad, 2010*). The morphology of the blends showed very low domain size indicating higher interfacial adhesion (discussed in later section) as also seen by Balamurugan et al.(*Prasath Balamurugan, 2008*) where, they have reported that the poor strength in blends is due to the dispersed phase which elongates individually rather than elongating along with the matrix.

For PA6/PP/PP-g-MA blend from figure 2.3b, with addition of compatibilizer, the tensile modulus decreased for 5 and 10 wt% PP content. This shows that the matrix

has plasticized due to higher PP-g-MA to PP ratio. At lower PP content, the compatibilizer could be present both at the interface and in the matrix. Hence, the compatibilizer and PP being low modulus compounds, deforms the matrix earlier by elongating and sliding between the PA6 layers. As the PP content is increased, the PP-g-MA to PP ratio reduces, and the compatibilizer tends to occupy the interface between PA6 and PP leading to higher tensile modulus. 20 wt% and 30 wt% PP had higher tensile modulus than PA6. Further when 50 wt% PP was added, the tensile modulus dropped only by 4.9% which shows that the compatibilization has occurred at higher PP content too.

Improved interfacial adhesion was found in higher PP content, where, in comparison to pure PA6, 28.9%, 4.9% loss in yield strength, tensile modulus was seen for 50 wt% PP content against 52.2%, 36% reduction in dry uncompatibilized counterpart. Ma et al. (*L. F. Ma, 2012*) observed 30% decrease in tensile strength for PA6/TPV blend of 80/20 wt/wt%, whereas in this study only 28.9% decrease is seen for 50 wt% PP content, which is economically beneficial. Dry compatibilized blend revealed 14%, 6% and 48.7%, 49% increase in yield strength, tensile modulus for 30 wt% and 50 wt% PP respectively compared to uncompatibilized blend, which could be due to the improved interfacial adhesion.

- *Effect of PP content on water absorption and yield strength (wet)*

All blends showed reduced water absorption than pure PA6 as seen from Figure 2.4. For uncompatibilized blends, water absorption decreases with increase in PP content. On addition of 5 wt% PP content, no significant decrease in water absorption was observed, however as PP content increased, water absorption decreased up to 75% for 50 wt% PP content, showing the ability of PP in hindering the water absorption due to its hydrophobic nature.
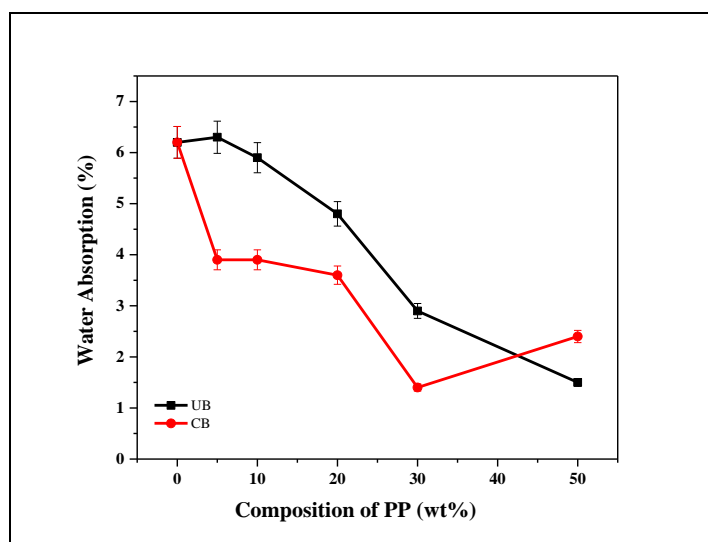
Figure 2.4: Water absorption by blends in absence and presence of compatibilizer (4phr PP-g-MA)

The effect of water absorption on yield strength of uncompatibilized blend can be seen from Figure 2.3a. Yield strength of wet pure PA6 reduced by 51.6% due to plasticization effect of water in comparison to dry PA6. In comparison to wet pure PA6, for uncompatibilized blends, the yield strength decreased with increase in PP content, in spite of decrease in water absorption. In comparison to dry uncompatibilized counterpart, highest reduction in yield strength was found for 10 wt% PP (61.7%) content, due to plasticization of PA6 & heterogeneous dispersion of PP causing capillary effect for increased water absorption in uncompatibilized blend (*Ohlsson, 1998*). For wet uncompatibilized blend, above 10 wt% PP content, there is no further reduction in yield strength value, in spite of increasing PP content and drastic decrease in water absorption.

Tensile modulus decreased drastically for PA6/PP blends post water absorption (Figure 2.3b). All blends except for 5 and 50 wt% PP content gave lower tensile modulus than wet PA6. With water absorption, the amorphous portions of matrix tend to slide easily due to plasticization. With increase in PP content, due to reduced water absorption, there is a 7% increase in tensile modulus at 50 wt% PP content.

For PA6/PP/PP-g-MA blends, that is in presence of compatibilizer as seen from Figure 2.4, the water absorption was constant for 5 wt% to 20 wt% PP content with

3.6% water absorption and drops drastically for 30 wt% PP content to 1.4% and then increases to 2.4 % for 50 wt% PP content. Reduction in water absorption was due to reactive compatibilization of the blend which aids in the formation of PP-g-PA6 (*Bhattacharyya, 2005*; *González-Montiel, 1995b*; *Ohlsson, 1998*) at interface. In comparison to pure PA6, 77.4% reduction in water absorption is found for 30 wt% PP blend. The drop in water absorption can be compared with the % crystallinity results (discussed later) where it was found that 70/30 blend had lowest % crystallinity due to higher reaction between PP-g-MA and PA6 which led to lower water absorption as it reduces the amount of free $-NH_2$ of PA6 which is responsible for water absorption (section 2.4). This leads to better interfacial adhesion and when reaction occurs, the PA6 becomes bonded to PP-g-MA leading to hindrance in crystallinity of PA6. 50 wt% PP content shows slightly higher water absorption which might be due to comparatively poor dispersion of PP and low reaction due to reduced PP-g-MA content. With increase in PP content, more amount of PP-g-MA occupy the interface, due to which more amount of PA6 end groups are anchored with PP leading to reduced water absorption.

Among wet compatibilized blends, higher yield strength was found for 20 and 30 wt% PP content in comparison to 5 and 10 wt% PP content. It was also found that, the yield strength value decreases up to 10 wt% PP content and then reaches a constant value (20 to 50 wt% of PP content). Also, above 10 wt% PP content, the yield strength of wet compatibilized blend was slightly higher than wet uncompatibilized blend counterpart.

Tensile modulus of PA6/PP/PP-g-MA blends was higher than wet PA6. All blends showed higher or equivalent tensile modulus as that of wet PA6. However, the tensile modulus did not vary among the compatibilized blend inspite of decreased water absorption. Similar effect was seen by Vlasveld et al. (*Vlasveld, 2005*) while using hydrophobic silicates for reducing water absorption of PA6. 10wt% to 30wt% blends showed higher tensile modulus than their uncompatibilized counterparts. Here, the effect of compatibilization, and extent of interfacial reaction can be understood. i.e. the effective compatibilization or ratio of PP to PP-g-MA is better between 10 to 30 wt% PP content.

From the wet yield strength and tensile modulus properties of blend it could be

concluded that above 10 wt% PP content the yield strength almost remains constant for both uncompatibilized and compatibilized blends which is good phenomenon as even though the amount of PP which has lower yield strength than PA6 is present in more amount the overall yield strength of the sample was not getting lowered. Tensile modulus of compatibilized blends was higher than wet PA6 and uncompatibilized counterpart between 10 wt% and 30 wt% PP content. Overall it could be found that the role of the compatibilizer becomes more significant post water absorption as it decreases the water absorption by reacting with amine groups and simultaneously retains the yield strength of the blends due to better interfacial adhesion. Considering the blends, even though the yield strength is lower than the PA6, the compatibilization is essential as these blends are to be used as matrix material for carbon fibre reinforced composites. In such case, without compatibilizer, the interfacial adhesion between fibre-matrix will be poor and retention of properties will be poor as discussed in chapter 3.

2.2.2. Theoretical model for yield strength of blends:
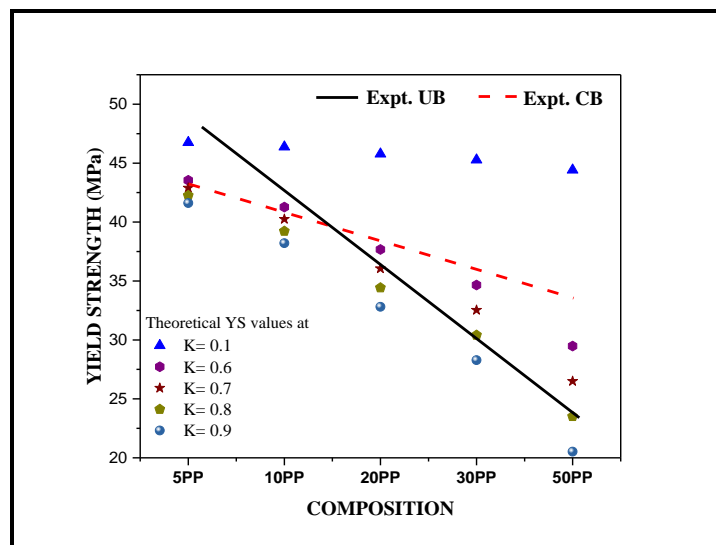
Figure 2.5: Plots representing theoretical yield stress using Nicolais-Narkis model with various K values for PA6/PP and PA6/PP/PP-g-MA blends (dry)

The theoretical yield strength of the blends can be calculated using models and by using the theoretical data, the experimental data can be further explained by the assumptions of the models. In this work, yield strength was calculated using Nicholais-Narkis model (eqn. 2.3) as this model gives the adhesion parameter along

with the yield strength (*Bliznakov, 2000*; *Kumar, 2007*).

$$y_c = y_m(1 - Kv_1^{2/3}) \qquad \text{(eqn. 2.3)}$$

Where, y_c represents yield strength of blend and y_m represents yield strength of matrix (PA6). *K* represents the interface interaction parameter and v_1 represents the volume fraction of the PP. *K* value is zero for pure polymer and maximum value of 1.21 is used for poor interfacial adhesion between the polymers considering all particles are spherical in shape.

In this study, the *K* value was varied from 0.1 to 1.2 to obtain various theoretical yield stresses. Lower the *K* value, higher the interfacial adhesion. In Figure 2.5, the solid line and dashed line represents experimental average yield strength value of uncompatibilized blend and compatibilized blend respectively. For uncompatibilized blend the *K* value increased with increase in the PP content. Initially, *K* value is 0.1 showing high interfacial adhesion and slowly transcends down to *K*=0.7 for 20 wt% PP content and *K*=0.9 for 50 wt% PP content. The increase in *K* value corroborates with the experimental yield strength value. However all *K* values were lower than unity which shows good adhesion between PA6 and PP blend.

In compatibilized blend as observed experimentally, for 5 wt% PP content the *K* value is 0.7, showing the reduced interfacial adhesion. As the PP content is increased the *K* value reaches 0.5 for 50 wt% PP content. This shows the effect of reduction in PP-g-MA to PP ratio and the advantage of using PP-g-MA as compatibilizer. Compatibilized blends had *K* value between 0.7 and 0.5 whereas uncompatibilized blend had varied *K* value from 0.1 to 0.9. Hence it can be considered that at lower PP content, PA6/PP blend interfacial adhesion is better, but at higher PP content, compatibilizer is essential. Also, optimization of PP to compatibilizer ratio is required for improving the yield strength of the compatibilized blend at lower PP content.

2.3. Impact strength of PA6/PP and PA6/PP/PP-g-MA blends:

Impact strength of uncompatibilized blend and compatibilized blend is depicted in Figure 2.6. All blends gave higher impact strength than pure PA6 with exception of 30 wt% uncompatibilized blend due to its higher domain size. In PA6/PP blends, when 5 wt% PP was added, the impact strength increased significantly by 162% and on

further addition of PP the impact strength decreased till 30 wt% PP content and again increased slightly for 50 wt% PP content in comparison to pure PA6. 10 wt% PP content gives 125% increment and 20 wt% PP content gives 107% increment which shows the ability of PP to hinder the crack propagation in PA6. But as the PP content increases, the interfacial adhesion decreases which leads to poor stress transfer causing reduced impact strength.
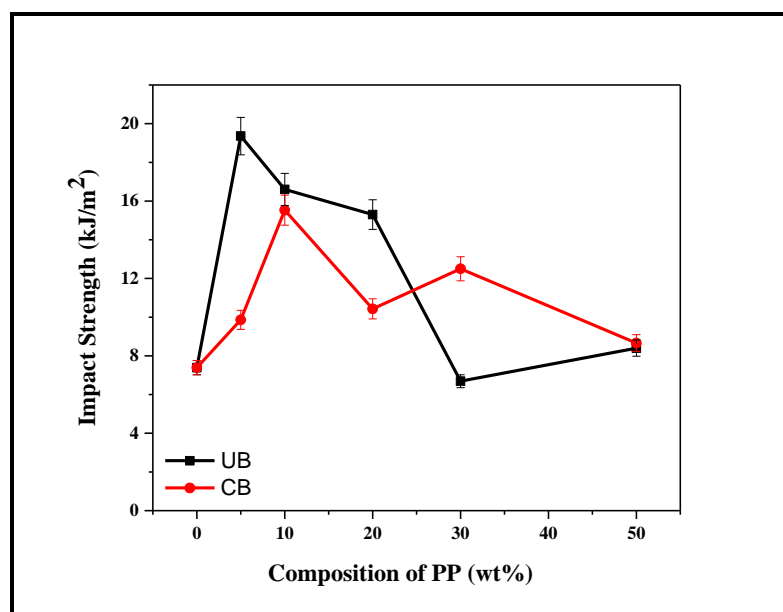
Figure 2.6: Variation of impact strength with increasing PP content for PA6/PP (UB) and PA6/PP/PP-g-MA (CB) blends

For PA6/PP/PP-g-MA (compatibilized blends), with increase in PP content, the impact strength increases eventually and higher value of impact strength was seen for 10 wt% and 30 wt% PP content. With addition of PP, the impact strength increased by 33%, 110% and 41% for 5 wt%, 10 wt% and 20 wt% PP content respectively in comparison to pure PA6. Unlike uncompatibilized blend when 30 wt% PP was added, 69% increase in impact strength was observed in compatibilized blend. In case of compatibilized blend, even though improvement in impact strength was achieved in comparison to pure PA6, the values were lesser than that of the uncompatibilized blends up to 20 wt% PP content. Generally compatibilized blends have higher impact strength than the uncompatibilized blends. However, at higher PP-g-MA to PP ratio, the domain size of dispersed phase becomes too low leading to poor toughening of the blend. When the domain size is smaller, the dispersed phase is not efficient in initiating and terminating the crazes, as the crazing of the matrix leads to higher impact strength. Hence, optimum domain size is required for obtaining tough blend

(*Fowler, 1988*; *Huber, 2014*; *Purnima, 2006*; *Ren, 2008*). In case of 30 wt% PP content, it was observed that compatibilized blends gave 87% increased impact strength in comparison to uncompatibilized blend counterpart.

Comparing the impact strength between the blends, it can be seen that at 50 wt% PP content the impact strength of uncompatibilized and compatibilized blends are almost equivalent. Also, 12 kJ/m^2 obtained for 70/30 weight ratio compatibilized blend is advantageous as it is cost effective and has lower water absorption (1.5 % from Figure 2.4). Moreover, the impact strength of PA6 and PP used in this study was 7.4 kJ/m^2 and 4 kJ/m^2 respectively (*Purnima, 2006*), however in PA6/PP blend, the PP domains act as crack arresters leading to higher impact strength. It is evident that brittle to ductile transition is seen for both uncompatibilized blend (5 wt% PP content) and compatibilized blend (10 wt% PP content) for impact strength studied at room temperature at domain size 3.5 µm and 0.45 µm respectively (discussed later).

Impact strength results were in agreement with the yield strength results before and after compatibilization. At 5 wt% PP content the ratio of PP-g-MA to PP was high which led to reduced impact strength & yield strength due to excess compatibilization. The reduction was visible up to 20 wt% PP content and then increases for 30 & 50 wt% PP content. Comparing yield strength and impact strength, it can be seen that at lower PP content, the uncompatibilized blend had better impact strength and yield strength than compatibilized blend which emphasizes that interfacial adhesion as well as the packing was better even without compatibilizer at lower PP content in this study. At higher PP content i.e. at 30 wt% PP content compatibilized blend had better properties than uncompatibilized blend, where the use of compatibilizer becomes essential. The fracture morphology was studied for further analyzing the factors responsible for higher impact strength in blends.

2.3.1. *Effect of PP content on impact fracture mechanism*

For uncompatibilized blends, with 5 wt% PP content in Figure 2.7a, the PP domains were seen in PA6 pockets, and a brittle fracture with stress whitening was seen. In this system, it can be seen that the PP particles are intact to PA6 phase and elongation of PA6 occurs as seen in Figure 2.7a. Shen et al.(*C. Shen, 2015*) observed that as the crack initiated, the triaxial stress (stress on PP domain in x, y and z-axis) has to pass

through the equator of the dispersed phase leading to cavitation of dispersed phase along with elongation of continuous phase every time the crack propagated through interface. The same phenomenon can also be seen in this system.
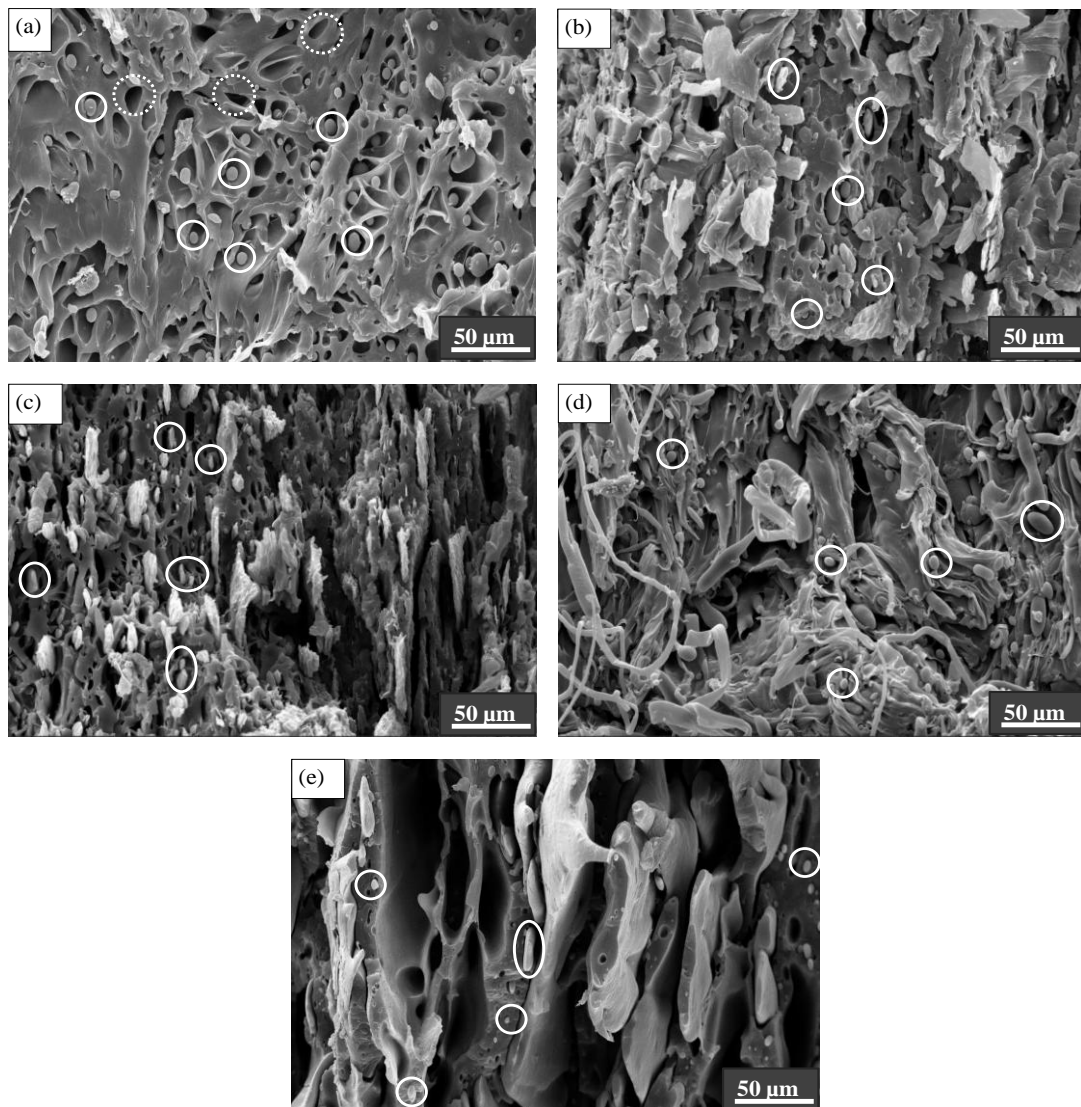
Figure 2.7: Impact fractography of PA6/PP blends (UB) a) UB1- 5 wt% PP, b) UB2- 10 wt% PP, c) UB3- 20 wt% PP, d) UB4- 30 wt% PP and e) UB5- 50 wt% PP. Solid circle: PP phase, Dotted circle: Cavitation due to PP

Since, interfacial adhesion was better, PA6 could elongate more due to better mobility of PA6 molecules. Some voids or PP cavitation is also seen for 5 wt% PP content. For 10 wt% PP content, cavitation of PP was observed along with elongation of PA6 phase (Figure 2.7b). For 20 wt% PP blend in Figure 2.7c, elongated PP domain along with PP cavitation was seen with brittle fracture of PA6 phase. For 30 wt% PP blend in Figure 2.7d, the cavitation of PP along with fibrillation of PA6 was seen. Here the

lack of compatibility is higher owing to higher PP content, leading to easy cavitation of PP phase and fibrillation of PA6(*Mehrabi Mazidi, 2018*). For 50 wt% PP blend Figure 2.7e, the PP phase was coalesced and complete energy was absorbed by cavitation of PP phase and brittle fracture of PA6.
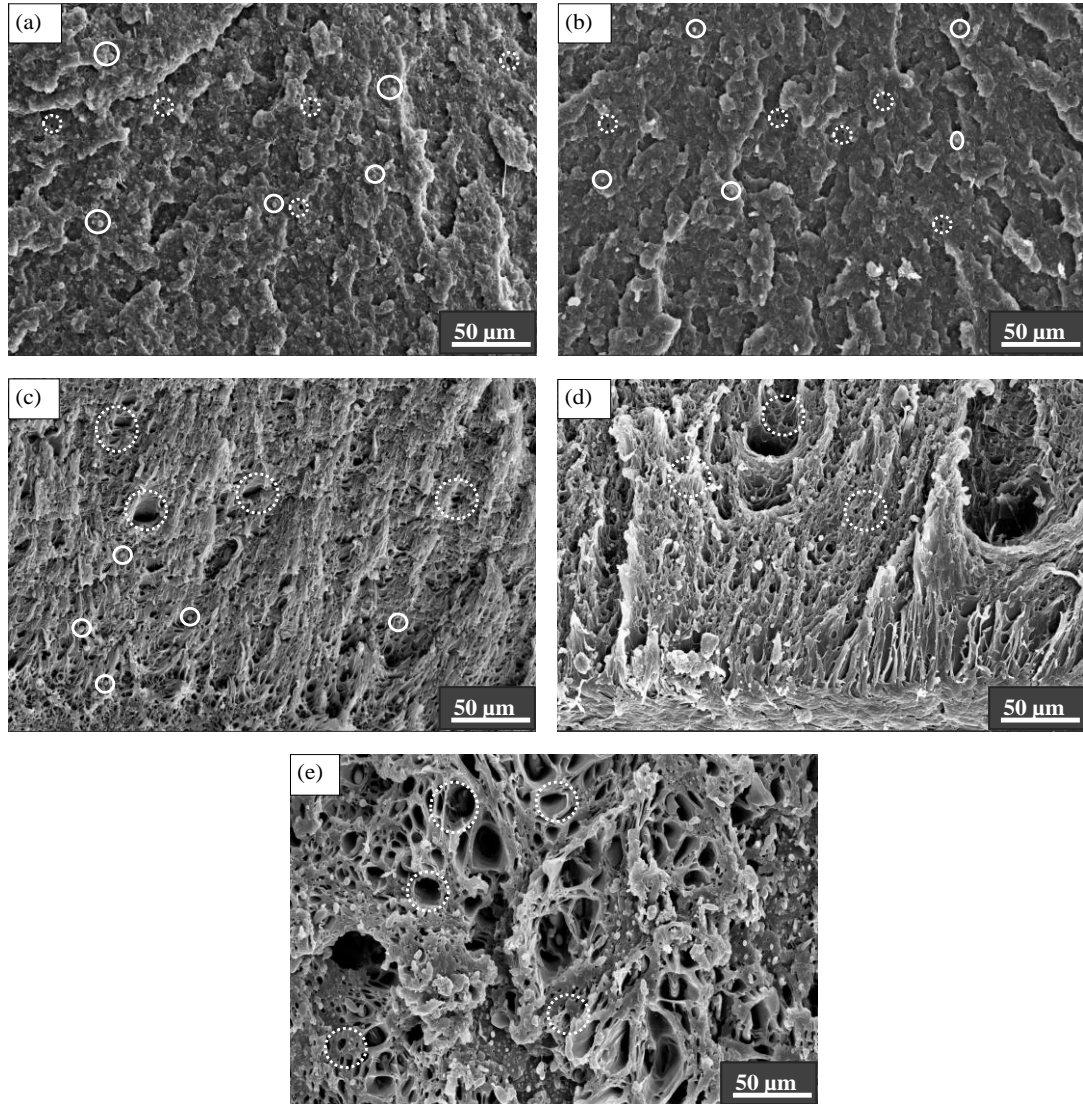
Figure 2.8: Impact fractography of PA6/PP/PP-g-MA (CB) blends a) CB1- 5 wt% PP, b) CB2- 10 wt% PP, c) CB3- 20 wt% PP, d) CB4- 30 wt% PP and e) CB5- 50 wt% PP. Solid circle: PP phase, Dotted circle: Cavitation due to PP

In presence of compatibilizer in Figure 2.8, stress whitening and brittle fracture was seen for all blends. For 5 wt% PP blends in Figure 2.8a, brittle fracture was observed with multiple feather like structure near notch area with low energy absorption to failure as similar to that of PA6, despite the presence of PP and PP-g-MA (*Balamurugan, 2007*; *Ren, 2008*; *Tjong, 1997*). For 10 wt% PP blend in Figure 2.8b,

larger feather like structure was seen, with cavitation of PP which led to higher impact strength. For compatibilized 20 wt% PP blend, Figure 2.8c, shows fibrillation of PA6. Here the elongated PA6 along with PP cavitation was seen. The size of PP was lower hence the energy absorbed is very less. For 30 wt% PP blend in Figure 2.8d, the cavitation of PP was seen with higher fibrillation of PA6 phase, but it is possible that PP also could have fibrillated as this blend showed higher impact strength than uncompatibilized counterpart owing to optimum PP-g-MA to PP ratio. In case of 50 wt% PP in Figure 2.8e, the lower PP-g-MA to PP ratio led to more cavitation of PP phase and brittle fracture of PA6 phase. The 50 wt% compatibilized blend had impact strength comparable to uncompatibilized blend at same composition which could be due to cavities formed in compatibilized blend being more in number and uniformly distributed leading to more distributed energy absorption during fracture leading to comparable impact strength. With respect to impact strength it can be concluded that optimum PP content and PP-g-MA to PP ratio plays a major role in determining the impact strength of the blends. The cumulative effect of cavitation of PP phase along with elongation of PA6 gives better impact strength than fibrillation of PA6 and cavitation of PP alone.

2.4. DSC study of PA6/PP (UB) and PA6/PP/PP-g-MA (CB)blends

Since, the first cycle of heating in DSC is for removal of thermal history, the second and third cycle of DSC are used to explain the crystallization and melting of the PA6 and blends. Figure 2.9 (a, b), 2.10a depicts the cooling cycle of PA6 and blends. The exotherms UB1 to UB5 represent uncompatibilized PA6/PP blend with varying PP content (5, 10, 20, 30 and 50 wt%). Two distinct peaks were visible for PA6/PP blend which proved the immiscibility of the blend. The first peak of exotherms corresponds to crystallization of PA6 at 190°C and the second peak corresponds to PP crystallizing at 115°C. For PA6/PP blends, it can be seen from Figure 2.9a that with increase in the PP content, the intensity of PA6 crystallization peak reduces which relates to the weight fraction of the PA6 (95, 90, 80, 70 and 50 wt%) in the blend.

The T_{peak} value representing crystallization temperature of PA6 in blends decreases with increase in PP content in comparison to pure PA6, but the difference in T_{peak} value was very low. Hence, all blends can be processed in the conditions similar to

that of PA6. The presence of PP in melt state and lack of compatibility may have led to reduced crystallinity of PA6 which would have led to lower yield strength in uncompatibilized blends (Figure 2.10).
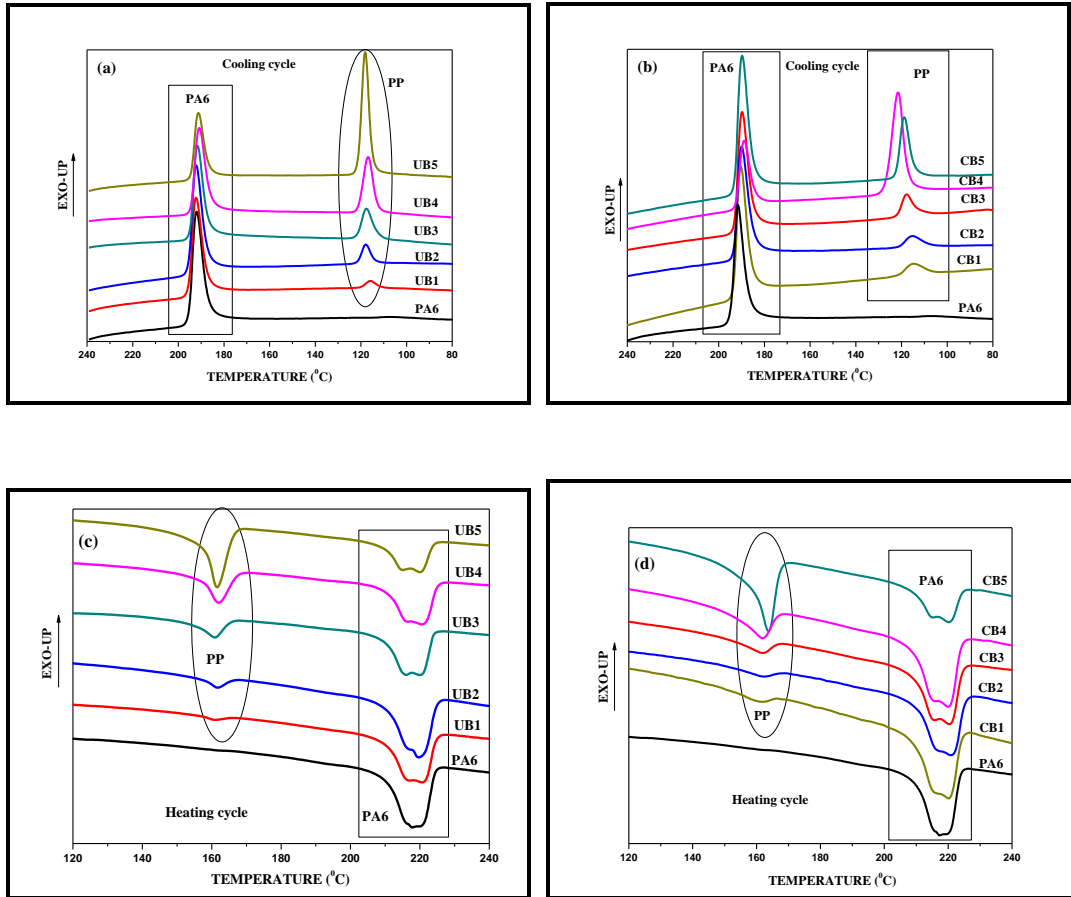
Figure 2.9: DSC thermogram of Cooling cycle of a) PA6 & uncompatibilized blends (UB) b) PA6 & compatibilized blends (CB); heating cycle of c) PA6 & uncompatibilized blends (UB) d) PA6 &compatibilized blends (CB)
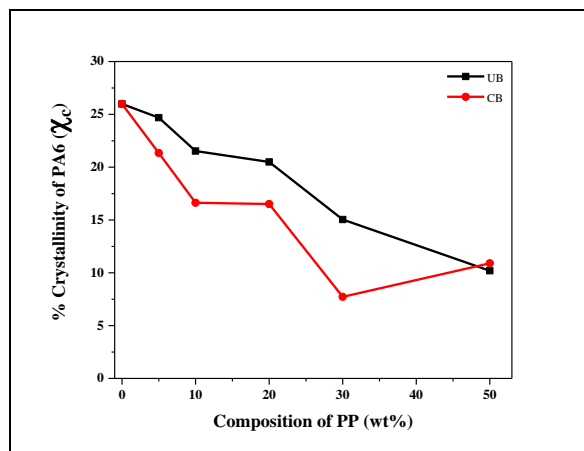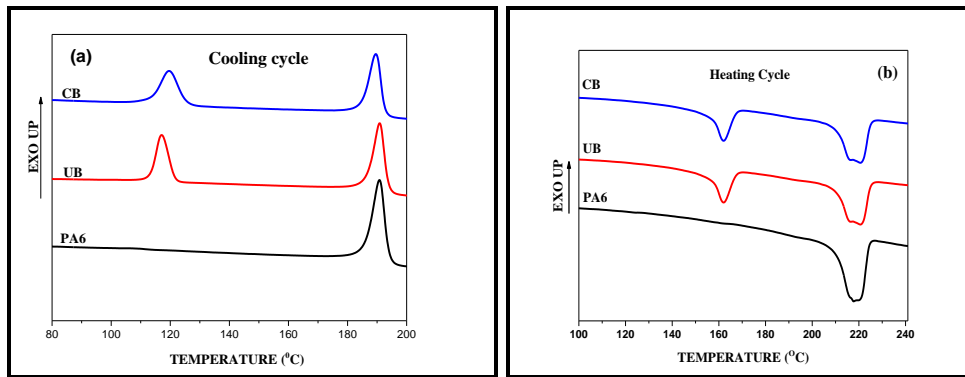
Figure 2.10: Representative DSC thermogram of PA6, PA6/PP (UB) and PA6/PP/PP-g-MA (CB) a) Cooling cycle b) heating cycle and bottom image shows %χ_c of PA6

In the heating cycle (Figure 2.9 (c, d), 2.10b), generally, PA6 shows single endotherm representing the melting of α-PA6 at 220°C (*Augustine, 2012*; *Lai, 2007*). For PA6/PP blends two distinct peaks for PA6 and PP were seen (Figure 2.9c & 2.10b). From Figure 2.10b, it was found that pure PA6 had very slight twin peak at 220°C and 214°C corresponding to α and γ structure of PA6 respectively (*Anstey, 2018*; *Augustine, 2012*; *L. P. Li, 2012*). The intensity of twin peak increases with increase in the PP content (5, 10, 20, 30, 50 wt%). The addition of PP acts as hindrance to crystallization of PA6 leading to development of two phases in PA6. Similar result was also observed by other authors (*Augustine, 2012*; *Lai, 2007*; *Ohlsson, 1998*; *Ren, 2008*). The occurrence of heterogeneous crystallization was affirmed (*Anstey, 2018*) from Figure 2.9c with increasing width and decreasing peak intensity of PA6 melting curve in comparison to pure PA6. α-PA6 is more thermodynamically stable form of

PA6 and as PP content is increased, the intensity of γ-PA6 increases confirming that the PP inclusion supports the growth of γ-PA6. This generally occurs during slower cooling rate or hindered crystallization (*Anstey, 2018*; *Lai, 2007*). As from Figure 2.9c, 2.10b pure PA6 shows α-PA6 more prominently, this proves the occurrence of hindered crystallization leading to development of two phase structure of PA6 in uncompatibilized blends.

Figure 2.9 (b,d) represents CB1 to CB5 compatibilized blends with varying PP content. In presence of compatibilizer (4 phr PP-g-MA), two exotherms are visible in cooling curve for CB1 to CB5 (Figure (2.9b & 2.10a)) which shows that the blends are immiscible. With increase in PP content, PA6 peak intensity was more pronounced in comparison to uncompatibilized blend. When 5 wt% PP was added the T_{peak} value decreases by 2.1°C and on further addition of PP, the T_{peak} reduces by 3.5°C in comparison to T_{peak} of pure PA6. This shift of T_{peak} value of PA6 to lower temperature represents the super cooling which is caused by compatibilization of the blend. Supercooling is the state of polymer in which it exists in liquid phase even after the crystallization temperature. Generally T_{peak} decreases in presence of PP or compatibilizer (*Ohlsson, 1998*). The %χ_c value was lower than that of uncompatibilized blend and decreases up to 30 wt% PP content as seen in Figure 2.10c. It was found that %χ_c of the compatibilized blends was lower than uncompatibilized blends due to lower chain mobility caused by increased interfacial reaction (*L. P. Li, 2012*; *Purnima, 2006*; *Ren, 2008*). Lower the %χ_c value, higher the reaction between PP-g-MA and PA6. Hence in the compatibilized blend 30 wt% PP content has the lowest %χ_c showing the better PP-g-MA to PP ratio. The higher %χ_c value at 50 wt% PP content shows the effect of lower PP-g-MA to PP ratio.

The melting peak width of PA6 increases with increase in PP content as seen in Figure 2.9d. The peak width was slightly broader than uncompatibilized blend due to heterogeneous crystallization in compatibilized blends. In presence of compatibilizer, the intensity of α-PA6 is higher than γ-PA6, which might have led to higher yield strength and impact strength in compatibilized blend at higher PP content (30, 50 wt% Figure 2.3, Figure 2.6).

2.5. PP domain size distribution:

A difference in two phase morphology and degree of dispersion of the second polymer is observed for uncompatibilized and compatibilized blends. The dispersion and the domain size distribution can be correlated with tensile and impact strength of blends(*González-Montiel, 1995b*; *Huber, 2014*; *D. Li, 2009*; *L. F. Ma, 2012*). Balamurugan et al.(*Balamurugan, 2007*) studied PA6/EBA poly(ethylene-co-butyl acrylate) blend and found that the average domain size of dispersed phase decreases with increase in compatibilizer content (EBA-g-MA), which improved the impact strength of the blend. Liang et al.(*Liang, 2000*)stated that there was optimum domain size which gave the toughening effect in PP/rubber based blends and higher domain size led to easier cavitation. Ma et al.(*L. F. Ma, 2012*) found that the impact strength increased with reduction in inter particle distance and Borgrevve et al.(*Borggreve, 1989*) studied the impact strength at various temperatures and found that the brittle to ductile transition is affected by domain size. From the above studies, it can be understood that the study of domain size and dispersion of PP in PA6 blends is important to decide the optimum PP content. The number average domain size (D_n) (eqn. 2.4), weight average domain size (D_w) (eqn. 2.5), interfacial area (A_i) (eqn. 2.6) and particle size distribution (σ) (eqn. 2.7, 2.8) can be calculated from the domain size using the following formula (*Balamurugan, 2007*; *L. F. Ma, 2012*). The D_w is generally compared with the impact strength values, which gives the brittle to ductile transition of blends (*González-Montiel, 1995b*; *L. F. Ma, 2012*).

$$D_n = \frac{\sum n_i D_i}{\sum n_i} ; \qquad \text{(eqn. 2.4)}$$

$$D_w = \frac{\sum n_i D^2_i}{\sum n_i D_i} \qquad \text{(eqn. 2.5)}$$

$$A_i = \frac{6\phi_d}{d} \qquad \text{(eqn. 2.6)}$$

$$\ln \sigma = \sqrt{\frac{\sum_{i=1}^{N} n_i (\ln D_i - \ln D)^2}{\sum_{i=1}^{N} n_i}} ; \quad \ln D = \frac{\sum_{i=1}^{N} n_i \ln D_i}{\sum_{i=1}^{N} n_i} \qquad \text{(eqn. 2.7, 2.8)}$$

Here, D_i represents diameter of PP domain, n_i is number of PP domains, ϕ_d represents weight fraction of PP in blend and d is average domain size of PP.
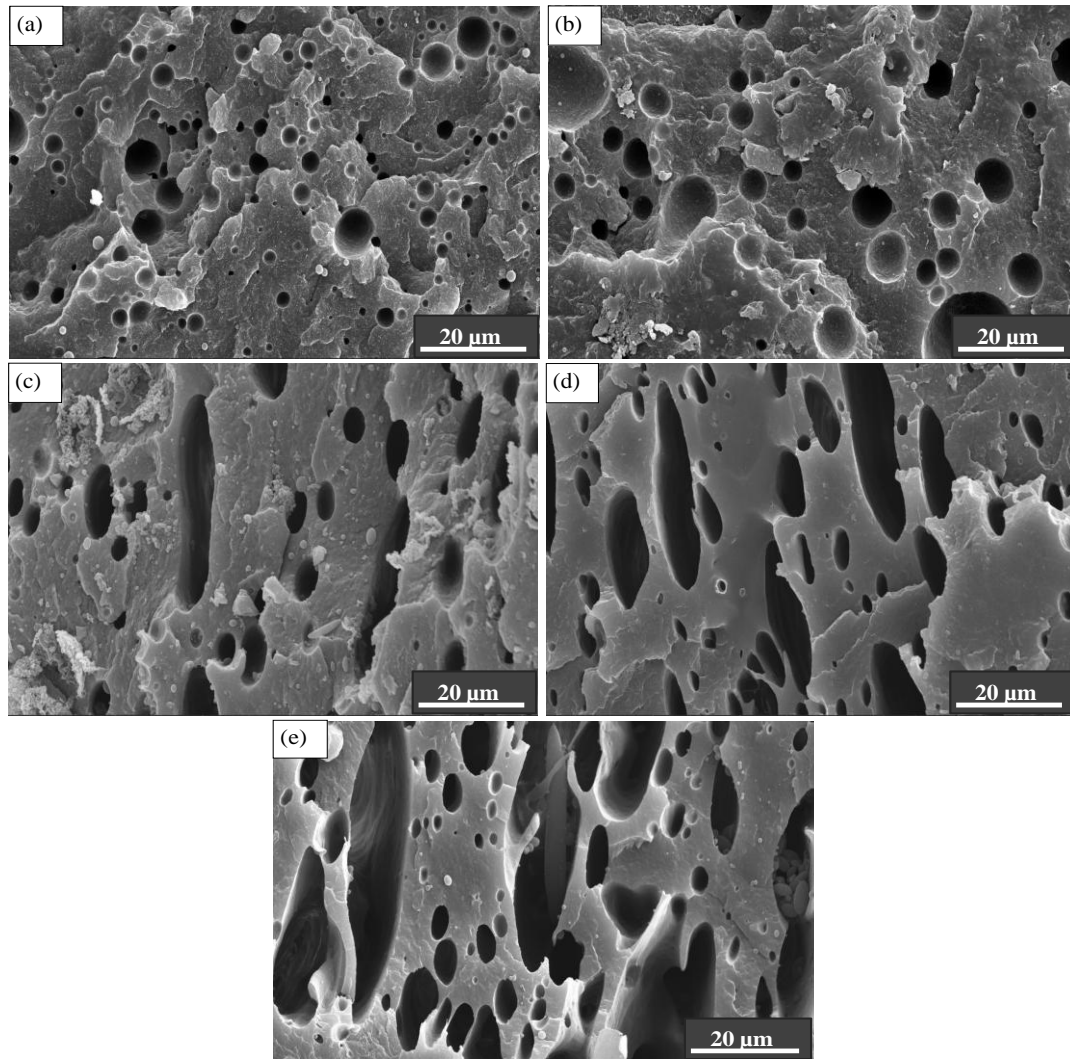
Figure 2.11: SEM micrographs of etched uncompatibilized blend a) UB1- 5 wt% PP, b) UB2- 10 wt% PP, c) UB3- 20 wt% PP, d) UB4- 30 wt% PP and e) UB5- 50 wt% PP

The final domain size is dependent on many parameters including blend composition, melt viscosity & viscosity ratio of two components, interfacial adhesion and processing history (*Tan NC, 2014*). In this work, the blends were processed at temperature suitable for PA6, which is 70°C higher than the melting point of PP. For uncompatibilized blend, during thermo-mechanical shearing, at lower PP content the shear on PP may be more because PP melts earlier than PA6 leading to higher flow of PP which disperses PP in the PA6 phase leading to lower size PP domains. Also, since the volume fraction is lower and PP is immiscible with PA6, the chances of agglomeration of PP become less feasible due to matrix area available for dispersion. As the PP content increases, the interfacial adhesion decreases & agglomeration or coalescence of PP becomes easier in the melt state which would have led to higher

diameter particles of PP in PA6 matrix (Figure 2.11 a-e). SEM micrographs of etched uncompatibilized blend samples are given in Figure 2.11 Diameter of PP (void size in Figure 2.11) increased with increase in PP content. As seen from Figure 2.11a; when 5 wt% PP was added, PP dispersed as spheres with PA6 as continuous phase. As the PP content increased, for 10 wt% PP content, the diameter of PP increased as seen in Figure 2.11b. PP shape was spherical up to 10 wt%, hence domain shape was calculated only for 5 and 10 wt% PP content. With increase in the PP content, 20 to 50 wt% PP blend showed change in morphology to ellipsoidal shape which may be due to coalescence of PP (Figure 2.11c-e).
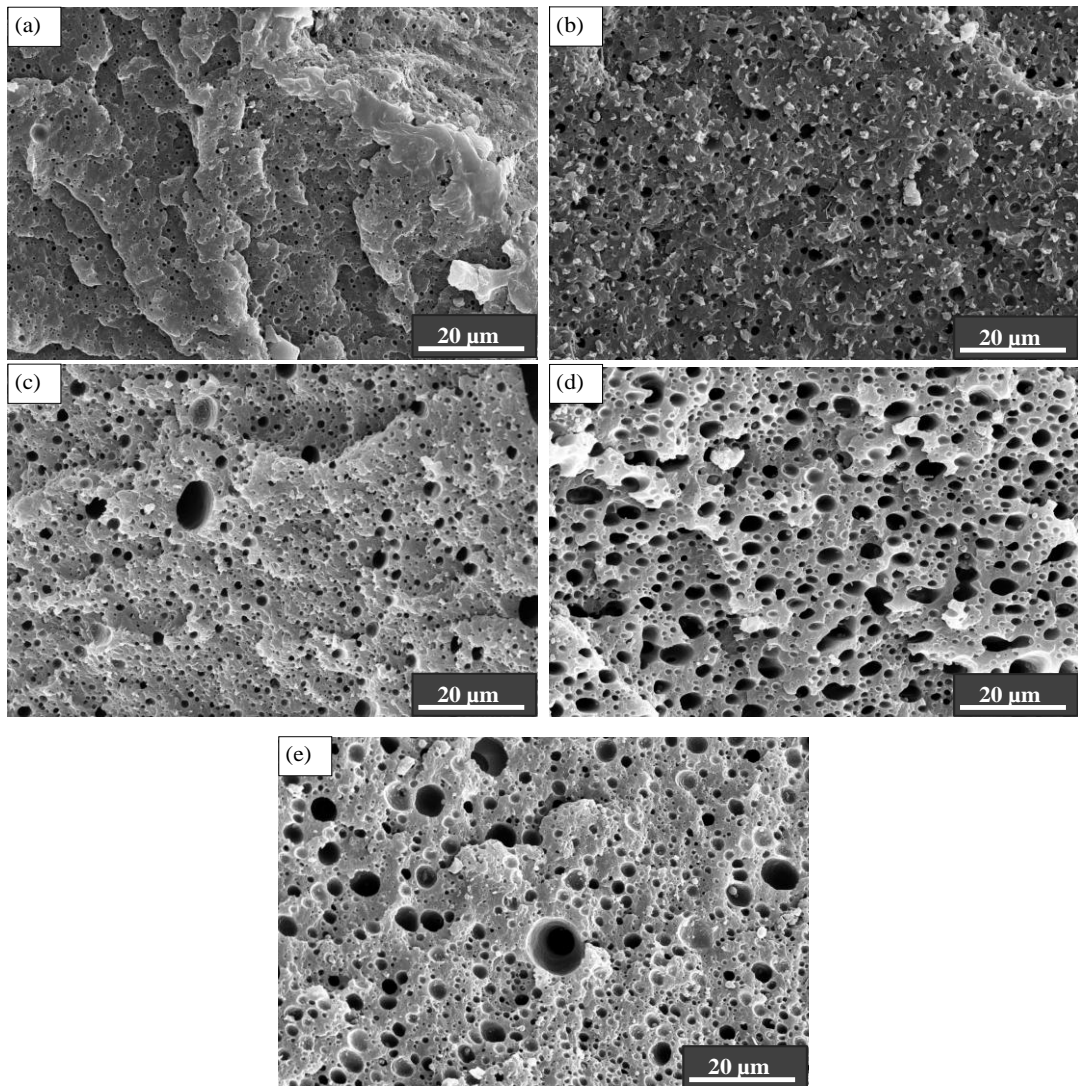
Figure 2.12: SEM micrographs of etched compatibilized blend a) CB1- 5 wt% PP, b) CB2- 10 wt% PP, c) CB3- 20 wt% PP, d) CB4- 30 wt% PP and e) CB5- 50 wt% PP

In compatibilized blend, the PP-g-MA increases the interfacial adhesion by reacting

with the end groups of PA6. Even though shear force in extrusion helps in dispersion of PP, the major contribution is due to improved interfacial adhesion in presence of PP-g-MA as it forms bond with PA6 at PA6-PP interface as mentioned in earlier studies (*Balamurugan, 2007*; *González-Montiel, 1995b*; *L. F. Ma, 2012*). Hence at lower PP content, size of PP is very low & uniform throughout and as PP content increases, the availability of MA decreases proportionately leading to higher PP size. SEM micrographs of etched compatibilized blend samples are given in Figure 2.12 and the corresponding derived data are given in Table 2.2.

For compatibilized blend, a finer PP domain with better dispersion was visible due to the compatibilization. The average size of PP domains drastically reduced to 0.3 µm for 5 wt% PP compatibilized blend in comparison to 3.5 µm for 5 wt% PP uncompatibilized blends. Initially, the PP domains were perfectly spherical in shape and as the PP content increases, distorted spherical domains appear (Figure 2.12a-e). Rather than ellipsoidal shape, PP attains spherical shape after compatibilization even at higher PP content.

Table 2.2: Domain size parameter of compatibilized blend (4 Phr PP-g-MA)					
Composition	**PA6/PP**	D_n **(µm)**	D_w **(µm)**	**Ai ($\mu m^2/\mu m^3$)**	σ
CB1	95/5	0.35	0.59	0.85	1.22
CB2	90/10	0.38	0.69	1.54	1.82
CB3	80/20	0.56	1.08	2.10	2.10
CB4	70/30	0.82	1.55	2.18	2.35
CB5	50/50	0.86	1.79	3.47	2.27

Note: For Uncompatibilized blend, D_n varied from 3.5-18µm

The PP-g-MA led to dispersed PP phase with average domain size lesser than the corresponding uncompatibilized blend. The A_i value increases with increase in PP content and due to highly dispersed PP domain. The σ represents distribution parameter of PP, when σ value is unity, it represents uniformly dispersed blend or monodispersity (*L. F. Ma, 2012*). As seen from the Table 2.2, the σ value increases with PP content. At lower PP content, σ value was 1.22 representing uniform distribution of similar PP domain size and as PP content increased it reaches a value higher than 2 showing dispersion of varied domain size of PP.

2.6.Conclusion:

For optimization of PP content in PA6/PP blends, yield strength, tensile modulus before & after water absorption, impact strength and the variation in morphology was investigated for both PA6/PP and PA6/PP/PP-g-MA blends. These properties were studied with increasing PP content i.e. 5, 10, 20, 30 and 50 wt% but in case of compatibilized blends PP-g-MA quantity was kept constant i.e. 4 phr. For uncompatibilized blends, good yield strength, tensile modulus and impact strength was observed for 5 and 10 wt% PP content. From impact fractography and PP etched morphology of uncompatibilized blends, it was understood that at 5 and 10 wt% PP content, the domain size of PP is smaller and homogeneously distributed in PA6 phase due to lower weight fraction.

From DSC of uncompatibilized blends, it was observed that the crystallization enthalpy of PA6 was higher for 5 & 10 wt% PP content as it did not hinder the crystallization of PA6 owing to lower weight fraction and smaller domain size in PA6 phase. From heating cycle, it was seen that the α-PA6 was present and the γ-PA6 was just being initiated due to the presence of PP, leading to better yield strength. The average domain size of PP in PA6/PP blend was 3.5μm and 4.5μm respectively for 5 wt% and 10wt% PP content. Since the domain size is smaller and uniformly distributed, it leads to better crack arresting during impact test leading to higher impact strength of uncompatibilized blend at lower PP content. In the case of higher PP content (20, 30, and 50 wt%) domain size of PP becomes higher as the PP agglomerates leading to lower impact strength. Hence, for uncompatibilized blend it is recommended to use lower PP content for optimized properties.

Since, the objective of the work was to find the optimum blend composition for high humid application, water absorption and its effect on yield strength was studied for uncompatibilized blends. Post water absorption, the yield strength decreased drastically, and hence the compatibilizer was added and their properties were studied.

 For compatibilized blends, at 30 wt% PP content, the water absorption was only 1.5% and the difference in yield strength between dry and wet blends was lower in comparison to other blends. Impact strength (30wt% PP content) was higher than the other compatibilized counterparts owing to better PP to PP-g-MA ratio and optimum

domain size (0.82 µm) distribution of PP in PA6 phase.

As the PP content increases the difference in yield strength between dry uncompatibilized and wet compatibilized blend samples decreases, which affirms that for high humid applications blends with higher PP content can be preferred due to their yield strength preserving capacity.

Comparing uncompatibilized and compatibilized blends, it is observed that the yield strength of the compatibilized blend is higher at higher PP content along with lower water absorption. From impact fractography, it was understood that the compatibilized blends showed cavitation of PP, whereas PP particles are seen in uncompatibilized blends. The % crystallinity of PA6 in compatibilized blend is lower than the uncompatibilized blend due to the occurrence of reaction at the PA6/PP/PP-g-MA interface. The crystallization temperature of PP is at same temperature for uncompatibilized blends, whereas for compatibilized blends, the crystallization temperature moves towards higher temperature due to compatibilization reaction. For PA6/PP uncompatibilized blends, the PP particles were spherical up to 10 wt% PP content and then became ellipsoidal in shape, but for compatibilized blend the PP domains were spherical for all compositions.

Overall, 70 wt % PA6, 30 wt% PP is immiscible, hence 4 phr compatibilizer was used to make compatibilized blend in order to increase the interfacial adhesion, water absorption reduction and retention of yield strength. Owing to better properties shown by this blend, this could be used as matrix material for making composites assuming that the compatibilizer will improve the fibre-matrix interaction. Hence, in the next chapter PP-g-MA will be optimized for composites with SCF as reinforcement.

CHAPTER 3

Effect of compatibilizer and short carbon fibre contents on PA6 blend based composites

3.0. Introduction
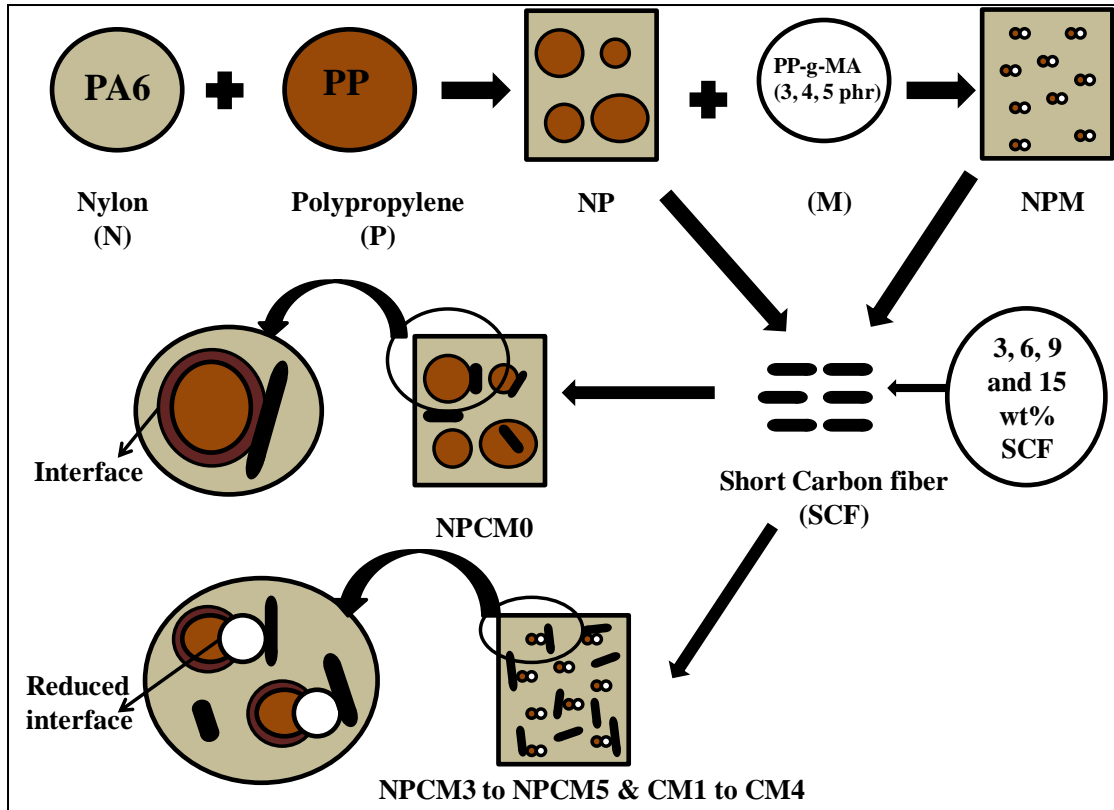
Figure 3.1: Schematic illustration of composites studied by varying PP-g-MA compatibilizer and short carbon fibres (1mm length)

In the previous chapter, the PP content was optimized for PA6/PP blends as 70/30 wt% of PA6/PP. In this chapter, properties of short carbon fibre (SCF) reinforced blend based composite is studied by varying PP-g-MA content and SCF content. Initially, PA6/PP blend reinforced with 5 wt% SCF content was used to optimize the compatibilizer content by varying the compatibilizer from 3-5 phr, as the effect of compatibilizer was to be studied directly for the composites. Later, after optimizing the PP-g-MA content to 3phr, the SCF content was varied from 3-15 wt%, and the effect of SCF content was studied. Processing of composites was done by extrusion followed by injection molding in a similar process to that of blends. Optimization of compatibilizer content was essential, as the property of the composites varies with the

compatibilizer content. When compatibilizer is absent or added in insufficient amounts, the wetting of the SCF will be affected due to the occurring phase difference (Figure 3.1) which in turn affects the fibre-matrix interfacial adhesion. At higher compatibilizer content, plasticization of matrix occurs, leading to matrix with high toughness, and lower strength & stiffness. Hence, it is important to optimize the compatibilizer to obtain composites with balanced stiffness and toughness.

Following this, the SCF content was varied and the effect of SCF content on tensile and impact properties were studied. For both "optimization of compatibilizer" as well as "effect of SCF content", tensile properties before (dry) and after (wet) water absorption were compared among, PA6, matrix blend (PA6/PP/PP-g-MA), and composites. After the composites were made, FTIR was used to understand the interaction between the fibre and the matrix. Impact strength was measured only for dry samples. In this chapter, initially, processing of composites and FTIR of composites for optimization of PP-g-MA content and varying SCF content (both dry and wet state) are explained. In-depth analysis was carried out using experimental and statistical method of "optimization of compatibilizer content" and "study on effect of SCF content" on composites by measuring mechanical properties and by conducting morphological studies in dry and wet states. Finally residual fibre length of fibres in SCF composites was measured and discussed.

3.1. Processing of composite

All materials shown in Figure 3.2 (a)-(d) were preheated for 5 hrs at 80°C in hot air oven, and then extruded in Berstorff Maschinenbau GmbH, Germany (ZE-25) which is a co-rotating twin screw extruder with L/D ratio 48, screw diameter 25 mm and screw speed 100 rpm (Figure 1.12). Temperature of screw gradually increased from zone-1 to zone-7 as 170°C, 180°C, 190°C, 210°C, 220°C, 230°C, and 235°C at the die. The profile (rod) (Figure 3.2e) coming out of the extruder was cooled in a water bath and pelletized (Figure 3.2f). Similar temperature and screw speed were maintained for compounding all compositions i.e. PA6, PA6/PP (blends) and composites. For blend, all the materials were mixed manually and added to hopper directly. For composites, the plastic pellets were added to hopper, and short carbon fibre (SCF with 1% epoxy coating having average length of 1mm and average diameter of 7μm, obtained from Sun Young industry, South Korea) was fed through

side feeder located at middle part of zone-1 at around 170°C. Details of compositions studied for optimization of compatibilizer content are given in Table 3.1 and composites studied for effect of SCF content on composite properties in Table 3.2.
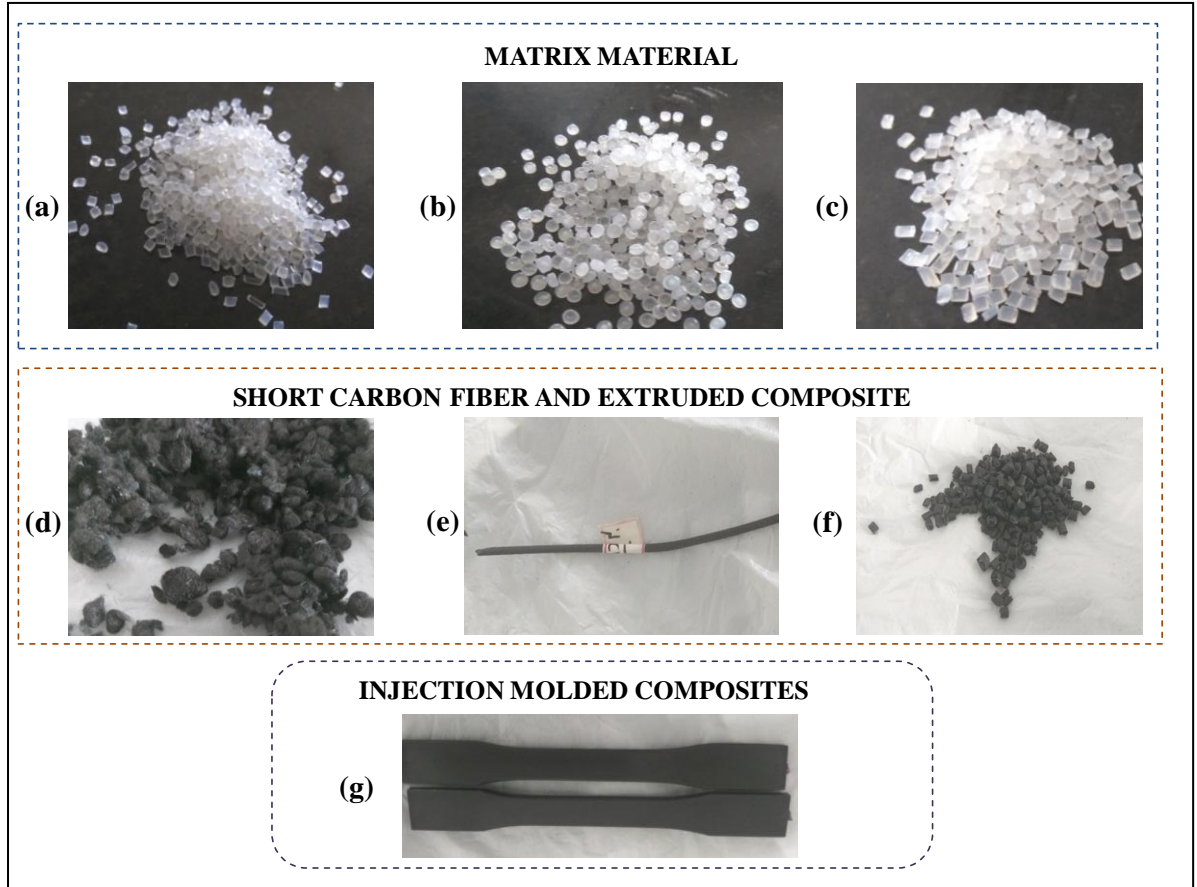
Figure 3.2: (a) PA6 pellets, (b) PP pellets, (c) PP-g-MA pellets, (d) Carbon fibres of 1 mm length, (e) Composite rod obtained from extrusion (f) pellets of composite and (g) Injection molded specimens of composite (NPCM5)

Table 3.1 Composition of blends and composites with varying the compatibilizer content				
Sample name	PA6 (wt %) (N)	PP (wt %) (P)	SCF (wt %) (C)	PP-g-MA (phr) (M)
N	100	-	-	-
NP	70	30	-	-
NPM	70	30	-	4
COMPOSITES				
NPCM0	70	30	5	0
NPCM3	70	30	5	3
NPCM4	70	30	5	4
NPCM5	70	30	5	5

Table 3.2
Composition of blends and composites with varying SCF content

Sample name	PA6 (wt %)	PP (wt %)	SCF (wt %)	PP-g-MA (phr)
PA6	100	-	-	-
CM0	70	30	-	3
COMPOSITES				
CM1	70	30	3	3
CM2	70	30	6	3
CM3	70	30	9	3
CM4	70	30	15	3

3.1.1. *Sample preparation of composites*

The pellets obtained from extrusion process were oven dried for 5 hrs at 90°C to remove the water absorbed during processing and injection molded to make dog bone specimens of 3.2 mm thickness (Figure 3.2g) required for tensile testing. Electronica Endura-90 injection molding machine was used to make all specimens with temperature range of 49°C to 249°C from the compression zone to the nozzle with cycle time of 40 seconds and injection pressure of 800 kg/m^2. At the temperature of 249°C, the matrix is in melt state and it aids in uniform dispersion of SCF in the composite. The high pressure applied to the polymer melt aids in orienting the short fibres partially in the flow direction. Pellets of pure PA6, PA6/PP (blends) and composites were processed similarly to make specimens for tensile test and impact test.

3.2. Estimation of Maleic Anhydride (MA) content in PP-g-MA

Initially, to understand the amount of MA in PP-g-MA pellets, titration method was used, as stated by Oromiehie et al. (*Oromiehie 2014*). 0.5 g of *PP-g-MA* was dissolved in 50 ml of xylene at 80°C, and 1 ml of water was added in order to hydrolyze the maleic anhydride to maleic acid, which was then titrated against alcoholic KOH (0.1 N). Bromo thymol blue was used as indicator. The end point was change of color from yellow to sky blue. The grafting percentage was calculated from the acid number value generated from the titration as given in equation (eqn. 3.1) and (eqn. 3.2).

$$G = (A.N \times M_m)/(2 \times 561) \qquad \text{(eqn. 3.1)}$$

$$A.N = (mlKOH \times N \times 56.1)/gr.polymer \qquad \text{(eqn. 3.2)}$$

Where, G is the MA grafting percentage, $A.N$ is the acid number, M_m is the molecular weight of the monomer to which MA is grafted and $mlKOH$ is the alcoholic KOH consumed for neutralizing the maleic acid present in 0.5 gram of PP-g-MA and N is the normality of the alcoholic KOH. Grafted MA content was determined to be 1.375% for PP-g-MA used in this study.

3.3. FTIR studies of blends and composites made with varying compatibilizer (PP-g-MA) content

For FTIR analysis, thin slices were peeled from both sides of injection molded specimens using blade which was then fragmented into small particles suitable for FTIR analysis using scissor. The small particles or powdered samples were mixed with potassium bromide to form pellets required for the FTIR analysis. The blends and composites were tested and analyzed using Jasco-FTIR4200 equipment.
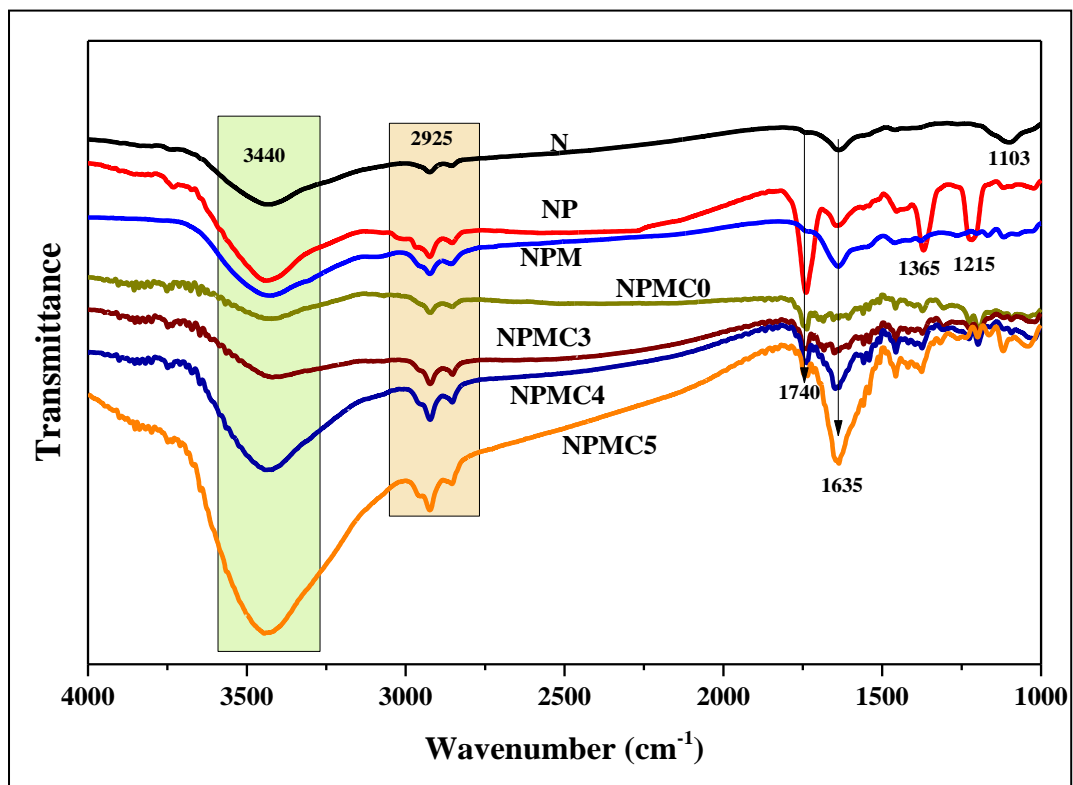
Figure 3.3: FTIR of N-PA6, NP-PA6/PP blend, NPM-PA6/PP/PP-g-MA blend,

FTIR results of pure PA6 gave the characteristic peaks which include -NH- stretch at 3440 cm^{-1}, -CH$_2$- stretch at 2925 cm^{-1}, overlapping C=O stretch of amide and N-H bend of secondary amide at 1635 cm^{-1} and C-OH stretch at 1103 cm^{-1} as shown in Figure 3.3 (*Anstey, 2018*; *Arsad, 2010*). On addition of PP, the intensity of -CH$_2$- stretch increased, and characteristic peaks of PP was seen at 1365 cm^{-1} and 1215 cm^{-1} representing the -CH$_3$- peak and -CH$_2$- twist respectively for the PA6/PP blend(*Prasath Balamurugan, 2008*). The peak intensity at 1635 cm^{-1} of PA6 shifted to 1740 cm^{-1} for PA6/PP blend which could be due to the resonance between PA6 and PP molecules(*Arsad, 2010*).

Introduction of PP-g-MA led to absence of peak at 1740 cm^{-1} and presence of broad single peak close to 1635 cm^{-1} denoting the reaction taking place between the PA6 and PP-g-MA in NPM blend. The reaction between PA6 and PP-g-MA occurs between C-O-C of MA and -NH$_2$- of PA6 to form C-N-C bond as reported (*Bliznakov, 2000*) in patent, where they have given the synthetic route of reaction between PA6 and PP-g-MA. The reaction occurring between PA6/PP blend and PP-g-MA has been illustrated in Figure 3.4.
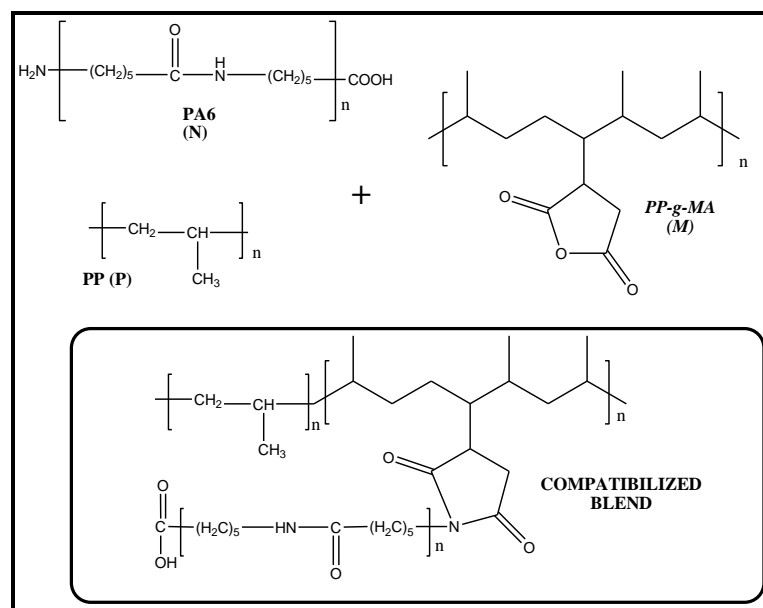
Figure 3.4: Reactive Compatibilization of PA6/PP/PP-g-MA blends

When SCF was compounded along with PA6/PP blend, smaller peaks at 1740 cm^{-1}, 1365 cm^{-1} and 1215 cm^{-1} was observed in comparison to PA6/PP system as shown in Figure 3.3. This reduction in peak intensity could be due to the reaction between "epoxy on SCF" and PA6. When SCF was compounded along with PA6/PP/PP-g-MA blend, with increase in PP-g-MA content (NPCM3 to NPCM5), the intensity of -NH- peak at 3440 cm^{-1} increased, indicating the possibility of reaction between PA6 and PP-g-MA, because of which there could be an increased adhesion between SCF and PA6/PP/PP-g-MA matrix (*Feng, 2013*).

Similar increase in peak intensity at 1635 cm^{-1} was observed with increase in PP-g-MA content, indicating the increased number of C=O groups from MA in the composite. Overall because of high reactivity of MA and end groups of PA6, it could be assumed that PA6 is forming bonds with both MA and SCF which could have led to compatibilization of blend and good adhesion between fibre and matrix respectively. Adhesion between fibre-matrix is important in composites, because it leads to higher stress transfer from matrix to the fibre indicating better mechanical properties (*Adusumalli, 2012*).

3.4. FTIR studies of blend and composites (dry and wet) made with variable SCF content
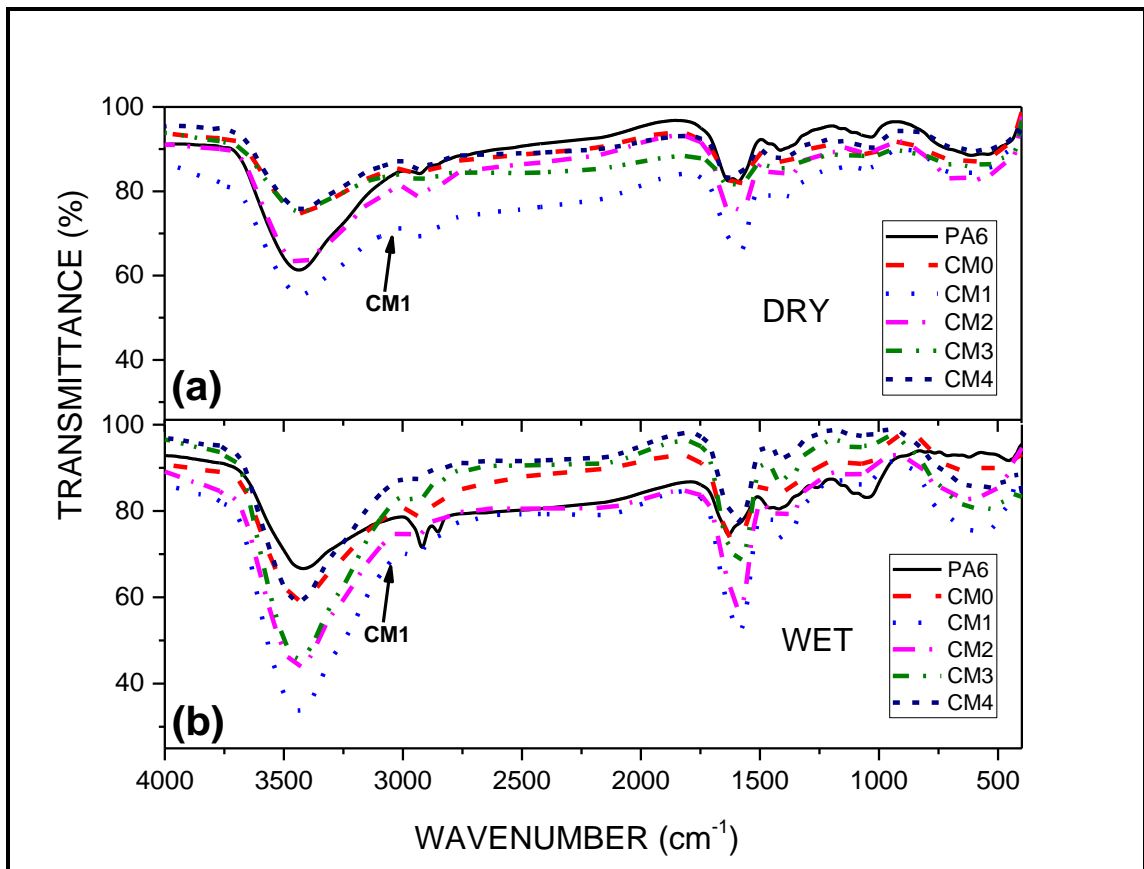
Figure 3.5: FTIR of PA6, CM0 (blend) & composites CM1 (3 wt% SCF), CM2 (6 wt% SCF), CM3 (9 wt% SCF) and CM4 (15 wt% SCF) in (a) dry & (b) wet state

FTIR of both dry and wet PA6, CM0 and the composites with varying SCF content are shown in Figure 3.5. FTIR was done to understand the reaction occurring between the matrix and fibre, before and after water absorption. Considering the raw materials used in making composites, PA6, PP, PP-g-MA and "epoxy on SCF", it is understood that reactions can take place between "PA6 and PP-g-MA", "PA6 and epoxy on SCF" and "PP-g-MA and epoxy on SCF". Hence, FTIR was done to understand the reaction combination occurring in the composite, resultant interfacial adhesion and plasticization (if any) before and after water absorption.
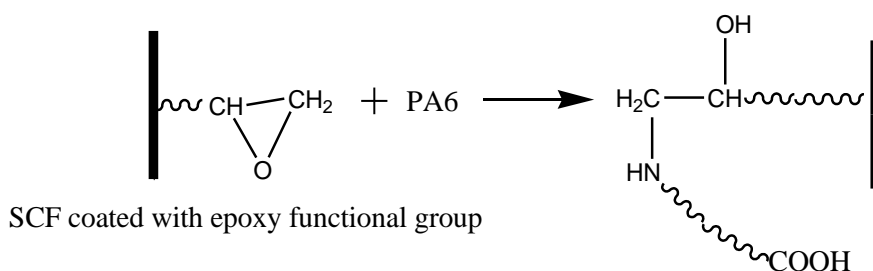
Figure 3.6: Schematic representation of reaction occurring in the composite Showing reaction between PA6 and epoxy on SCF adapted from (*Feng, 2013*)

As seen in Figure 3.5a, which shows the FTIR of dry samples, PA6 showed a broad peak between 3000-3600 cm^{-1} corresponding to –NH- amide stretch and carboxyl –OH- stretch; and a twin peak at 1630 cm^{-1} and 1589 cm^{-1} corresponding to C=O of amide and –NH- of amine group respectively as also seen in section 3.4. Considering the blend CM0, it is seen that PA6 reacts with PP-g-MA through the free amine and forms bond with maleic anhydride. Since the reaction yields a complex structure, the end groups become lesser and lower intensity wavelet is observed at 3000-3600 cm^{-1} as well as at 1630 cm^{-1} for CM0 as discussed in section 3.4. For dry composite samples, in comparison to pure PA6, the –OH- peak broadens for the composite CM1-CM2 at 3300-3500 cm^{-1}, which indicates the increase in the –OH- groups. For CM1, sharp peaks can be observed at 1630 cm^{-1}, which corresponds to C=O peak of carboxylic acid.

Considering the reaction (Figure 3.6) discussed by Feng et al. (*Feng, 2013*), the reaction between PA6 and epoxy yields more –OH- and –NH- as the "–H-" in the amine group reacts with cyclic "–O-" in epoxy leading to ring opening of epoxy with more –OH- groups. Hence the bonding between PA6/SCF could be better in CM1. For CM2, as the peaks are similar to that of PA6 with increased twin peak intensity at 1630 cm^{-1} and 1589 cm^{-1} denoting the reaction occurring at PA6/SCF interface. However, as the SCF content increases, for composites CM3-CM4, the resultant wavelet is similar to that of CM0. Here the peak intensity at 3400 cm^{-1} is reduced due to lower amount of –OH- group and twin peak intensity is also reduced, showing lesser amount of free amine at 1590 cm^{-1}and lesser C=O group at 1630 cm^{-1} which may be due to the PA6/PP/PP-g-MA compatibilization reaction. Li et al.(*Minggang Li, 2014*) has elaborated the reaction occurring between PP-g-MA and epoxy which resulted in more of –OH- groups of carboxylic acid and ester groups which would

appear at 1740 cm^{-1}. But such peak was not seen in our study, and to affirm the type of reaction occurring in the composite, PP was etched out selectively from the matrix blend and composites, and morphology was studied using SEM as explained in chapter 3.7.5.

Considering the FTIR of wet samples from Figure 3.5b, it was observed that the amount of, -NH- and –OH- of carboxylic acid peak intensity increases at 3400 cm^{-1} in comparison to the dry counterparts. For comparison, CM1 dry and wet are highlighted with arrows in Figure 3.5. This shows the interaction of water along the interface between the fibre/matrix and PA6/PP forming more –OH- bonds which could decrease the interfacial adhesion. As mentioned in the earlier chapter, water reacts with free –NH$_2$- as well the amorphous regions containing amide linkage leading to attachment of –OH- and –H- groups of water with C=O and –NH- of amide linkage respectively. Hence the peak intensity at 1630 cm^{-1} as well as 1415 cm^{-1} was more in comparison to the dry samples. This might lead to plasticization of the matrix. To further understand the effect of water absorption tensile test was carried out in both dry and wet states.

3.5. Optimization of compatibilizer content using experimental and statistical analysis

The effect of compatibilizer on PA6/PP (70/30 wt/wt) blend based composites was studied in detail. The compatibilizer (PP-g-MA) content is varied as 3, 4 and 5 phr and properties of PA6/PP/PP-g-MA/SCF have been studied in comparison with pure PA6, PA6/PP and PA6/PP/PP-g-MA. Here the SCF content was fixed as 5 wt % as the aim of the work was to optimize the compatibilizer content and it is easy to disperse the fibres uniformly in a matrix via extrusion and injection molding at lower fibre content. The other reason is that with increase in fibre content, the residual fibre length decreases i.e. losing the effect of reinforcement(*Zhang, 2015*). In this study SCF of 1 mm length and diameter of 7 µm is used. PA6, its blends and composite were prepared by first mixing in a twin-screw extruder and then injection molding in order to make homogeneous and isotropic composites (due to lower amount of SCF) which could maintain its strength even at higher humidity condition. So, the effect of compatibilizer content on tensile properties of composites was studied before water absorption (dry) and after water absorption (wet) or water saturation. Impact studies were restricted to dry samples only. Morphology of the tensile fractured specimen was

also studied using SEM to correlate it with the tensile properties. Statistical analysis was carried out using Grey relational analysis (GRA) to find the optimum compatibilizer content.

3.5.1. Water absorption studies of blends and composites

Water absorption test showed reduction in water intake in presence of compatibilizer and SCF as shown in Table 3.3. The significant reduction in water absorption in NP (PA6/PP) is due to the hydrophobic nature of PP, and further 16.4% decrease in water absorption in NPM is due to the compatibilizer, as compatibilizer reacts with PA6 and reduces the free $-NH_2-$ groups as mentioned in FTIR analysis. Water absorption of PA6 blend has been studied previously by Li et al (*H. Li, 2017*) and Do et al. (*Do, 2016*), where the reduction in water absorption due to PBT (Polybutylene terephthalate) and PP has been reported respectively. Water absorption in PA6 is due to the free amine and the amorphous parts of PA6, where the -OH- group of water forms bond with $-NH_2-$ group, leading to plasticization of PA6 chain. The reduced water absorption in NPCM0 might be due to the water resistant nature of SCF and PP. With addition of PP-g-MA, the water absorption capacity is reduced by 60% for both NPCM3 and NPCM4 compared to N (PA6). Incorporation of 5 phr PP-g-MA to composite led to 64% reduction in water absorption showing the combined effect of PP, SCF and PP-g-MA (and reactivity of PP-g-MA and SCF).

Table 3.3 Influence of water absorption on weight and tensile properties (compared to dry samples)				
Sample	% Increase in weight	% Reduction in Tensile Strength	% Increase in Elongation	% Reduction in Tensile Modulus
N	6.2	37.1	11	71.9
NP	2.9	53	519.7	72.7
NPM	2.5	44.7	160	52.6
NPCM0	2.2	22.3	23.7	47.7
NPCM3	2.4	10.7	56.1	30.9
NPCM4	2.4	18.8	53.6	37.7
NPCM5	2.2	20.7	51	30.5

3.5.2. Tensile properties of composites with varying compatibilizer content (dry and wet)

The tensile test was carried out using Universal Testing Machine (Micro-control systems) at a crosshead speed of 5mm/min and a gauge length of 50mm as per ASTM D638 standard. Tensile properties of all dog bone specimens were studied before (dry) and after water absorption (wet). Wet samples were tested after 45 days of water saturation and tested immediately after surface drying. During the test, few wet specimens elongated beyond 300%. Tensile strength, modulus and % elongation were obtained from the stress-strain plots.

- **Yield strength**

In design calculations, yield strength is preferred than maximum strength for ductile materials. Considering the yield strength and yield strain values from stress-strain plots (Figure 3.7a), it could be deduced that NPCM3 has 25.8%, 35.8% higher yield strength than N and NPM respectively. So, compatibilized composites have higher yield strength values than blends and uncompatibilized (NPCM0) composites. The lowest yield strength is shown by NP, due to lack of compatibilization between PA6 and PP. Conversely, NP had highest yield strain than other blend and composites, but fractured in brittle manner without any plastic zone indicating the need of compatibilization. Compared to N and NPM, the compatibilized composites showed high yield stress, tensile strength, low elongation and higher stiffness due to SCF and PP-g-MA.
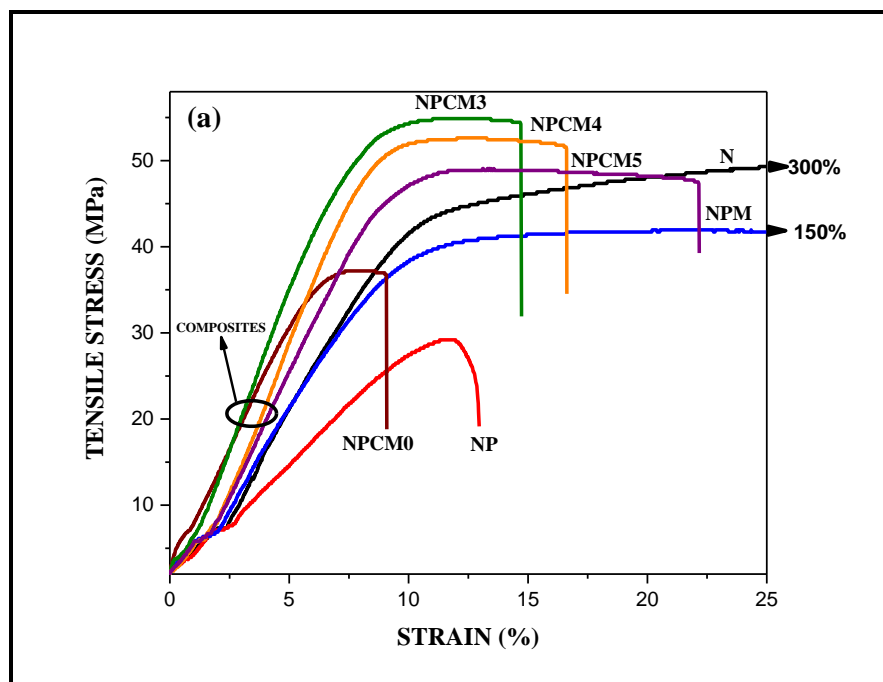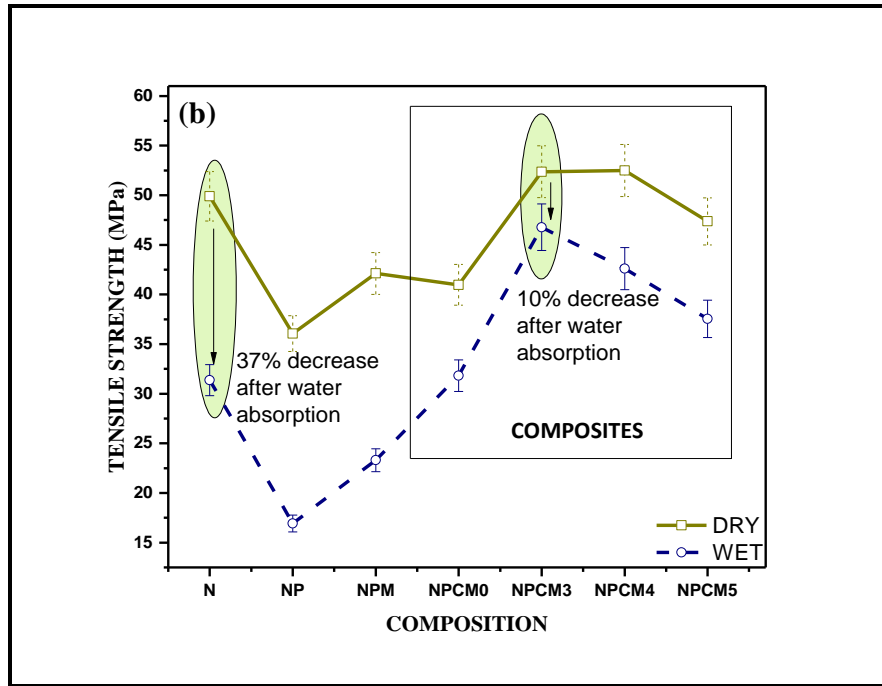
**Figure 3.7: a) Stress-strain plots of dry samples, b) Variation of tensile strength of samples in dry and wet condition. N- PA6, NP-PA6/PP blend, NPM-PA6/PP/*PP-g-MA* blend, NPCM0 to NPCM5: Composites with 0,3,4,5 phr compatibilizer content**

- **Tensile strength (dry)**

PA6 showed tensile strength of 49.5 MPa as shown in Figure 3.7b. On addition of PP, the tensile strength is reduced by 26.5% than PA6, which is due to the lower tensile strength of PP. Addition of PP-g-MA improved the tensile strength of PA6/PP blend by 12.2%, but still it is 14.2% lesser than PA6, which is also reported by Huber et al. (*Huber, 2014*). The increase in the tensile strength in NPM when compared to NP could be attributed to the reduced interfacial tension between PA6 and PP(*González-Montiel, 1995a*) due to the reactivity of PA6 with PP-g-MA as confirmed by FTIR. Addition of SCF to PA6/PP (NPCM0) led to 10 % increase in its tensile strength in comparison to NP as shown in Figure 3.7b. This is due to the reinforcing effect of SCF as reported in the literature(*Karsli, 2013*; *Molnár, 1999*; *S. Zhou, 2013*), but the reduction in tensile strength compared to N could be due to lower compatibility of PA6/PP system. The adhesion between SCF and PA6/PP improved when compatibilizer PP-g-MA was used as observed from the peak intensity variation of FTIR. So, the addition of PP-g-MA led to increase in tensile strength of NPCM3 and

NPCM4 (30% increase compared to NPCM0). The tensile strength was same for 3phr & 4phr PP-g-MA compatibilized composites, but decreased for 5phr PP-g-MA. The trend is similar to that of study reported by Arsad et al.(*Arsad, 2010*), where above 2 phr compatibilizer content, the tensile strength of the blends decreased due to excess compatibilizer content.

- **Tensile strength (wet)**

As shown in Table 3.3 and Figure 3.7b, PA6 had 37 % reduction in tensile strength and PA6/PP blend had 53 % reduction in tensile strength due to the water absorption. With respect PP-g-MA and SCF, same trend is followed in tensile strength values by blends and composites before and after water absorption (dry and wet). As expected, for NPM, the tensile strength was higher than NP, proving the effect of compatibilizer which led to lower water absorption and lesser reduction in tensile strength than NP. On addition of SCF to PA6/PP blend (NPCM0), the % reduction in tensile strength decreased from 53 % to 22% indicating the homogeneous dispersion of SCF fibres. Surprisingly, the tensile strength values of N and NPCM0 almost became equal (32 MPa), but with the addition of compatibilizer (NPCM3) in composites, the value increased to 45 MPa. For all three composites PA6/PP/PP-g-MA/SCF, the % reduction of tensile strength due to water saturation was between 10-20%, least being NPCM3 composite and highest being NPCM5 composite and it might be due to plasticization of matrix by 5 phr PP-g-MA.

- **Tensile elongation (dry)**

% Elongation is shown in Figure 3.8 which confirms that PA6 is a tough engineering plastic. Inclusion of PP to PA6 drastically reduces the elongation to 12.5 % which can also be seen from the brittle fracture of PA6/PP blend. PP has low elongation and PA6/PP blend has lower resistance to crack propagation due to lower compatibility i.e. large PP globules poorly dispersed in PA6 matrix. Addition of PP-g-MA to PA6/PP blend increased the elongation from 12.5 to 150 % which showed the effective compatibilization of PA6/PP blend because of good dispersion of PP in PA6. Similar results were reported by other authors (*Agrawal, 2010*; *Kudva, 1999*). On addition of

SCF to PA6/PP/ PP-g-MA blend, the elongation again decreased to 10 %, due to the restriction of chain mobility and brittle nature of SCF(*B. Li, 2009*; *Tjong, 1999*). NPCM3 had similar % elongation as NP, but with further increase in compatibilizer content, the % elongation of composites increases slightly. Compatibilized composite NPCM5 showed 71.4% higher elongation than NPCM0, which indicates the excessive plasticization of PA6/PP due to the presence of PP-g-MA(*Sharma, 2009*), which also led to the reduction in tensile strength (Figure 3.7b). The compatibilization effect is optimum in NPCM3 and NPCM4 where higher tensile strength and lower increase in elongation was observed.

- **Tensile elongation (wet)**

As shown in Figure 3.8, PA6 showed 11% more elongation after water absorption and it did not break during the test, rather slipped out of the grip due to the reduction in thickness and width during the test. An average of 2 mm reduction of thickness was observed. For PA6/PP blends, the elongation increased in comparison to dry sample because of plasticization of PA6 phase due to water absorption, and had highest increase in elongation (>500 %) as shown in Table 3.3. Similar to PA6 and PA6/PP, the compatibilized blend showed 100% increase in elongation and this system also slipped out of the grip before break. Among the composites, the uncompatibilized composite (NPCM0) which had lowest water absorption also had a lower increase in elongation because of presence of PP and SCF. Whereas the compatibilized composites had higher increase in % elongation due to plasticization of PA6 by water and PP-g-MA (NPCM3-56%, NPCM4-53%, NPCM5- 50%) but the trend of elongation change remained same for dry and wet conditions as shown in Figure 3.8.
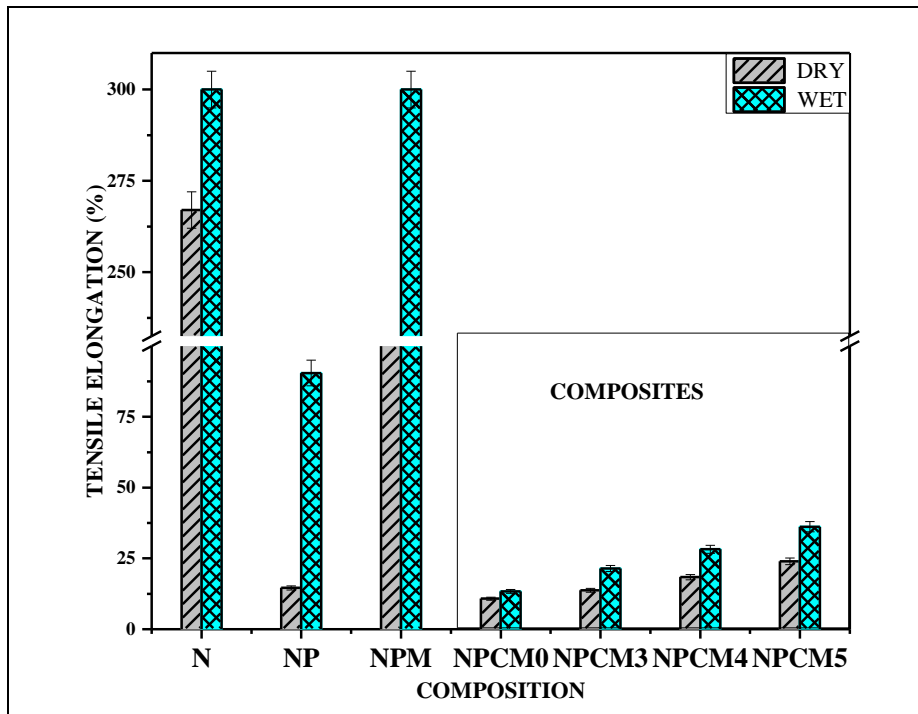
Figure 3.8: Variation of tensile Elongation of samples before (DRY) and after (WET) water absorption. N- PA6, NP-PA6/PP blend, NPM- PA6/PP/PP-g-MA blend, NPCM0 to NPCM5: Composites with 0,3,4,5 phr compatibilizer content
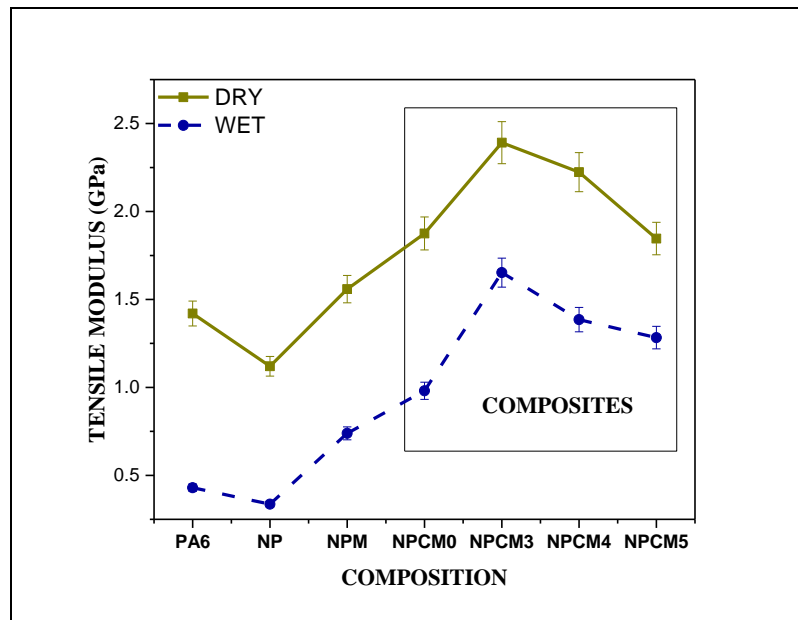
Figure 3.9: Variation of tensile modulus of samples before (dry) and after (wet) water absorption. N- PA6, NP-PA6/PP blend, NPM- PA6/PP/PP-g-MA blend, NPCM0 to NPCM5: Composites with 0,3,4,5 phr compatibilizer content

- **Tensile modulus (dry)**

Variation of stiffness for blends and composites has been illustrated in stress-strain curves shown in Figure 3.7a and Figure 3.9. PA6 (N) had less stiffness and high elongation than the composites. PA6/PP (NP) had 15% lower modulus than N owing to lower modulus of PP. NPM had higher tensile modulus than NP as observed in tensile strength which justifies the decrease in interfacial tension due to lack of compatibilization of PA6/PP(*Huber, 2014*). NPCM0 had higher stiffness than N, NP and NPM due to the reinforcing effect of SCF because SCF has very high tensile modulus in comparison to matrix material. High tensile modulus was also observed for NPCM3 and it decreases slightly with increase in compatibilizer content, which proves the plasticization effect of compatibilizer as observed in SEM analysis (discussed below) and elongation measurements. From the stress-strain curve shown in Figure 3.7a, brittle to ductile transition (increase in elongation, decrease in strength) can be observed with increase in compatibilizer content (NPCM3-NPCM4-NPCM5).

- **Tensile modulus (wet)**

Tensile modulus values of wet samples followed the same trend as that of tensile modulus for dry samples (Figure 3.9). The reduction in tensile modulus for wet samples is shown in Table 3.3. The stiffness of all composites was higher than that of PA6, showing the effect of plasticization of water on PA6 in absence of PP, PP-g-MA and SCF. NPM had higher modulus than N and NP. NPCM0 had lower stiffness than compatibilized composites. In both cases (blends and composites) compatibilizer is causing increase in stiffness. Compatibilized composite with 3 phr PP-g-MA content had highest tensile modulus than other systems similar to that of dry samples. % reduction in stiffness due to water absorption is low for composites (30-38%) compared to PA6 and blends (52-72%), so these composites can be considered for applications in high humid conditions with factor of safety into consideration.

From the tensile strength, elongation and stiffness values, it can be said that 3phr PP-g-MA is the optimum compatibilizer content for PA6/PP/SCF system with minimum reduction in tensile strength (10%), stiffness (30%) and minimum increase in weight

(2.4%) due to water absorption or saturation. Among the dry composites there was not much increase in properties was obtained, but for wet composites the composites gave much higher properties than PA6. There is 30-38% reduction in tensile modulus, but reduction in tensile strength 10-20%.

3.5.3. *Fractography of blends and composites after tensile testing*
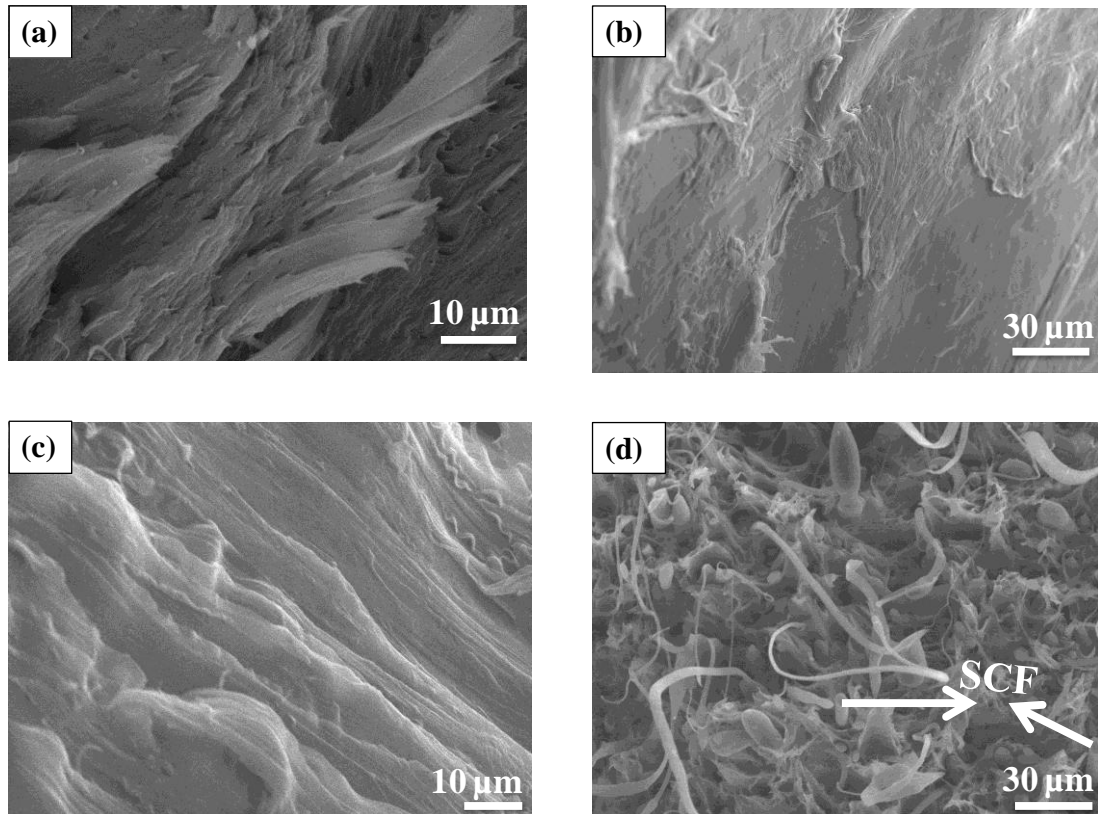
Figure 3.10: SEM images of tensile fractured surface of (a) N-PA6, (b) NP-PA6/PP, (c) NPM- PA6/PP/PP-g-MA, (d) NPCM0- PA6/PP/SCF

Morphology of the fractured samples of blends and composites were studied using SEM (Hitachi S3700N VP-SEM). From SEM fractography shown in Figure 3.10, it can be said that PA6 under tensile load failed due to excessive pull out (Figure 3.10a). PA6/PP (NP) had a smooth fracture (Figure 3.10b) across the width showing no pull out of matrix, which could be due to the brittle nature of PP as observed from elongation measurements (only 12 % elongation for PA6/PP compared to 300 % elongation for PA6). It can be said that crack initiated and propagated at the PP interface because it is not bonded well to PA6. When compatibilizer was added to PA6/PP blend, it showed again pull-out on the fractured surface as it is noticed in the

74

case of PA6 (elongation also increased to 150%; Figure 3.10c), but the intensity of pull out is low in comparison to PA6 indicating the reaction between PA6- PP-g-MA-PP. Because of the brittle nature of SCF and bonding between SCF and PA6, little matrix pull out could be seen in NPCM0 system, which showed brittle fracture like NP with exception of slightly fibrillated PA6 because of phase difference existing between PA6 and PP (Figure 3.10d).
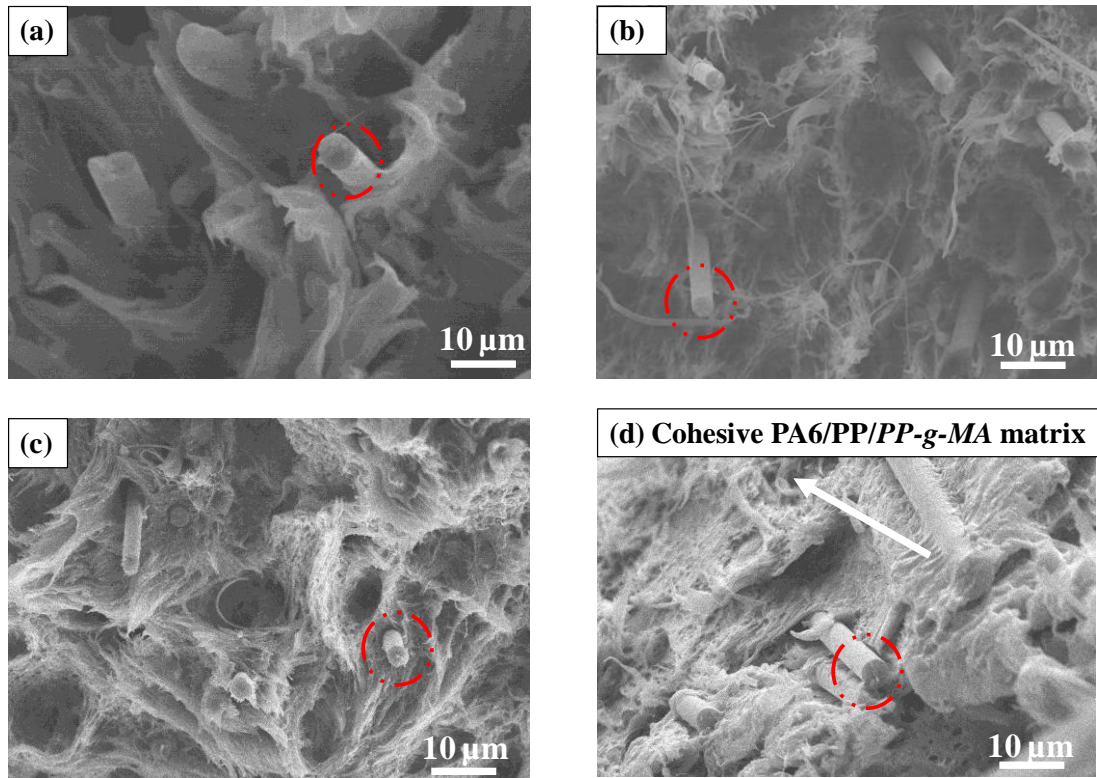
Figure 3.11: SEM images of tensile fractured surface of (a) NPCM0-PA6/PP/SCF (b) NPCM3-PA6/PP/PP-g-MA (3phr)/SCF, (c) NPCM4-PA6/PP/PP-g-MA(4phr)/SCF, (d) NPCM5-PA6/PP/PP-g-MA(5phr)/SCF. Circles denote the carbon fibres. (Cohesive failure of matrix: inset)

SEM images of fractured composite specimens are shown in Figure 3.11. Comparing the fractography of compatibilized composite systems, the SCF gets more wetted and adhered into the matrix system as seen in Figure 3.11d, where the fibre is fully surrounded by the matrix. The interfacial adhesion between the fibre (SCF) and matrix (PA6/PP/PP-g-MA) is clearly seen in Figure 3.11d because cohesive failure of the matrix is observed. For 3phr and 4phr compatibilizer content, little matrix pull out and transverse fracture of matrix could be the reason for composite failure, but in the case of 5 phr compatibilizer, matrix shearing led to composite fracture. Comparing

NPCM0-NPCM5 (Figure 3.11a to 3.11d) fractographs, thread like appearance has turned to network or web like appearance, which could be due to the increased interfacial adhesion between the PA6/PP and compatibilizer. It is also seen that higher amount of compatibilizer leads to poor dispersion of SCF resulting in the web like appearance of the matrix, and it also resulted in reduction of tensile strength and increase in elongation of the composite system (Figure 3.7 and 3.8). SCF are circled in Figure 3.11d indicating the fibre diameter of 7 μm. For 5phr PP-g-MA content, the composite had ductile failure, showing the plasticizing effect of PP-g-MA on PA6/PP/SCF. SEM results correlates well with the FTIR and tensile results, showing that the increase in compatibilizer content is causing gradual change in fracture pattern from brittle to ductile in composites.

3.5.4. Impact strength of blends and composites with varying compatibilizer content
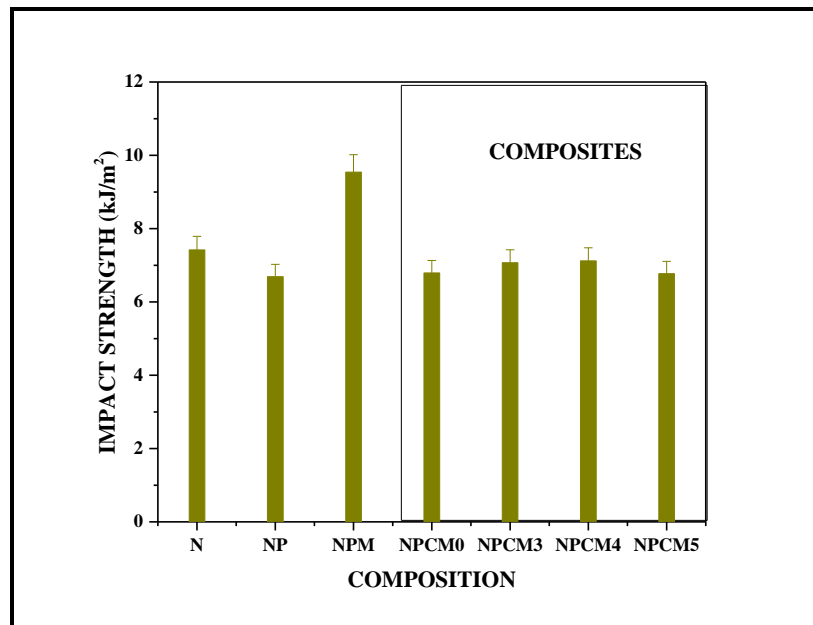
Figure 3.12: Variation of impact strength of sample dry samples. N- PA6, NP-PA6/PP blend, NPM- PA6/PP/PP-g-MA blend, NPCM0 to NPCM5: Composites with 0, 3, 4, 5 phr compatibilizer content

The notched-izod impact test was conducted as per ASTM D256 standard on (CEAST 9050) pendulum type impact tester for all compositions. Flat specimens of 3.2 mm thickness and 64 mm length obtained from injection molding were used for impact

test (dry). Comparing the impact strength values of N, NP and NPM in Figure 3.12, it can be seen that NPM gave highest impact strength followed by N and NP which could be due to the improved interfacial adhesion between PA6 and PP in presence of compatibilizer. The low impact strength of NP might be due to the poor dispersion of PP phase in PA6 phase as explained before. Impact strength values of the blends are matching with published results reporting that MA based compatibilizers improved the impact strength of the blends by reactive compatibilization (*Purnima, 2006*).

Comparing composites in Figure 3.12, there is a slight increase in impact strength up to 4phr compatibilizer content and then slight decrease on addition of 5 phr compatibilizer similar to that of the result observed by Huber et al. (*Huber, 2014*) where decrease of impact strength was seen on using higher maleated PP-g-MA for compatibilizing PA6/PP blend. The NPCM0 had comparable impact strength to that of NP. This indicates that SCF is not contributing to impact strength, but it increased the yield strength, modulus and maximum strength of the composite. NPCM4 had 1.4% increased impact strength than NPCM3, so from Figure 3.12 it can be concluded that not much change in impact strength values due to the addition of compatibilizer content from 0 to 5 phr. It could also be seen that, impact strength follows the same trend as that of tensile strength in composites, which again confirms that 3phr PP-g-MA content is the optimized compatibilizer content for PA6/PP/SCF composite.

3.5.5. *Statistical analysis using GRA method*

Grey Relational Analysis (GRA) is a statistical tool used for process optimization. In this study optimum PP-g-MA and SCF content required to achieve maximum tensile strength, modulus, elongation and impact strength of the composites (before water absorption) was investigated. Hence "larger–the-better" quality characteristic was used to find the Signal to Noise (S/N) ratio. Grey relational grade (GRG) was obtained from GRA using four step procedure (*Krishnaiah, 2012*). First step is to find the S/N ratio for individual property followed by normalization of the S/N ratio data (range 0-1) and the third step is to find the grey relational coefficient for individual property (ranges between 0.5-1). Finally GRG was calculated by taking average grey relational coefficient value of tensile and impact property. In above calculations distinguishing coefficient was taken as 1.

<table>
<tr><td colspan="5" align="center">**Table 3.4:**
Factors and their assigned Levels considered Grey Relational Analysis (GRA)</td></tr>
<tr><td>Control Factors</td><td>Level 1</td><td>Level 2</td><td>Level 3</td><td>Level 4</td></tr>
<tr><td>PP-g-MA (phr)</td><td>0</td><td>3</td><td>4</td><td>5</td></tr>
<tr><td>SCF (wt %)</td><td>0</td><td>5</td><td></td><td></td></tr>
</table>

Trial no	TS	TM	% E	IS	S/N ratio	Normalized S/N Ratio	Δ	G_CTS	G_CTM	G_CE	G_CIS	G_{IC}

Table 3.5: GRA calculation for the eight trials

Trial no	TS	TM	% E	IS	S/N ratio	Normalized S/N Ratio	Δ	G_CTS	G_CTM	G_CE	G_CIS	G_{IC}
1	36.07	4.88	14.60	6.69	29.352	0.0000	1.0000	0.0329	0.6075	0.5362	1	**0.5441**
2	40.97	5.79	10.79	6.79	30.429	0.8092	0.1908	0.0318	0.7135	0.5	0.9456	**0.5477**
3	42.12	3.81	108.26	9.54	30.724	0.9396	0.0604	0.0315	0.5	1	0.5	**0.5078**
4	52.37	7.42	13.71	7.07	32.604	1.1939	0.1939	0.0298	1	0.5317	0.8293	**0.5976**
5	42.12	3.81	108.26	9.54	30.724	0.9396	0.0604	0.0315	0.5	1	0.5	**0.5078**
6	52.50	6.90	18.40	7.12	32.639	1.1454	0.1454	0.0297	0.8966	0.5702	0.8126	**0.5773**
7	42.12	3.81	108.26	9.54	30.724	0.9396	0.0604	0.0315	0.5	1	0.5	**0.5078**
8	47.37	5.71	23.96	6.77	31.74	1.0000	0.0000	0.0305	0.7163	0.6152	0.9558	**0.5794**

Note: TS-Tensile strength, TM-Tensile Modulus, %E- % Elongation, IS- Impact strength, G_C- Grey relational coefficient, G_{IC}-Cumulative grey relational grade

PP-g-MA content (0, 3, 4 and 5 phr) and SCF (0 and 5%) content were chosen as factor-level combinations as shown in Table 3.4, which are the input parameters considered in the GRA analysis. Tensile strength, tensile modulus, elongation and impact strength are considered as output responses. With two factors and four levels, the number of experiments is eight, and the corresponding GRG for all output responses were found as explained (Table 3.5). The factor and level having highest GRG is considered as the optimum parameter for obtaining better combination of mechanical properties.

Table 3.6
Response Table for Grey Relational Grade. Bold Figures represent the higher (optimal) value. Total mean value of the GRG is 0.7186. Note that SCF is more influencing than PP-g-MA on tensile and impact properties

Control Factors	Level 1	Level 2	Level 3	Level 4	Difference (Max-Min)	Rank
PP-g-MA (phr)	0.6751	**0.7477**	0.7389	0.7130	0.0726	2
SCF (wt %)	0.6587	**0.7787**			0.1200	1

From the GRG value as tabulated in Table 3.6, higher value of GRG is observed for 3 phr PP-g-MA content and 5 wt% SCF content. As the GRG values are well above 0.5,

it could be said that both PP-g-MA content and SCF content plays a major role in determining the mechanical properties of the composites. To affirm this, the difference between maximum and minimum value among levels was found, and the rank was given. From the difference it can be seen that the PP-g-MA has Rank 2 and SCF has Rank 1 denoting that SCF content plays better role than PP-g-MA content in determining the mechanical properties of PA6/PP/PP-g-MA/SCF composites. Overall from GRA analysis, it is understood that for obtaining higher strength, stiffness and toughness, 3phr PP-g-MA and 5 wt% SCF is the most optimum composition which corroborates with the experimental data where NPCM3 was considered to be the most optimum composition as shown in Figure 3.7-3.9. Despite the fibre breakage during processing, the contribution of SCF is slightly better than the PP-g-MA content in obtaining optimum composite properties as seen from Table 3.4c, but for obtaining stiffer composite higher SCF content and for obtaining tougher composite higher PP-g-MA content should be used.

3.6. Effect of Short Carbon Fibre content on mechanical properties

After optimizing the PP content of 30 wt% (chapter 2) and PP-g-MA content of 3 phr (section 3.6), the following work focuses on influence of SCF content on mechanical properties of composites in both dry and wet states. Here, PA6/PP/PP-g-MA (70/30/3 wt/wt/phr) matrix blend with varying SCF content (CM0-0, CM1-3, CM2-6, CM3-9 and CM4-15 wt %) has been studied (Table 3.2). The effect of SCF content on tensile properties before (dry) and after (wet) water absorption and on impact strength (dry) was studied. Additionally, effect of SCF on PP size distribution in composites has been elaborated by selectively etching out PP. Residual fibre length of the composite was measured using matrix burn out method as it plays a major role on determining the composite mechanical properties.

3.6.1. Water absorption studies of blend and composites

Water absorption of the samples was carried out until saturation for 45 days and the resultant weight gain is shown in Figure 3.13. Water absorption occurs through diffusion of water through the interfacial defects existing between fibre and matrix and also through the matrix voids (*Tsenoglou, 2006*). On prolonged exposure, water

accumulates at the interface leading to swelling of samples and also water starts to bond with the matrix material. CM0 had 2.6% water absorption, which is 58% lesser in comparison to pure PA6. In PA6, the water absorption takes place through the reaction between the –OH- group of water and end groups of PA6 as explained in the FTIR (section 3.4). Whereas for blend, this reaction is restricted as the end group react with PP-g-MA due to which the water absorption decreases drastically as also explained in FTIR (section 3.4). For composites, water absorption decreases drastically showing the synergistic effect of hydrophobic PP and SCF. Here, the reactivity between the compatibilizer with "epoxy of SCF" as well as the compatibilization of blend aids in reduction of water absorption (section 3.4 and Figure 3.6). With addition of up to 6 wt% SCF, the water absorption is similar to CM0, and then decreases drastically as shown in Figure 3.13. In comparison to PA6, CM4 had 72% reduction in water absorption. From the morphology of PP dispersion discussed later, it could be understood that as SCF content increases, the dispersion of PP becomes better which led to better reduction in % water absorption. It can be concluded that, SCF along with PP acts as barrier for water absorption indicating the importance of SCF reinforced PA6/PP composites for wet or high humid applications.
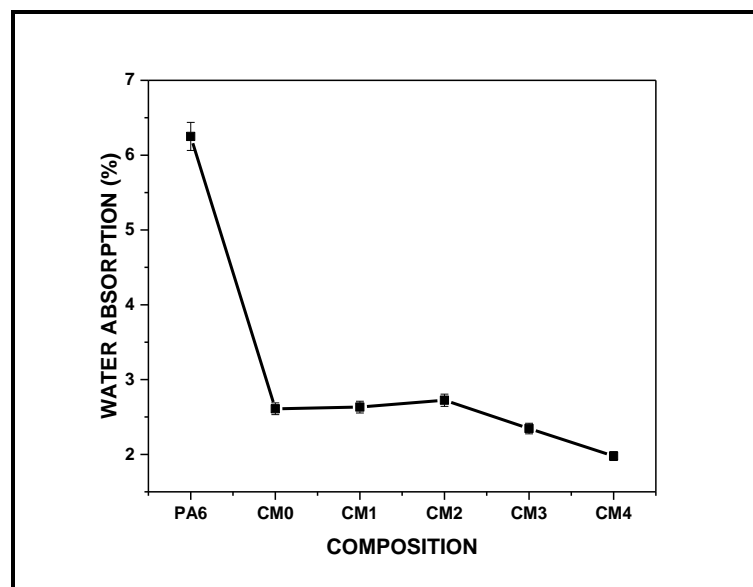
Figure 3.13: Water absorption of PA6, CM0 (PA6/PP/PP-g-MA) and composites (CM1-3, CM2-6, CM3-9 and CM4-15 wt% SCF content)

3.6.2. Tensile properties of PA6, matrix blend (PA6/PP/PP-g-MA) and composites (dry, wet) made with varying SCF content

The tensile test was carried out using Universal Testing Machine (Zwick Roell) at a crosshead speed of 5 mm/min and a gauge length of 50mm as per ASTM D638 standard. Tensile properties of all dog bone specimens were studied before (dry) and after water absorption (wet). Tensile modulus and elongation was calculated using contact type extensometer attached to the specimen until yield point.

- **Tensile strength (dry)**
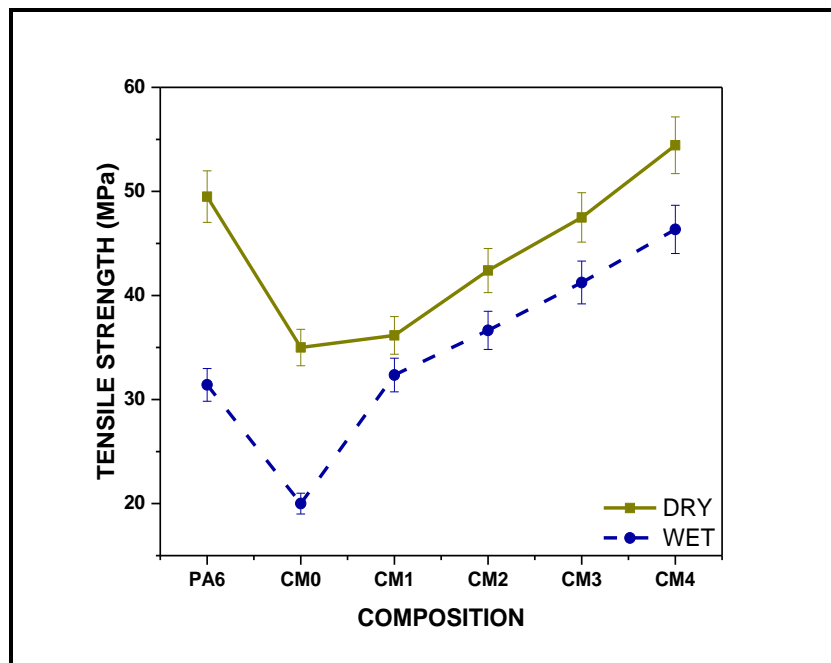
Figure 3.14: Tensile strength of PA6, CM0 (matrix blend) and composites (CM1-3, CM2-6, CM3-9 and CM4-15 wt % SCF content) at dry and wet states

Figure 3.14, represents the tensile strength of PA6, matrix blend (CM0) and composites (CM1-CM4) before and after water absorption. Considering the tensile strength of the dry samples, as more amount of SCF was added, the tensile strength improved consistently, but not significantly. CM4 resulted in 10% higher strength than pure PA6 and 55% more strength than CM0 blend. This proves the reinforcing effect of SCF as reported by other authors(*Feng, 2013*; *Karsli, 2013*; *Luo, 2014*; *Molnár, 1999*) which is due to the high tensile strength of SCF fibres. Figure 3.14

clearly indicates that adding PP to PA6 is contributing in strength reduction (lowest for CM0), but it also contributes in reduction in water absorption as discussed (Figure 3.13). The tensile strength reduction due to addition of PP/PP-g-MA was also seen by Do et al.(*Do, 2016*). It was understood that most of the authors have used SCF of length ≥ 3mm, and most of the studies were based on PA6/SCF, where the tensile strength doubled in comparison to pure PA6 at 20 wt% SCF content (*Karsli, 2013*; *Luo, 2014*). The residual carbon fibre length in composite was reported as 50 μm even though the initial fibre length was 6 mm (*Karsli, 2013*). Similarly, in this study, the residual fibre length was found to be 50 μm (see section 3.8), due to which, the increase of tensile strength is minimal at CM1 (3 wt %) and gradually increasing with increase in SCF content.

- **Tensile strength (wet)**

As seen from Figure 3.14, there is drastic reduction in tensile strength for PA6 (37%) and CM0 (42%) post water absorption, as water acts as plasticizer and aids in mobilization of the PA6 chains. With addition of SCF, the tensile strength increases similar to that of dry samples. It is reported earlier that water not only acts as plasticizer, but also reduces the interfacial adhesion between the fibre and the matrix (*Do, 2016*; *Minggang Li, 2014*). As seen in the FTIR of wet samples, the number of –OH- group increases in the wet samples, which would lead to reduction in mechanical properties. Comparing the dry and wet samples, it was seen that, tensile strength of wet CM1 decreased by 10.5% in comparison to dry CM1, whereas wet CM4 showed 14.8% reduction in comparison to dry CM4. Even though the % water absorption is very low (Figure 3.13), there is "reduction in tensile strength" at higher SCF content, which might be due to the combined effect of compatibilization of the blend and SCF induced defects in the composite. Wet CM4 gave 133% higher tensile strength than wet CM0 (matrix blend) indicating the reinforcing effect of carbon fibres in wet condition.

- **Tensile modulus (dry)**

The tensile modulus of the dry samples increased drastically with addition of SCF as seen in Figure 3.15. Initially CM1 had 78% higher tensile modulus than pure PA6, whereas CM4 revealed 255% higher tensile modulus than pure PA6. It is commonly

seen that carbon fibre improves the stiffness of the polymer matrix by 2-10 fold depending on the fibre volume fraction and also due to the higher ratio of fibre modulus to polymer modulus (*Agarwal, 2006*). The drastic increase in modulus shows better interfacial adhesion and uniform fibre dispersion in the composite.
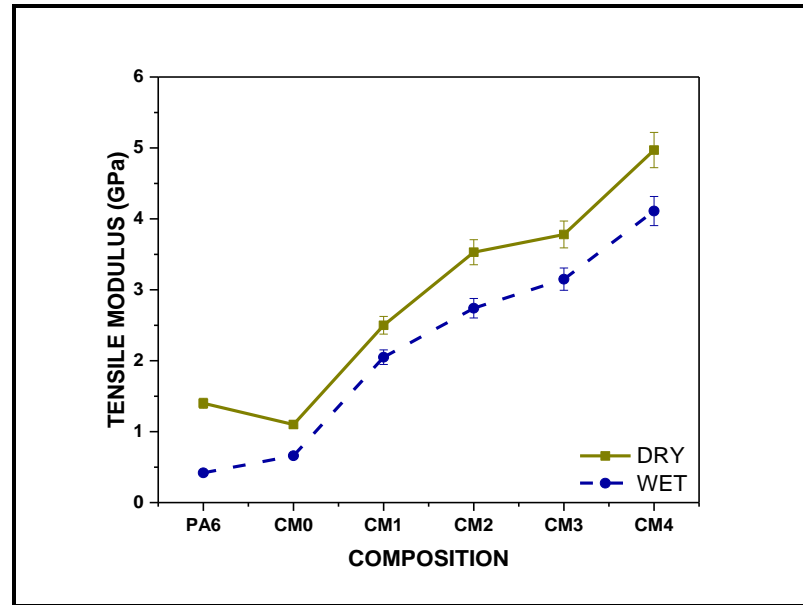
Figure 3.15: Tensile modulus of PA6, CM0 (matrix blend), and composites (CM1-3, CM2-6, CM3-9 and CM4-15 wt % SCF content) in dry and wet state

Here it is noteworthy that tensile strength and modulus of the blend based composite (CM4-15 wt% SCF) is 55% and 351% higher than the pure CM0 respectively. The tensile strength increment is lower than that of modulus, which could be due to the huge difference in "elongation at break" of matrix and the fibre and also due to the "presence of interfacial defects" in the composite. But from modulus increment it is understood that the packing of the composite is good, which indicates less number of "micro" defects. Hence, the low increase in tensile strength could be due to random orientation of SCF. Unlike in thermoset composites, the plastic deformation in these thermoplastic composites might lead to crack initiation at the weak interfaces i.e. randomly oriented fibre zones on skin side, which then propagates through the core zone of the composites. Molnar et al.(*Molnár, 1999*) found that fibres are aligned at the core zone, but fibres are randomly oriented at the skin side in injection molded composite specimens. Hence, for dry composites, both fibrillation of matrix and brittle fracture of composite were observed which led to low increment in tensile

strength as shown in Figure 3.14.

- **Tensile modulus (wet)**

The tensile modulus reduction was 71.9% for PA6 and 40% for CM0 post water absorption (Figure 3.15). However, with addition of SCF, the reduction in modulus was around 18% for all composites in comparison to its dry counterparts. It was observed that CM4 had nine-fold and five- fold increase in modulus in comparison to wet PA6 and wet CM0 respectively. This increase in tensile modulus reflects the reinforcing effect of SCF fibres even in wet condition, which also confirms the homogeneous dispersion of SCF and good interfacial adhesion between fibre-matrix in wet state. As also seen from FTIR, due to the occurrence of reaction between the "sizing on fibre surface" and compatibilizer, the reduction in modulus is lower for all composites. The addition of compatibilizer (3 phr) proved to be beneficial as it could aid in retention of strength and modulus of the composite even in wet condition.

- **Tensile elongation (dry)**
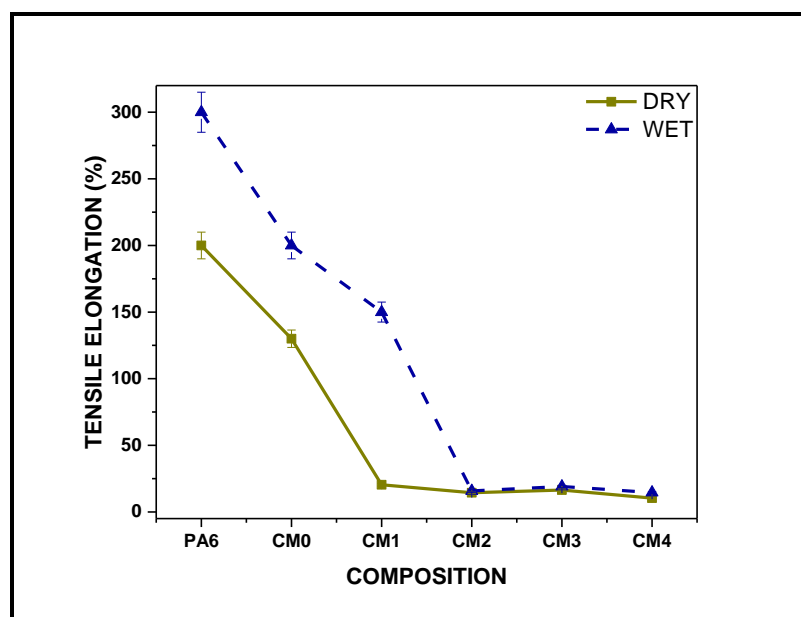
Figure 3.16: Tensile elongation of PA6, CM0 (matrix blend) and composites (CM1-3, CM2-6, CM3-9 and CM4-15 wt % SCF content) in dry and wet state

The elongation at break reduced for the blend and composites in comparison to pure PA6 (Figure 3.16). In case of matrix blend, the compatibilization led to restriction of chain movement of PA6 due to the reaction occurring at the interface of PA6-PP. In

case of composites with increase in SCF content, elongation at break remained same for all SCF contents indicating no effect of SCF content on elongation which is beneficial as tensile strength and modulus are increasing without any reduction in elongation. This shows the existence of excellent interfacial bonding between PA6 and SCF. Since the average residual fibre length is only ~50 μm (section 3.8), the number of fibre ends are very high leading to lower elongation because fibre ends acts as stress concentrators (crack arresters) and do not allow the matrix to elongate (*Karsli, 2013*).

- **Tensile elongation (wet)**

The elongation at break of PA6 and CM0 increased post water absorption due to the plasticization of PA6 (Figure 3.16). However, it was seen that composite CM1 did not break during the test and this increase in elongation in comparison to its dry counterpart could be due to plasticization of PA6 in its amorphous phase. As the SCF content increases (CM2-CM3-CM4), water absorption decreased and the plasticization effect is decreasing, hence the elongation at break becomes saturated and not much difference was observed between the wet and the dry counterpart at 6 wt%, 9 wt% and 15 wt% SCF contents.

3.6.3. *Fractography of blend and composites after tensile testing (dry and wet)*

To further understand tensile properties of composites, fractography was carried out using SEM analysis. Figure 3.17, represents the tensile fractography of the dry and wet CM2, CM3 and CM4 specimens. Dry samples of CM0 did not break during the tensile test, rather elongated to the maximum extent and slipped off from grip due to excessive thinning of the sample. Dry fractography of PA6 showed fibrillation as reported in Figure 3.10. Among the wet samples tested, PA6, CM0 and CM1 did not break. Hence the tensile fractography of these samples are not discussed.

Considering the tensile fractography of the dry samples, CM1 revealed matrix fibrils that could have occurred due to the ductile fracture of the matrix (not shown). Even though the weight fraction of SCF was very low (3 wt %), these fibres acted as crack arresters owing to better interfacial adhesion, due to this elongation at break was reduced by 19.6% in comparison to CM0 but the fractography resembled matrix

fibrillation. Fibre pull-out or breakage was not seen for this sample. In Figure 3.17a fibres are oriented in random direction and this is due to the fibre pull out and elongation of the matrix. As the SCF content increased, the stress transfer from the matrix to the fibres is becoming prominent. It was observed that the fibres were covered with a layer of matrix (cohesive failure) which indicates better wetting of fibres by the matrix.
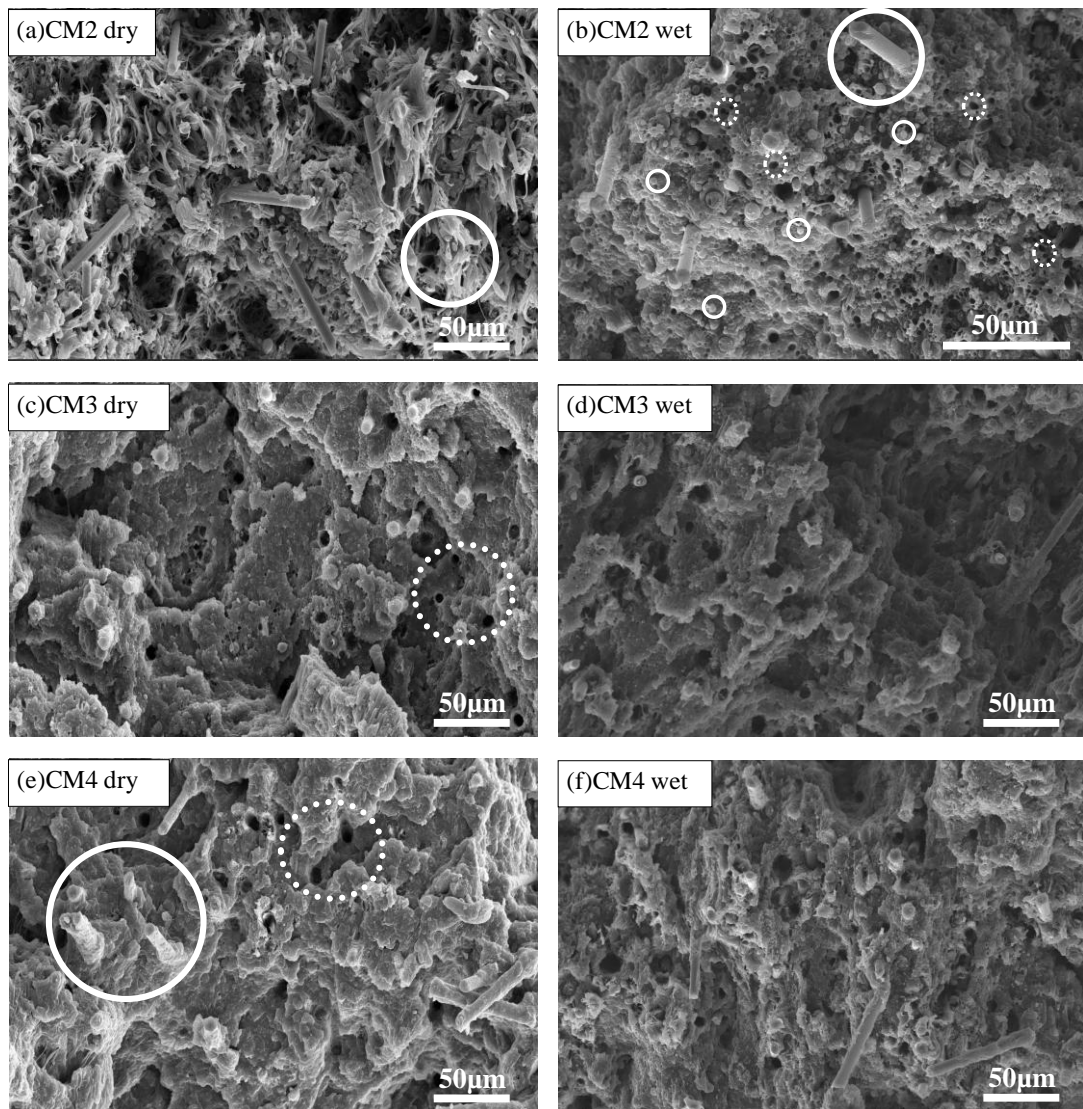
Figure 3.17: Tensile fractographs of CM2 (6 wt% SCF), CM3 (9 wt% SCF) and CM4 (15 wt% SCF) composite samples are shown in a-b, c-d and e-f respectively. In (a) big solid circle indicates matrix fibrillation and in (b, e) indicates lesser pull out of fibres. In (b) small solid circles show PP droplets and small dotted circles indicate voids due to PP removal. In (c) big dotted circle indicate voids due to fibre pull out.

In Figure 3.17c, very little fibre pull out was visible along with the feather type/ridge-like fracture (*Ishak, 1994*; *Ogunsona, 2017*) of matrix indicating good bonding. More numbers of voids due to fibre pull-out on the fracture surface was seen, which indicates better dispersion of SCF fibres. As shown in Figure 3.17e for highest SCF content (CM4), the fibre pull out, feather type fracture of matrix and agglomeration of SCF was observed. In CM3 and CM4 composites, small voids due to pull out of PP and smaller size PP droplets are visible (dotted circles), whereas in CM2 fractography bigger size PP droplets are visible.

Considering the fractography of the wet samples in Figure 3.17 b, d, f, it was observed that for CM2, very little fibre pull out and small to big size PP droplets are contributing in fracture. Dark ring i.e. adhesive failure, around PA6 was observed for few fibres showing the effect of water absorption in weakening the fibre-matrix interface. As the SCF content increased, more voids due to fibre pull out was seen which yet again proved the reduced interfacial adhesion in comparison to dry samples. Few fibres in wet samples showed adhesive failure (no matrix on fibre surface). Hence, due to water absorption, the interface between PA6/PP and between fibre/matrix is getting affected due to which lower tensile strengths are observed for the wet samples in comparison to the dry samples. This result also correlates with the peak intensity enhancement in wet samples of FTIR which also proved the reduced interfacial adhesion.

In dry sample, it was observed that fibre is covered with a layer of matrix (cohesive failure) and well embedded in the matrix. On the contrary, in wet sample, the fibre is not fully covered with matrix (both cohesive and adhesive failure) and severe fibre pull-out, and ductility of the matrix (fibrillation) surrounding the fibre (*Ishak, 1994*) was seen which shows the reduction in the interfacial bonding between the fibre and the matrix and plasticization of matrix due to water absorption. Even though water absorption of PA6 decreased with addition of PP and SCF, it still resulted in reduction of the properties of composite due to the chemical bonding between the PA6 and water molecules. But, due to the use of PP-g-MA as compatibilizer, the weakening of interfacial bonding was reduced which led to increase in tensile strength and modulus in wet composites with increase in SCF content (Figure 3.14 and 3.15).

3.6.4. Impact strength of blend and composites with varying SCF content

Impact test of injection molded specimen were carried out as mentioned in section 3.6.4. Figure 3.18, shows the impact strength of PA6, CM0 (matrix blend) and the composites. PA6 had impact strength of 7.4 kJ/m^2 and the composites had impact strength in the range of 8-12 kJ/m^2, which is slightly higher than the PA6. Around 47.5% reduction in impact strength was seen for CM1 in comparison to CM0, which is due to the brittleness and crack arresting nature of fibres, and reduced number of interfacial defects.
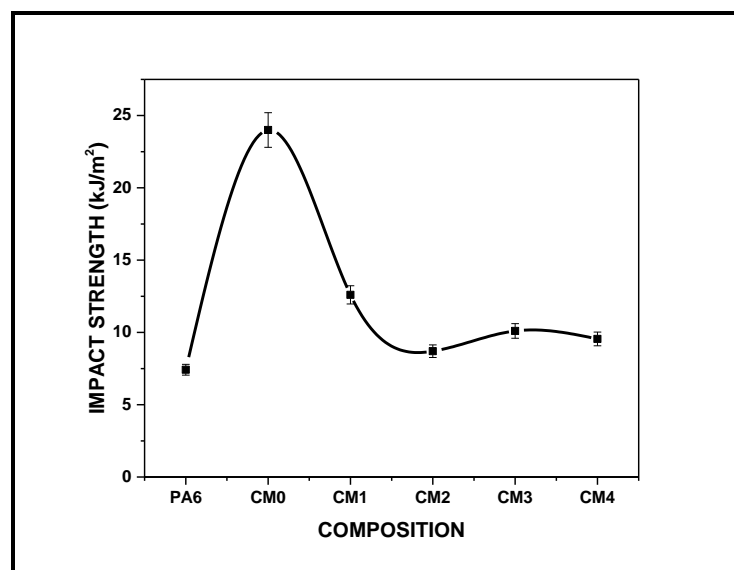
Figure 3.18: Impact strength of PA6, CM0 (matrix blend) and composites (CM1-3, CM2-6, CM3-9 and CM4-15 wt % SCF content)

With the addition of SCF, Luo et al.(*Luo, 2014*) and Feng et al. (*Feng, 2013*)found that the impact strength of the composite increased (higher than PA6) as the SCF acts as barrier to crack propagation. Increase in number of fibre ends lead to effective interfacial adhesion in SCF composite, wherein cracks would propagate around the fibres leading to higher impact strength in case of sized fibres. Feng et al. (*Feng, 2013*) compared the impact strength of PA6/ desized CF and PA6/ 8 wt% DGEBA coated CF, confirmed that the desized CF composites had equivalent or lower impact strength than PA6, while the DGEBA coated CF composites had higher impact strength than PA6 owing to better interfacial adhesion between the fibre and the matrix. Similarly, in this study, due to lower amount of sizing, the improvement in

impact strength of composites was equivalent or slightly higher than PA6.

Fibre pull out and matrix deformation aid in improving the impact strength of the composites. In this study, matrix is a blend containing reactive compatibilizer which can bond with both PA6 and epoxy sizing on SCF, the impact strength of composites is reduced in comparison to CM0. As the reaction between "PA6 and epoxy on SCF" becomes prominent for CM1 and also because of 3 wt% SCF, it gave better impact strength in comparison to other composites. For Feng et al. (*Feng, 2013*), at 15 wt% SCF content, the impact strength was 100 J/m (~ 10 kJ/m^2) for PA6/ DGEBA modified CF, whereas in this study the impact strength of the blend based composite at 15 wt% SCF content is 9.5 kJ/m^2 which is considered to be advantageous because PP is also present along with PA6, which aids in reduction of water absorption thereby extending its applications to high humid and under water components without compromising impact strength.

- **Fractography of blend and composites after impact testing**

Figure 3.19 illustrates the impact fractography of the blend and the composites. In all composites, PP is dispersed as droplets and it could be considered that the impact fracture could have occurred at PA6/SCF interface or PA6/PP interface. Considering the blend fractography in Figure 3.19a, cavitation due to pull out of PP can be seen (dotted circles) along with low-medium size PP droplets (solid circles). Feather type fracture was seen for the blend. Cavitation due to removal of 3μm PP droplet could have led to higher impact strength (due to more PA6/PP interfacial defects) and the blend had the highest impact strength in comparison to PA6 and other composites (*Kirk, 1984*) (Figure 3.18). The effective compatibilization can be assumed with the homogeneous distribution of PP droplets in the PA6 matrix. In Figure 3.19b, smooth fracture of matrix with fibre-matrix debonding was visible. Since matrix deformation occurs around the fibres (due to the high elongation of matrix), the impact strength of CM1 is higher than other composites. In Figure 3.19c-d, it was observed that cohesive failure of the matrix is dominating in fracture of the sample, which could be due to cavitation of smaller PP/PP-g-MA droplets present in the matrix. As the SCF content increases, due to better PP dispersion, the impact strength of composite did not decrease in comparison to PA6. It could be seen that the fibres are covered with

matrix (cohesive failure) which suggest that the interfacial adhesion exists between the matrix and fibre but it was not enough to prevent fibre pull out as seen in the impact fractography of CM4 in Figure 3.19d which might be due to the random orientation of SCF fibres. It could be concluded that, the interfacial adhesion did not decrease as the fibre content increased because interfacial defects are almost same in CM2, CM4, but slightly more number of defects were found for CM3 (not shown) which also showed slight increase in impact strength as shown in Figure 3.18. Overall, the presence of SCF decreased the impact strength in comparison to the matrix material, but was slightly higher than PA6.
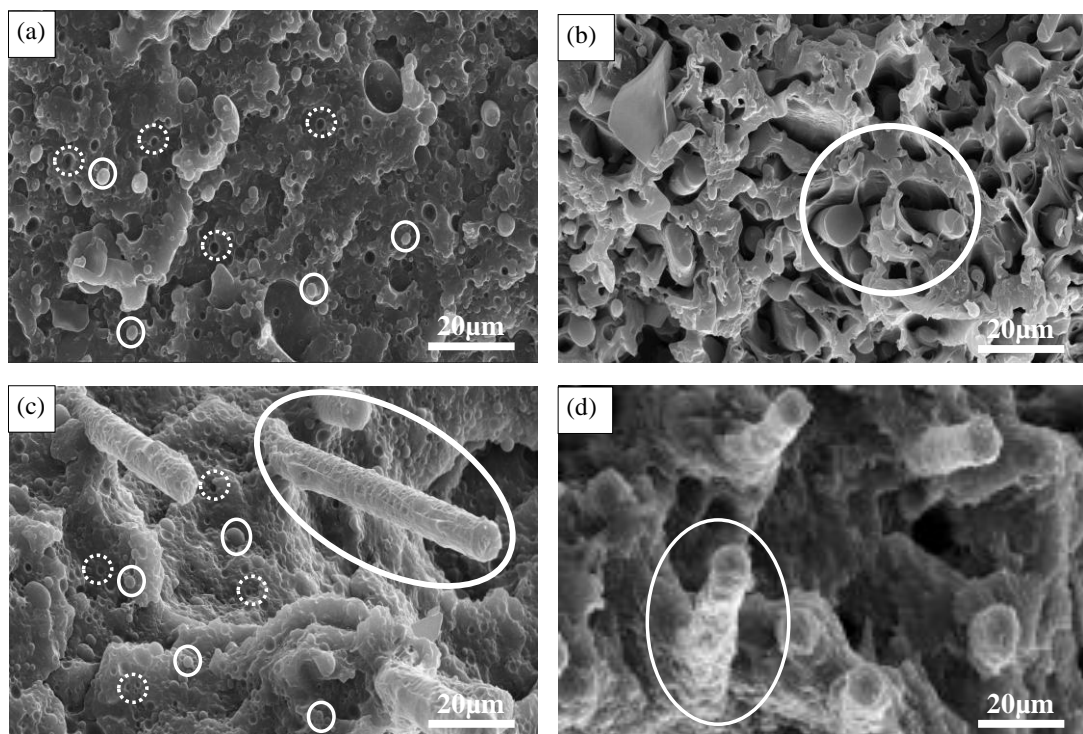
Figure 3.19: Impact fractography of a) CM0 (matrix blend), b) CM1-3 wt% SCF , c) CM2-6 wt% SCF and d) CM4-15wt% SCF composites

3.7. Fractography of PA6, matrix blend (PA6/PP/PP-g-MA) and composite after PP etching

The matrix blend (PA6/PP/PP-g-MA) and composites (PA6/PP/PP-g-MA/SCF) were dipped in liquid nitrogen for five minutes and then broke manually which was considered as cryogenically fractured. The fracture end of composite samples was cut into small fragments (13 x 5 x 3.2 mm^3) and PP was etched using xylene as solvent at

140°C and 48 hrs of heating and refluxing using soxhlet set-up. These fractured samples were also analyzed using SEM to understand the dispersion of PP. Similar to explanation given for PA6/PP blends where PP content was varied from 5-50 wt% section 2.6. Since PP is removed by dissolution, only PA6/SCF will be visible while studying the fractography of cryogenically fractured samples.

As shown in Figure 3.20a-d, the structure of PP in composite differs with increase in SCF content. For matrix blend in Figure 3.20a, it can be seen that PP droplets are of two different shapes, spherical as well as elongated elliptical shape. Mostly PP was in spherical shape, and few PP droplets had higher radii, which resembles the morphology of compatibilized PA6/PP blend (Figure 2.14d). For composite CM1 (Figure 3.20b), it is seen that PP domains are bigger and are mostly elongated elliptical in shape which resembles uncompatibilized blend.
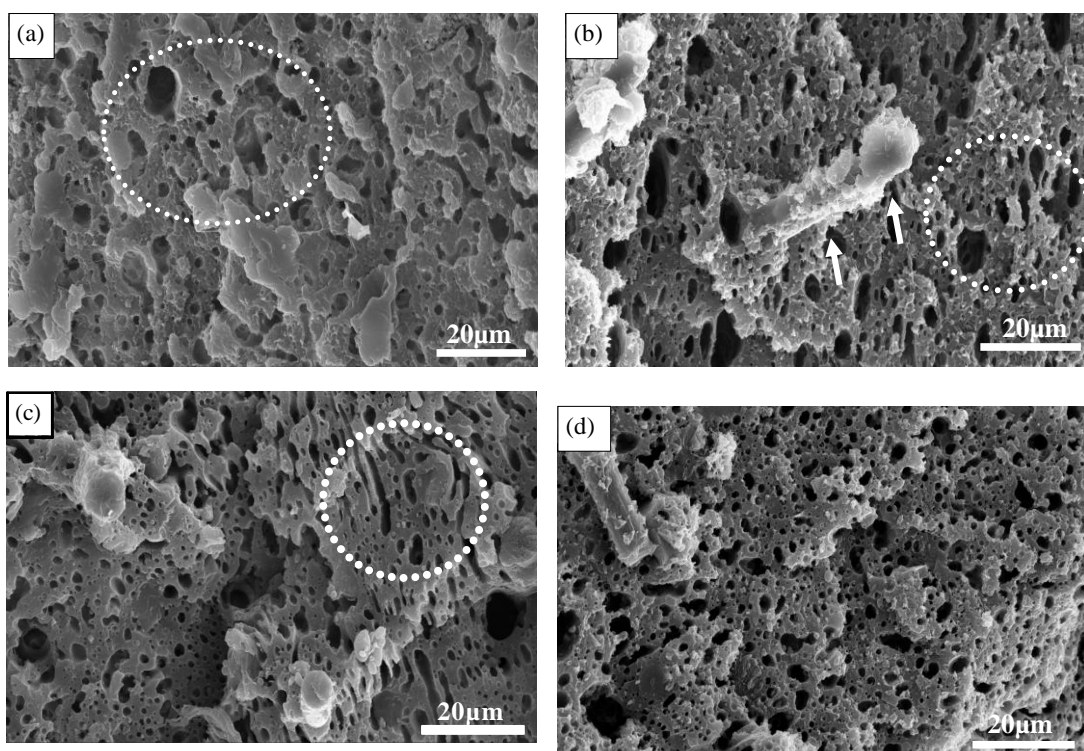
Figure 3.20: PP domain size distribution in a) CM0 (matrix blend), b) CM1-3 wt% SCF content, c) CM2-6 wt% SCF content and d) CM4-15wt% SCF content composites. Dotted circle: etched PP, Arrow: SCF

Cohesive failure is observed in Figure 3.20b i.e., SCF is covered with matrix indicating better interaction between PA6/SCF, as also seen in FTIR of CM1

composite. Hence it can be deduced that at lower SCF content, the reaction between "PA6- epoxy on SCF" becomes more feasible than "PA6-PP/PP-g-MA". CM2 also resembles the uncompatibilized blend morphology (Figure 3.20c). As the SCF content increases, in (CM3-CM4 Figure 3.20d), PP is well dispersed, domain size is found to be low and spherical in shape, in comparison to CM1. The PP domains become finer and resemble compatibilized blend morphology with increase in SCF content. As seen in FTIR, the composites CM3-CM4 resembled the blend (CM0) wavelet. Similarly, the morphology of CM3-CM4 also resembles CM0 which proves the effective compatibilization of the blend. It could be observed that the surface of SCF is covered with matrix in Figure 3.20b-d, which shows better compatibility between fibre and the matrix, and the pull-out of the fibres is low. At lower SCF content, "PA6 – epoxy on SCF" reaction is favored, but as SCF content increases the reaction 1 and reaction 2 shown in Figure 3.6 are occurring simultaneously.

3.8. Residual fibre length in composites

Optical microscopy (Metavis U-400) was used for finding the residual fibre length in the samples post injection molding using surface polishing technique. Samples were polished carefully with fine sand paper to remove the outermost matrix layer so that fibre length can be measured accurately using optical microscope (reflection mode) and toupview software. Alternatively, matrix was burnt by keeping the composite specimens at 550°C for 20 min. Here a sample from gripping portion of the tensile test was used. After degradation of the matrix, fibres were collected carefully, washed in acetone and dried. Since PA6, PP and PP-g-MA have degradation temperatures below 550°C and carbon fibres remains stable until 2000°C, this method was adopted to measure the residual fibre length using laser scanning confocal microscope (Leica DM18).

Composite strength and stiffness depends on fibre diameter and residual fibre length especially when extrusion and injection molding are involved due to their extreme shearing effects. The reduction in average fibre length (from original length of 1000 μm to 75 μm) is due to breakage occurring in twin screw extrusion and injection molding as the fibre is very weak in transverse direction and also due to the shearing effects involved in processing such as fibre-screw attrition and fibre-fibre attrition

(Karsli, 2013; Luo, 2014; Zhang, 2015). Since PA6/PP is a thermoplastic blend, when SCF is added, due to the high screw speed, the fibres are sheared while getting dispersed in the melted blend matrix. The major reduction of fibre length could have occurred in extrusion process only. Residual fibre length should be equal or higher than the critical fibre length to get the reinforcing effect of fibres. Since no change in fibre diameter was observed, only fibre lengths and their distribution in all composites (for a fixed content of 5 wt% SCF) were studied. From the surface polishing method (not shown) it could be understood that the average residual fibre length varies from 50-125 μm, lowest being for NPCM3, followed by NPCM4 and then by NPCM5 composites. Average fibre length of more than 100 μm was observed for NPCM0 which does not have any compatibilizer, which could be due to lower interaction between PA6 and PP. Zhang et al.(*Zhang, 2015*) reported a critical fibre length of 260 μm for PA6/CF composite, but no data has been reported for PA6/PP/PP-g-MA/SCF composite.
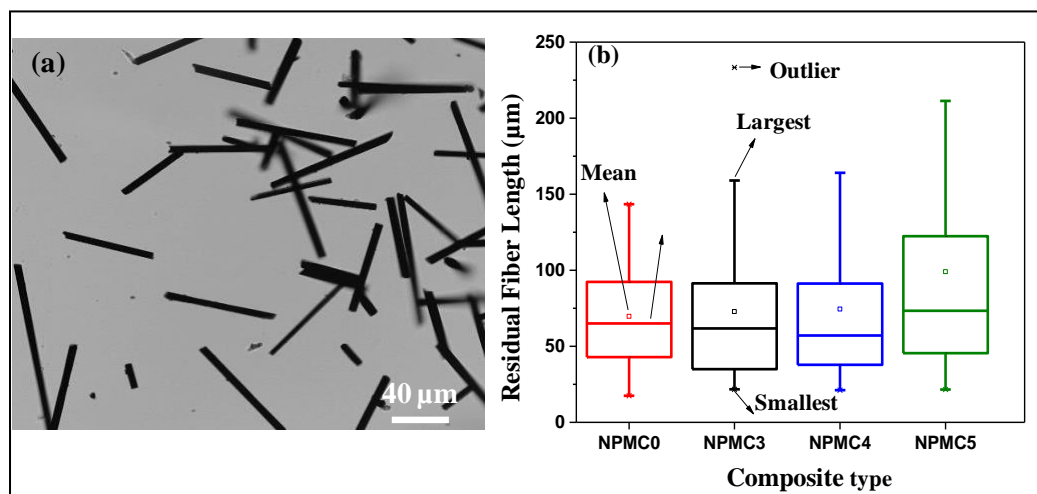
Figure 3.21: a) Optical microscopy of residual fibres after removing matrix and b) residual length distribution of fibres in injection molded composites made with varying compatibilizer content (0, 3, 4 and 5 phr)

Figure 3.21a shows the residual fibres in a composite (NPCM3) after removing the matrix. Similarly, the residual fibre lengths (50 readings) of each composite were measured and represented as a box-and-whiskers plot in Figure 3.21b. This plot gives the lowest, highest and mean value of the residual fibre lengths of the each composite.

It could be understood that the average residual fibre length is same as that of surface polishing method, but the highest values were observed for NPCM5 composite. Slight increase in residual fibre length was observed with increase in compatibilizer content and average residual fibre length was found to be around 75 μm. The reduction in average fibre length (from original length of 1000 μm to 75 μm) is due to breakage occurring in extrusion and injection molding as the fibre is very weak in transverse direction and also shearing effects involved in processing. It is assumed that ~75 μm of residual fibre length is almost equal to the critical fibre length of SCF fibres in PA6/PP/PP-g-MA/SCF composite because 140 % increase in tensile strength (after water saturation) was observed with the addition of SCF fibres
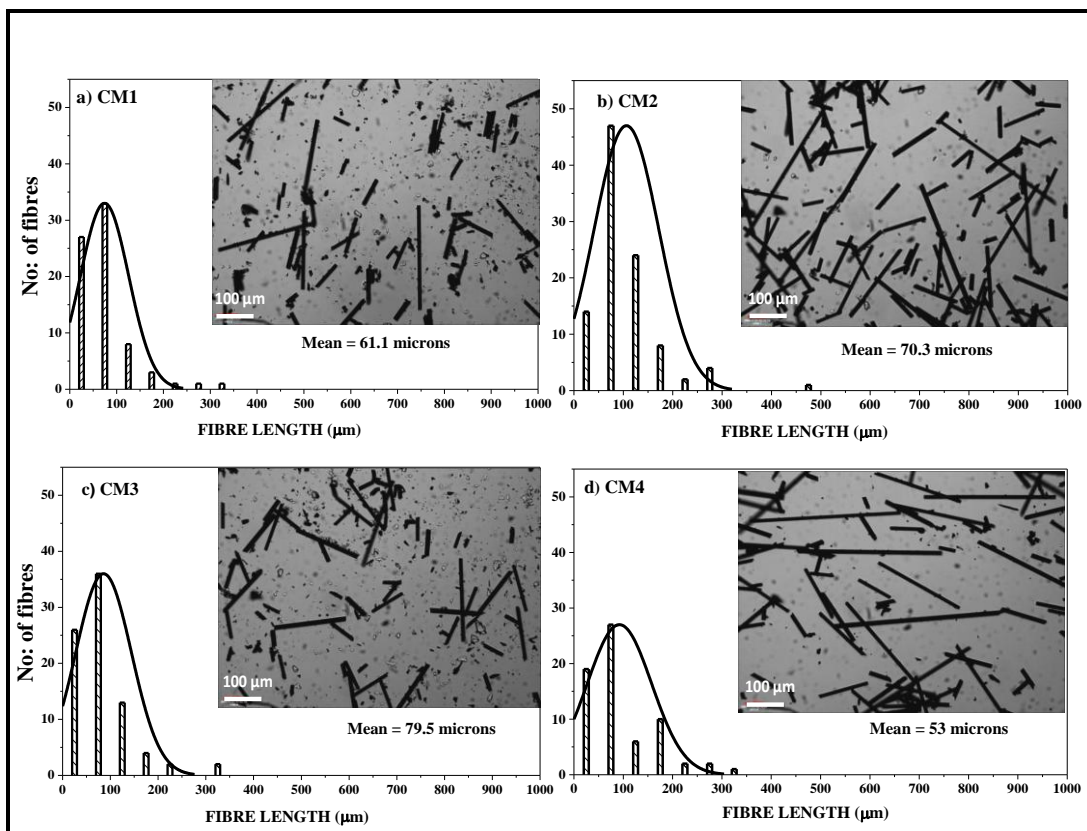
Figure 3.22: Residual fibre length distribution in composites made with varying SCF content CM1 to CM4 (3, 6, 9 and 15 wt%)

Zhang et al. (*Zhang, 2015*) also reported the reduction of the fibre length from 12 mm to 1.9 mm for PA6/ 5wt % CF composite processed via melt pultrusion followed by injection molding and their study showed that fibre length is decreasing further with increase in wt % of CF. Hence to obtain the reinforcing effect of the fibres, it is important to increase the residual fibre length of the SCF fibres to above their critical fibre lengths by adjusting the processing parameters, which is a challenging especially

during extrusion. Figure 3.22, illustrates the fibre length distribution post injection molding found using matrix burn-out method for the samples with varying SCF content (CM1 to CM4). The fibre length reduces during processing due to fibre-matrix attrition, fibre-screw attrition and fibre-fibre attrition (*Karsli, 2013*; *Luo, 2014*; *Zhang, 2015*). From this analysis it was found that the residual fibre length increases up to 9 wt% SCF (CM3) content and decreases for 15 wt% SCF content. With increase in the residual fibre length, the tensile strength of the composites increases as the fibre-matrix interaction improves due to the higher surface area of interaction. Considering CM1, the lower fibre length might be due to shear on SCF by highly viscous matrix and the different melting points of the matrix components. While in CM2 & CM3 the increase in SCF length could be due to reduced fibre-matrix attrition, but in CM4, fibre-fibre attrition might have led to lower residual fibre length.

From Figure 3.22, it can be seen that, maximum number of fibres are in the range of 20-100 μm length. But, the range of fibre length is 20-320 μm, except for CM2 having a range of 20-470 μm. Hence the reduction in fibre length is around 90% compared to the original length of 1000 μm. The average fibre length in CM1 was 61.1 μm, CM2 was 70.3 μm, CM3 was 79.5 μm and CM4 was 53μm. Comparing the tensile strength results, it can be seen that strength increased with either increase in fibre length (CM1-CM3) or the fibre content (CM1-CM4). It is known that the reinforcing effect of fibre can be obtained only if the fibre length is greater than the critical fibre length (*Monetfe, 1993*). From this study it could be understood that critical fibre length is around 50-80 μm for SCF. As mentioned above, the fibre length and dispersion are very crucial factors to obtain higher strength and stiffness in composites. In this study, in comparison to pure PA6 in dry and wet state, the modulus was 2.5 times and 9.2 times higher for CM4 composite. This significant increase shows the reinforcing effect of SCF even at such lower residual fibre length. From literature it was also understood that maximum number of fibres have 50-100 μm length irrespective of starting length of the SCF (*Karsli, 2013*). Hence the critical fibre length could be in the range of 50-100 μm. But we were unable to measure it using microbond technique and single fibre fragmentation technique due to the matrix blend's high melting point and high viscosity.

3.9. Conclusion:

- **Effect of PP-g-MA compatibilizer content on composite properties**

i. PA6/PP/SCF composites with and without water saturation has been studied. With increase in the compatibilizer content from 3 or 4 to 5 phr, tensile strength, stiffness and impact strength decreased slightly, but the elongation increased. Around 40 % increase in tensile strength was observed due to the effect of 5 wt % SCF reinforcement for 3phr PP-g-MA content.

ii. The composite containing 3 phr PP-g-MA had only 10% reduction in tensile strength, 30% reduction in modulus and 56% increase in elongation due to water absorption in comparison to dry sample of same composition.

iii. From SEM fractographs it was found that brittle fracture was seen for PA6/PP/SCF system, but with the addition of compatibilizer, the fracture patterns were more of ductile in nature (matrix pull out) indicating the good interfacial adhesion within the matrix (blend) and also between matrix and fibre. But at higher PP-g-MA content (5 phr), the matrix gets plasticized leading to early yielding and low tensile strength of the composite system.

iv. Fibre breakage during processing resulted in residual fibre length of around 75 μm in case of composites with 3phr or 4phr compatibilizer and 100 μm in the case of 5 phr compatibilizer. From the experimental results, it was also found that 3 phr PP-g-MA is the optimum compatibilizer content for PA6/PP/SCF composites which was also confirmed using Grey relational analysis.

v. 3 phr PP-g-MA is fixed as optimum compatibilizer content for PA6/PP/SCF based composites.

- **Effect of SCF content on composite properties**

i. PA6/PP/PP-g-MA blend based SCF reinforced composites were studied by varying the SCF content (3, 6, 9 and 15 wt%). From FTIR results, the interaction between fibre and matrix was found and, at lower SCF content "PA6- Epoxy on SCF" reaction was prominent and at higher SCF content "PA6/PP/PP-g-MA compatibilization" reaction was found to be prominent in addition to the above reaction.

ii. Water absorption reduced with addition of PP to 60% and on further addition of SCF (CM4) the value reduces to 72% in comparison to pure PA6 value indicating the synergistic effect of PP and SCF in reducing the percentage of water absorption.

iii. For both dry and wet composites, tensile strength and modulus increased with SCF content, whereas the elongation at break decreased drastically and saturated at 6 wt% SCF content. The reduction in tensile strength of composites post water absorption was 10-15% in comparison to its dry counterparts. At 15 wt% SCF, composites revealed 55% and 133% higher strength than PA6/PP/PP-g-MA blend in dry and wet condition respectively indicating the importance of these composites in high humid applications.

iv. Post water absorption, tensile modulus reduction was 18-20% in all composites. At 15 wt% SCF, composites showed 3.5 fold increase and 5.5 fold increase in tensile modulus in comparison to PA6/PP/PP-g-MA blend in dry and wet condition respectively. The drastic increase in modulus especially in wet state shows good dispersion and good packing of SCF in the composite.

v. The tensile fracture occurred due to fibrillation of matrix initially and at higher SCF content, fibre pull out led to fracture. Post water absorption, tensile fractured samples showed more pull out, showing reduction in interfacial adhesion due to water absorption which was also seen in FTIR.

vi. Impact strength of composite was much lesser than the matrix blend, but almost equivalent to pure PA6. Impact fractography showed that the fibres act as stress concentrators and cavitation of 3μm size PP droplets caused the fracture of the composites.

vii. From residual fibre length measurements, it was found that most fibres had 20-100 μm length and the critical fibre length could be in the range of 50- 80 μm for composites.

viii. Low residual fibre length (75 μm in case of 3 and 4 phr, 53 μm in case of 15 wt%) resulted in higher tensile strength which could be due to the good dispersion, good packing and less number of defects in the composite.

CHAPTER 4:

Processing and testing of PA6 blend based UDCF Laminate composites

4.0. Introduction

Compression molding is the widely used technique for manufacturing of laminate composite. It is also one of the techniques to make thermoplastic laminate composites (film stacking method). Modified blend as discussed in chapter 2 (PA6/PP 70/30 wt%) and chapter 3 (3 phr PP-g-MA) will be used as matrix material. In this chapter, the optimization of parameters for processing of matrix sheet and UDCF composite laminate has been discussed in detail. The matrix sheet and composite laminates were processed using compression molding machine (in-house modified). The mold having a size is 20 x 27 cm^2 was used for making both matrix sheets as well as composite laminates. The preforms or reinforcement used was UDCF. Desizing of UDCF was tried and found that, it further increases the brittleness of the fibres and also it became difficult to handle the fibre rovings. Hence the UDCF and BDCF reinforcements were used with the sizing agent (3 wt % epoxy resin). The rovings in UDCF fabric are 12K (12000 single fibres in each roving) and in BDCF (bidirectional carbon fabric) rovings are 3K type (3000 single fibres in each roving). UDCF is generally used to improve the tensile strength of the composite in longitudinal direction and BDCF is generally used to make composites having similar properties in longitudinal and transverse directions.

4.1. Processing of PA6 blend (matrix) sheets using Compression molding

The optimized conditions for making matrix sheet are as follows. 1mm spacer plate is used for making the matrix sheet of thickness of 700-900 µm. The top and bottom mold temperatures were set at 240°C and 260°C respectively. Once the bottom mold is heated to 230°C, mold is opened and high viscous silicone oil is applied as release agent. Immediately after applying the release agent, 35 gm of matrix pellets were spread uniformly using wooden spatula and the mold was closed. Once the bottom mold reaches 240°C, pressure of 80 bar (Figure 4.1) is applied for a period of 30 minutes while the temperature of the bottom mold increases and stabilizes at 260 °C.

The heaters are turned off and water is circulated for cooling the mold while specimen is under 80 bar pressure. Once the mold temperature reaches 100 °C, the pressure is reduced to 1 bar and mold is opened. With the help of ejector pins, spacer plate is moved up and the sheet is removed from the lower mold. Overall time taken for making matrix sheet is 2.5 hrs. The flow rate of cooling water is 4 l/min and cooling rate is 7 °C/min.
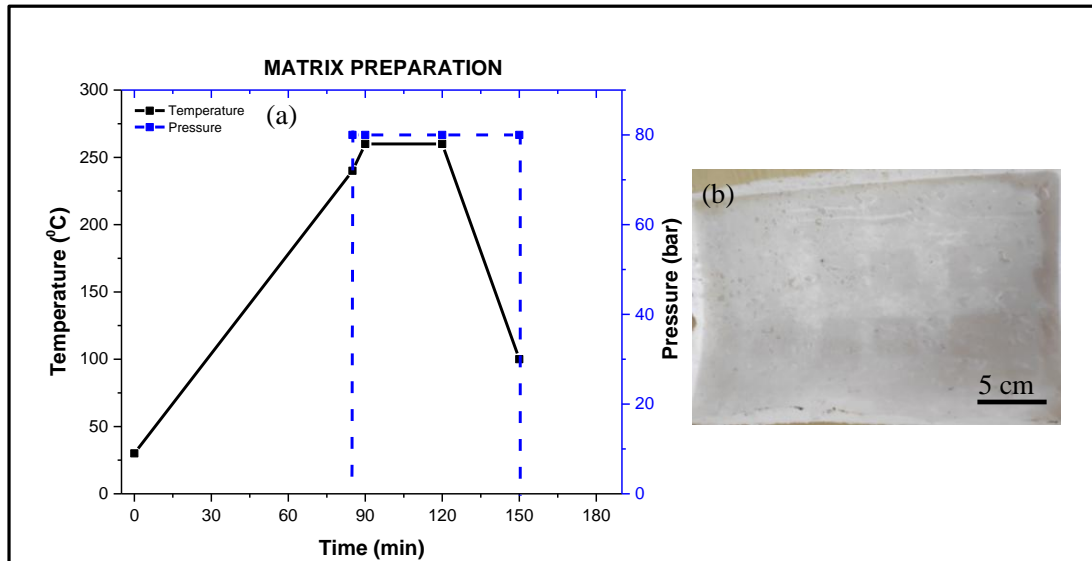
Figure 4.1: a) Temperature-time-pressure plot for compression molding of matrix sheet b) Matrix blend sheet of 900 μm thickness c) Pellets of PA6/PP-g-MA blend spread on bottom mold of compression molding machine

4.2. Processing of PA6 blend based UDCF Composites (Laminates)
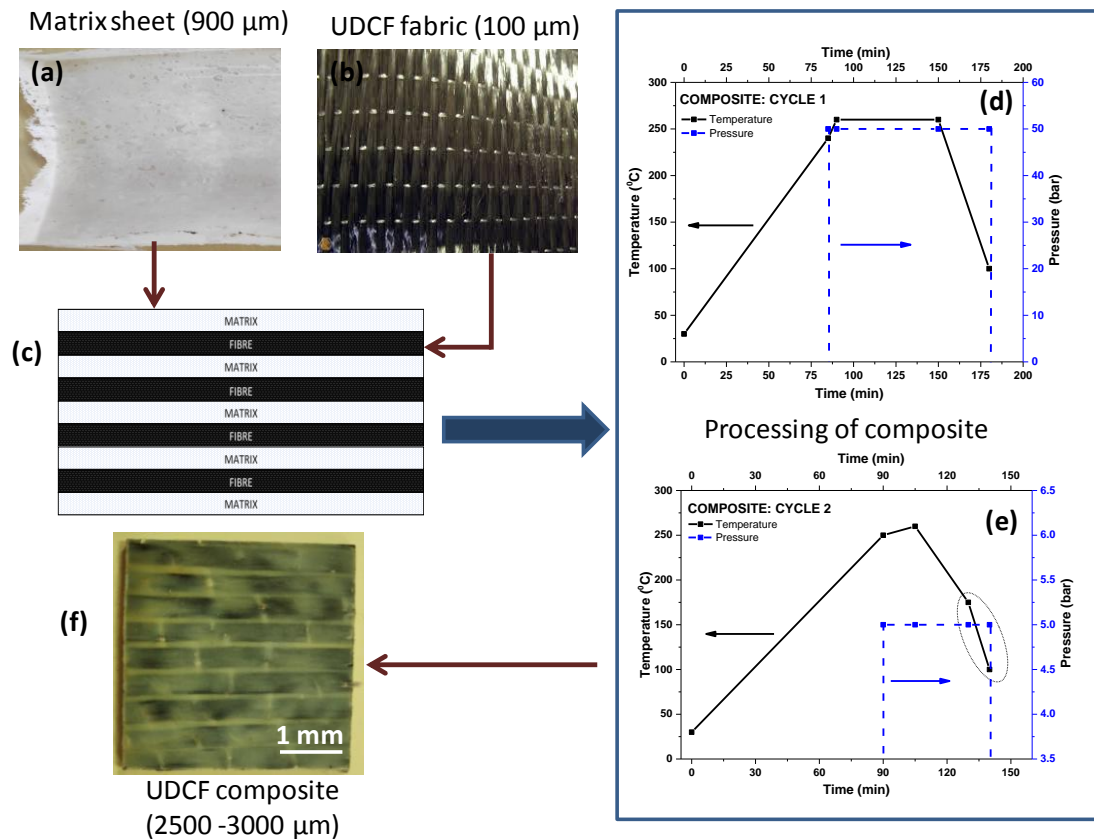
Figure 4.2: a) Blend matrix sheet of 900 µm thickness b) UDCF mat of 100 µm thickness, c) Schematic of alternate layer of matrix and fibre as arranged in compression molding machine. Processing of composite d) Cycle-1, e) Cycle-2, dotted oval represents the water cooled zone and f) final composite.

Optimum conditions for making UDCF Composites are discussed in this paragraph. Trials followed prior to reaching optimum conditions are given in section 4.9. Unlike processing of matrix sheets, UDCF composites are made using two cycles as shown in Figure 4.2. The first cycle ensures that the fibre and matrix layers are compacted without any misalignment resulting in 3-4 mm thick laminate, whereas the second cycle aids in better wetting of fibre and removal of excess matrix due to more compaction (spacer plate of 2 mm instead of 4 mm is used) resulting in 2-3 mm thin laminate composite. Details of Cycle 1 and 2 are given below.

Cycle-1 used to process thick composite laminate

- Weigh the matrix sheets and fibres (UDCF fabric sheets)

- Apply thin layer of high viscous silicone oil on 4 mm spacer plate

- Place the alternating layers of matrix and fibre sheets/mats on the mold (4 layers of UDCF mats, 5 layers of matrix sheets) and close the mold (Figure 4.2 a-c)

- The top and bottom mold temperature is set at 240°C and 260°C respectively

- Once the bottom mold reaches 240°C, apply 50 bar pressure (Figure 4.2d)

- Hold it for 60 min and turn off the heater

- Water is used for cooling the composite sample. Once the temperature reaches 100°C , composite sample are removed using ejector pins

- Composite having a final thickness of 3-4 mm with all fibres aligned in longitudinal direction are obtained

Cycle-2 used to process thin (2-3 mm) composite laminate:

Further processing of the composite obtained from cycle-1 with thickness of 4mm is carried out so as to decrease the composite thickness to 2mm, so that fibre wettability can be improved. Since, thermoplastic matrix is used; the reprocessing of composite is feasible and is advantageous in obtaining better fibre-matrix adhesion. The steps followed in cycle-2 are given below:

- The excess matrix at the sides of the composite is removed and weighed

- Apply thin layer of high viscous silicone oil on 2mm spacer plate

- Place the composite (obtained from cycle-1) in the mold and close the mold

- The top and bottom mold temperature is set as 240°C and 260°C respectively

- Once the bottom mold reaches 250°C, apply 5 bar pressure (Figure 4.2e)

- Hold it for 10-15 min until the excess matrix seeps out of the mold

- Turn off the heater, and allow the sample to be air cooled up to 175°C

- Then the sample was water cooled up to 100°C

- Remove the composite sample along with spacer plate from the mold which is found to have a thickness of 2-3 mm wherein all fibres are aligned in longitudinal direction

4.3. Mechanical properties of PA6 blend based UDCF Composites

4.3.1. Physical Characteristics of UDCF composite laminates

While processing, the weight of the matrix and weight of fibre (reinforcement) is noted to calculate the weight fraction of the fibres in the composite. The weight fraction of fibre in composite was ~30%. This can be converted to volume fraction by knowing the density of the composite or fibre and matrix. Theoretically using the eqn.4.1, the density of the composite is found to be 1.17 g/cm^3.

$$\rho_c = \frac{1}{(W_f / \rho_f) + (W_m / \rho_m)} \qquad \text{(eqn. 4.1)}$$

But experimentally, the density of the sample found using its mass and volume is 1.04 g/cm^3. This shows the presence of voids in the composite sample. The density difference is 12.8%.

Similarly the strength and modulus of the composite can be predicted theoretically using the rule of mixtures as shown in eqn.4.2 and eqn.4.3.

$$E_c = E_m V_m + E_f V_f \qquad \text{(eqn. 4.2)}$$
$$\sigma_c = \sigma_m V_m + \sigma_f V_f \qquad \text{(eqn. 4.3)}$$

Where, E_c, E_m, and E_f are the elastic modulus of the composite, matrix and fibre measured in longitudinal direction respectively; V_m and V_f is the volume fraction of matrix and fibre respectively. σ_c, σ_m and σ_f are the tensile strength of composite, matrix and fibre respectively. With the conversion of weight fraction to volume fraction using density data, the volume fraction of fibres in composite was around 20 vol%. Hence the maximum theoretical tensile modulus and tensile strength was calculated to be 46.8 GPa and 586 MPa respectively. The tensile strength and modulus of the matrix sheet was found experimentally (section 4.7) and that of fibre was taken from the datasheet as mentioned in the Chapter 1. Experimentally, tensile strength and modulus of the composite was obtained by performing tests on Universal Testing Machine (UTM) as discussed below.

4.3.2. Tensile properties of the composite laminates

Tensile test of the UDCF composite laminates was conducted as per ASTM D3039, where the specimen size was 250 x 12.5 x (2-3) mm^3. Samples from the composite sheet were cut using diamond knife. For UDCF composites, end tabs are used for

better gripping of samples during testing. Generally, ±45° glass fibre reinforced epoxy composite blocks are used as end tabs. These tabs are attached to the composite specimen ends using suitable adhesive such as loctite 406. Other than end tabs, emery paper can be used around the composite ends while testing the samples. In this study, emery paper instead of tabs was used to enhance the gripping. It is reported that it is very difficult to conduct the tensile strength of UDCF composite, as the strength of the fibres are very high in longitudinal direction, and the exact fracture of the fibre may not be obtained if the gripping is poor (*Agarwal, 2006*; *Chawla, 1998*). UTM (ADMET, Figure 4.3a) with load cell of 200 kN was used for conducting the tensile test. Strain gauge was used for obtaining the modulus data (Figure 4.3c). Strain gauges were removed once the modulus was calculated. In this study, satisfactory gripping (no slippage) was obtained using emery paper (Figure 4.3b). The composite samples had the average tensile strength of 353 MPa as shown in Table 4.1. Compared to the theoretical value of 586 MPa, the obtained experimental value is 39% lower. Generally, the factors influencing the tensile strength of composite laminates are listed below:

a) Alignment of fibres
b) Non-uniformity of fibre length
c) Interfacial adhesion
d) Residual stresses
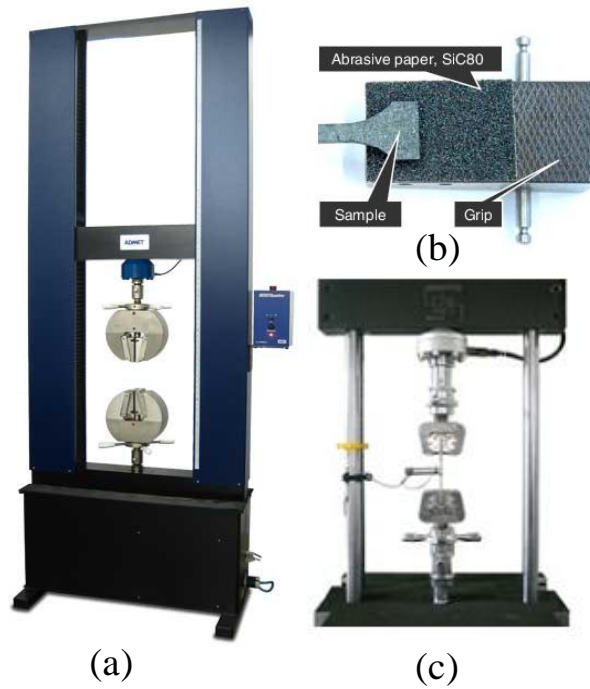
Figure 4.3: Representative image of a) Tensile test set-up (UTM), b) using abrasive/emery paper for gripping of tensile specimen, and c) strain gauge fixture for measuring tensile modulus

Sample	Dimension (w x t) mm	Load (N)	Stress (MPa)	Dimension (w x t) mm	Load (N)	Stress (MPa)
Table 4.1: Tensile strength of PA6/PP/PP-g-MA/UDCF composite laminates in dry and wet states (in longitudinal direction)						
	Dry			**Wet**		
1	12.45 x 2.97	14.09	381	12.97 x 2.88	10.43	279
2	14 x 3.15	15.38	349	13.03 x 2.94	11.43	298
3	12.83 x 2.72	13.21	379	13.01 x 2.96	8.60	223
4	12.83 x 2.95	14.57	385			
5	12.90 x 2.88	12.28	331			
6	12.89 x 3	11.37	294			
		Average	**353 MPa**		**Average**	**267 MPa**

During the tensile test, owing to difference in elongation between the fibre and matrix, the fibres break first leading to the fracture of the specimen. Accordingly, the carbon fibres broke first which led to matrix breakage during the tensile test. Interfacial adhesion plays a major role in providing strength to the composites, as the load has to be transferred from matrix to fibre. Stronger the interface better the stress transfer. In this case, the interfacial adhesion between the fibre and matrix was tested using short beam shear test which is discussed in the following sub section. Inter laminar shear strength (ILSS) value obtained was lower than epoxy/UDCF composites; due to which lower tensile strength was observed. The lower ILSS value along with lower tensile strength shows the presence of interfacial defects. Residual stresses are dependent on orientation of the fibres in the composite. If the orientation of the fibre is not the same in every layer, it might cause residual stresses. In this composite, some misalignment was observed, as it was processed twice and the fibres tend to move along with the matrix due to the higher viscosity of the matrix material. This could have also led to the lower tensile strength of composites. Also, the difference in thermal expansion of matrix and fibre leads to residual stresses in the composite. The PA6 has coefficient of thermal expansion (CTE) of 95×10^{-6} K^{-1}, whereas the carbon fibre has CTE of -0.83×10^{-6} K^{-1} in longitudinal direction and 6.84×10^{-6} K^{-1} in transverse direction (*Guo, 2019*) as shown in Table 1.1 of chapter 1.
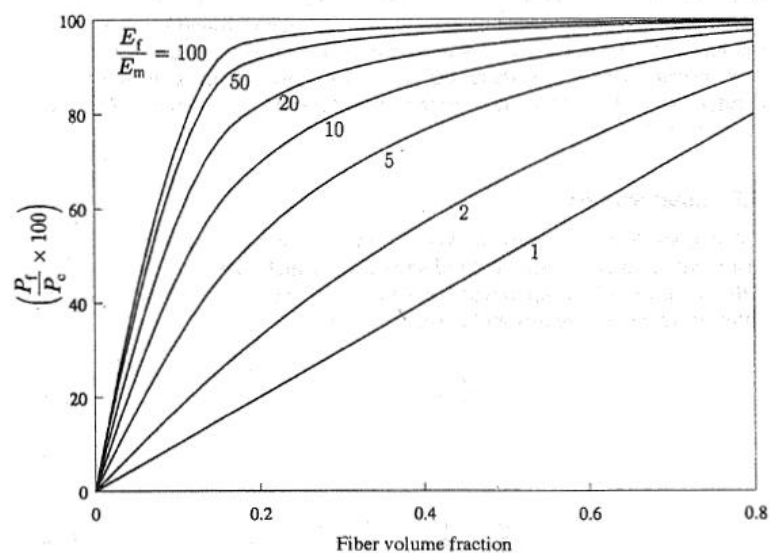
Figure 4.4: Percentage load carried by fibres in a unidirectional composite loaded in the longitudinal direction. Where, P_f is load carried by fibre, P_c is load carried by composite, E_f is tensile modulus of fibre and E_m is tensile modulus of matrix (*Agarwal, 2006*)

The tensile strength of the composite is dependent on type of fibre used, its distribution in matrix and volume fraction of fibre in the composite. The fraction of load carried by the fibres can be calculated in terms of the ratio of the tensile modulus of the fibre to the matrix as shown in the Figure 4.4 (*Agarwal, 2006*). In this case, the modulus ratio is around 109, so the percent load carried by fibres is 96 at 20 % volume fraction of the fibre as per the Figure 4.4. If the modulus difference between the fibre and the matrix is high, then lower amount of fibre volume fraction can be used to obtain maximum load sharing as seen in Figure 4.5. Above 40 vol% fibre, no change in load sharing is seen in the composite as shown in Figure 4.4. Hence, volume fraction of 20-30% is sufficient for utilizing the maximum fraction of the load carried by the fibre. So the volume fraction was fixed as 20 vol% in this study.

The behavior of composite during tensile test depends on the individual tensile strength of the matrix and the fibre. If the matrix and fibre shows linear stress-strain curves (like epoxy-glass composite) under uniaxial tensile loading, then the composite will also have linear stress strain curve. If the matrix has non-linear stress strain curve, then the composite will also have non-linear stress-strain curve. With increase in fibre fraction, the behavior of composite is closer to that of the fibre. Since the current study involves thermoplastic matrix, which is non-linear in nature and volume fraction of fibre is low (20-30 %), the behavior of the composite resembles matrix i.e. non-linear.

From the stress-strain curve of composite, it was seen that initially elastic deformation dominates even above 1.5% strain which corresponds to the elongation at break of the fibre. The overall elongation of composite was found to be 13.8%, which is eight-fold higher than the fibre "elongation at break". Hence, composite is able to behave plastically up to the point of break. This shows the existence of better interfacial adhesion between the matrix and the fibre. In case of better interfacial adhesion, the load is transferred from matrix to fibre, and the matrix can withstand the load even after the fibre fails. In this case, even though the interfacial adhesion was good, the failure was due to the crack initiated by fibres at the poorly wetted zones (core regions in the rovings). Hence the micro-cracks led to breakage of matrix.

Two types of failure have been discussed widely (*Y. Ma, Ueda, 2017*), cohesive failure, where the complete matrix breaks into parts in step like fashion and other is

the adhesive failure, where the matrix slips out or delaminates from the fibres locally leading to broom like structure at the failure end. In the current study, the matrix and the "fibre attached to the matrix" broke showing cohesive failure, but the fibres in the central part of roving, which were not wetted, found dislocated from its positions looking like an adhesive failure. Assuming fibres are being wetted only on the sides (opposite surfaces), the existence of this type of interfacial adhesion is evident because the experimental value of the tensile strength is only 60% of the maximum value (theoretical value). Hence, if the wetting would have been improved, and composite with lower number of misaligned fibres would have been made, then the maximum strength of the composite could have been achieved.

The tensile modulus of the composite determines the packing of the composite as stated earlier. Here the experimental tensile modulus was found to be 27.4 GPa which is 41% lesser than the expected theoretical value. This could be due to the few unwetted fibres in thick roving. Since the core part of every roving is not fully wetted, the fibres can slide from its position easily leading to lower tensile modulus. However, the measured strength, stiffness, and elongation at break are only possible due to the better interfacial adhesion existing between the fibre and the matrix on both sides of the composite. To increase the wetting and interfacial adhesion in the entire composites, the matrix thickness has to be reduced, as it will aid in better wettability of fibre in final composite, and viscosity of the matrix should be reduced, for which plasticizer was included, which is discussed in the later section.

4.3.3. Tensile properties of the composite after water saturation (wet)

Water absorption was carried out in the similar way as explained in chapter 2. The composite laminates (prepared using compression molding) had water absorption of 7.4% which is higher than all the blends and SCF composite (prepared using injection molding). The voids formed due to the unwetted fibres in the rovings acted as spaces for storing water, which further increases the chances of water absorption at the interface. Hence due to water absorption, the interfacial adhesion would have become weaker, which could be understood using the tensile test (Table 4.1) results of the wet samples, which were 24.5% lower than dry samples. Compared to other studies where more than 50% loss in tensile strength is observed due to water absorption of laminate

composites (*Arhant, 2016*; *Pillay, 2009*), it can be seen that this low reduction (24.5%) was possible because of the presence of PP and PP-g-MA. Also, it can be understood that in PA6 based laminate composite, the water bonds with the matrix chemically. Since a modified blend has been used as matrix in this study, the water is physically occupying the voids with reduced interaction with the PA6. Hence, it is advantageous to use modified blend as matrix material for making composite laminates which are intended for humid applications.

4.3.4. *Compression properties of composite laminates*

Further to analyze the composite mechanical behavior, shear compression test (ASTM D3410) was conducted. The compression test of UD composites can be conducted in three ways:

a) End loading Compression – ASTM D695-15

b) Shear loading compression– ASTM D3410

c) Combined loading compression – ASTM D6641

The end loading compressive test is the initial compressive test designed for testing the compressive strength of unreinforced plastic materials and for composite materials having modulus up to 40 GPa. It cannot be used for UDCF composites because it involves compressing the specimen with tabs at the gripping zone which leads to micro buckling. When the composite is processed, the carbon fibre rovings tend to bend or curve depending upon the flow pattern of high viscous PA6 blend resin. In tensile test, these fibres straighten up while load is applied, whereas in compressive loads, these fibres tend to buckle and break, leading to lower compressive properties. Gripping of sample for testing was an issue in this method. The samples tend to broom at the edges if they weren't gripped properly. Another drawback of this method was that, different tests had to be conducted for measuring the modulus and strength. Modulus was determined using flat rectangular specimen and for strength, tabbed sample with lower gauge length (10 mm) had to be used. Hence, this method ASTM D695-15 was modified by Boeing and better fixtures were developed.
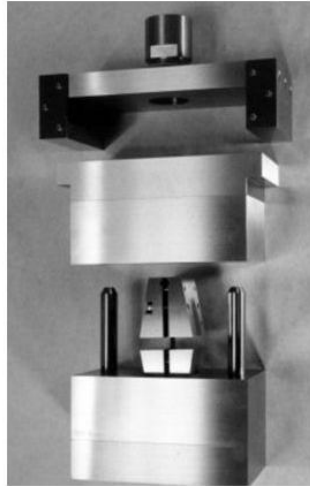
Figure 4.5: Shear compression test fixture- ASTM D3410

To overcome the effect of buckling, shear loading method ASTM D3410 (Figure 4.5) was introduced where the samples were held by the wedge shape fixture called the celanese fixture. The test length was 10 mm only and the rest of the length is under gripping zone. In this method, the buckling was avoided, but due to the higher gripping region, misalignment of samples during testing occurred leading to early failure of the material. Keeping the material parallel to test load was difficult. Hence, IITRI fixture was introduced. In this method, the guiding rods for celanese fixture was introduced which helped in making the composite to stay parallel to each other. Further, the gripping torque was also specified, so that the gripping does not cause stress on the samples. This method stands good for short fibre reinforced composite, unidirectional tape and other textile based composites. This method measures the in-plane compressive properties of the specimen and is called as "compression under shear loading" method. Since the test length is very small, the tensile and compressive forces cannot act on the sample, and the composite is forced to shear between its layers. However, the amount of bending of samples can be calculated by attaching an extensometer on both sides and according to test standards, the bending should be lower than 40% and the test stands true when the bending is lower than 10%. In this method test length as low as 5 mm can be used, but with this length the extensometer cannot be fixed, hence, 10-11mm is used as test length in this study. The only drawback of this method is the weight of the fixture is too high.

In this study, we have used ASTM-D3410 for testing the compressive properties of UDCF composites. In this method, specimen of 110 x 12.7 x (2-3) mm was used. The test length was 10 mm and other 100 mm was used gripping (top 50 mm and bottom 50 mm). This method resulted in a compressive strength of 42 MPa and modulus of 4.5 GPa. Since the Compressive stress-strain plots were non-linear, the compressive modulus was calculated by tangent method. The compressive strength was almost $1/8^{th}$ of the tensile strength of the composite, whereas the modulus was $1/6^{th}$ as that of the tensile modulus. While the test was conducted using IITRI fixture, bending was observed, but the exact values of compression was measured. The specimens were used directly without tabs. From the optical microscopic analysis of the samples, it was understood that due to the ductility of matrix and unwetted core fibres, the samples tend to bend along with the fibres as the fibres can slide within the matrix (instead of shearing). The other factor is that the tensile strength is influenced by the fibre properties whereas the compression strength is influenced by the fibre micro-buckling, matrix yielding, debonding, transverse tensile failure and shear failure. Here the un-wetted fibres aided in bending of matrix and widened the space between the matrix and fibre leading to lowering of the compressive strength. The fibres attached to matrix did not delaminate and no shearing effect was found in the samples. With comparison to literature, it was found that at shear loading, PA6/UDCF with 40 vol% CF gives 22-27 MPa strength (*Botelho, 2003*), so the values obtained in this study is comparable to the literature value.

4.3.5. *Impact strength of composite laminates*

The impact strength of the UDCF composite was found using low velocity impact (LVI) test ASTM D5420-16. In this method, composite specimen of 40 x 40 x (2-3) mm is placed on the bottom support and is hit by the free falling hemispherical tup. The height from which the tup is falling and weight of tup can be varied and the corresponding energy imposed on the sample is calculated using potential energy principle in terms of joules. For laminate composites, izod and charpy impact test cannot be conducted as the composite fracture mechanism is much complex than monolithic plastic or short fibre reinforced composites. In izod and charpy test, the notched specimens are used. So the notch act as stress concentrator and when the pendulum strikes the samples, it only provides the energy required for crack

propagation in sample as the crack has already been initiated by the notch (*Agarwal, 2006*). Since crack initiation, crack propagation and termination follows a different mechanism in UDCF laminated composite, it is important to measure the total energy required to break the sample, hence low velocity impact (LVI) test is used.

Table 4.2: LVI test data of PA6/PP/PP-g-MA/UDCF composites (dry), Weight of indenter = 1.8kg		
Height (mm)	**Energy (J)**	**Remark**
300	5.30	fine Crack found
325	5.74	fine Crack found
337	5.94	fine Crack found
350	6.18	one deep crack found (sample is intact)
400	7.06	one deep crack found (sample is intact)
425	7.50	Major fracture (two halves)
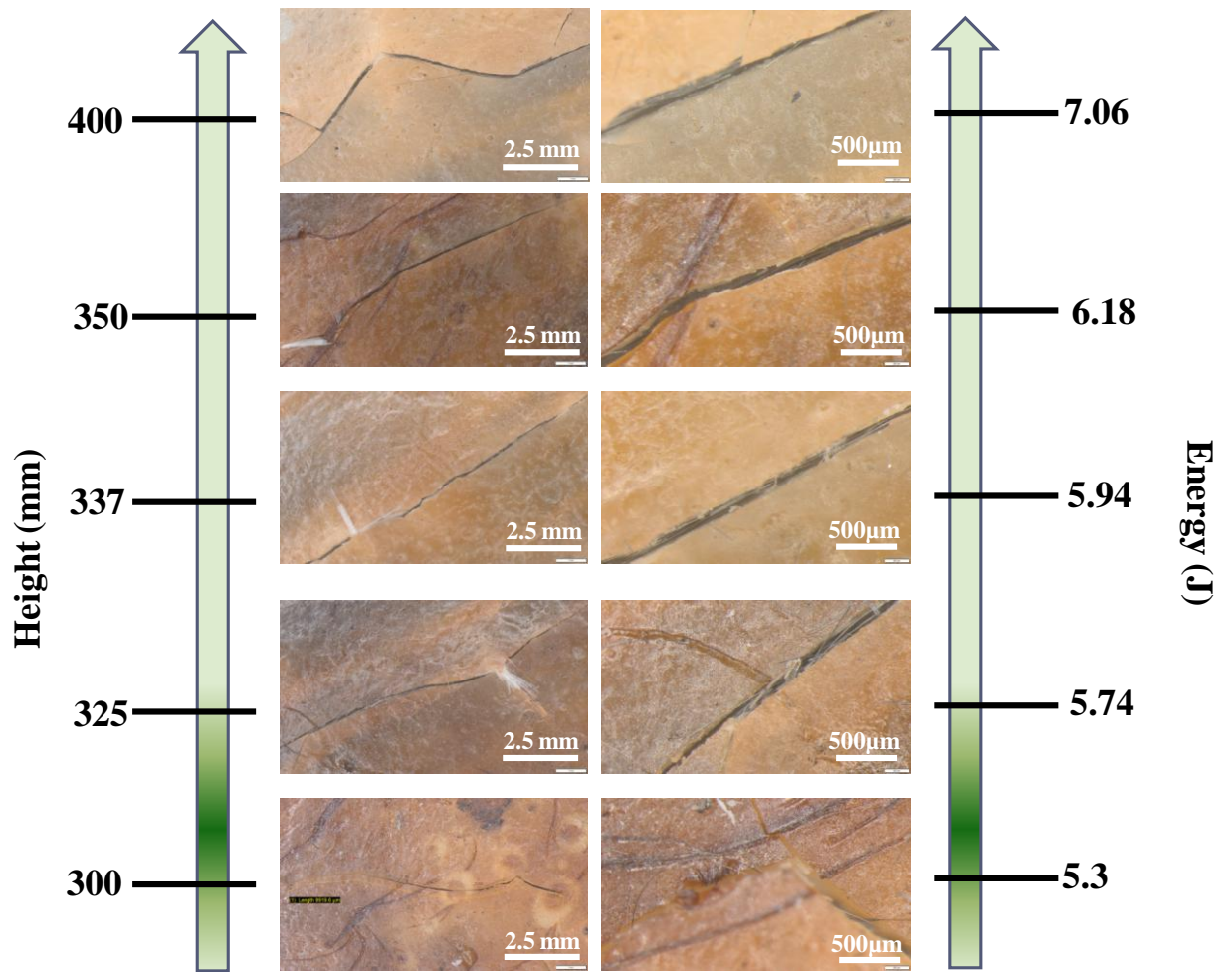
Figure 4.6: The expanding crack with increase in energy level as seen from optical microscopy at 0.8x (left) and 3.2x (right) of dry specimen (bottom surface of the tested specimen)

The reinforcement effect of UDCF was visible with the increase in the energy absorbed by the composites (compared to PA6 and PA6/SCF). In this case, two results were found, fracture or no-fracture. At particular energy level, the composite broke into two halves and at energy lower than that. For confirmation, indented samples were checked through optical microscope, but no visible cracks were found on the surface of the sample. The laminated composites absorbed 7 J of energy for fracture. The test was conducted in iterative method. The samples were struck by the tup with increasing height repeatedly on same specimen until fracture occurred. The weight of the tup or indenter was 1.8 kg. The generally observed fracture path was going through the carbon fibre roving. It is observed that when the tup strikes the sample, the interfacial zone between the matrix and the fibre absorbs the energy and dissipates to other layers. Once the threshold energy for breaking the interfacial adhesion is

reached, the crack propagates instantaneously to other layers of lamina, and eventually the composite fails. This test was repeated with different samples for different energy levels and the results are shown in Table 4.2.

The imprint of the tup on the top surface of the sample was not clearly visible, but the associated cracks can be seen at the bottom surface of the sample. Since, sudden load was applied to the sample, the sample could not bend and rather it transferred the energy from top layer to other layers and eventually it broke. Here, it can be understood, that even though the core rovings are not fully wetted, it effectively passed the load to the next layer during the impact load, where the samples are undergoing a sudden compression at particular point while the edges of the sample are undergoing tension. Hence, the stress is concentrated at the point of contact of the tup to the sample. The crack formed at the bottom surface of sample is parallel to the direction of fibre orientation. Hence, the crack travels from one weaker spot to the other in the composite. The samples were examined using optical microscopy and the crack formed at various energy levels are illustrated in Figure 4.6. From Figure 4.6, it can be understood that with increase in energy level, the crack intensity increases. Initially, at lower energy level, the cracks are very thin and extend to shorter distance where only matrix crack is observed. As the energy level increases, the crack deepens and extends further along the fibre direction. Fibre pull-out is also visible.

UDCF specimens were soaked in water for a week and impact test was carried out to measure the impact strength of the wet samples. Post water absorption the impact energy absorbed by the composites is increased. The composites did not break up to 11.4 J of energy (Table 4.3). The samples broke when the energy was further increased to 12.3J. Comparing dry and wet samples, it is understood that, the impact strength has increased by 64%. This is due to the plasticization of the matrix. The important point to be noticed from this testing is the interfacial adhesion is not severely affected during water absorption, because of which the load is effectively transferred from the matrix to the fibre. The ductility of matrix increases which is clearly visible through the wet impact results. Similar results were observed for matrix blend and SCF composite (discussed in chapter 5). Similar to dry samples, these samples also showed expanding crack with increasing energy level. The crack at 11.4J energy level resembled partial fracture of the sample (Figure 4.7) (visible crack

at the contact area hit by the tup). This showed the increased ductility of sample, as the dry samples broke into two halves, but the wet sample broke around the contact area only.

Table 4.3: LVI test data of PA6/PP/PP-g-MA/UDCF composites (wet), Weight of indenter = 1.8kg		
Height (mm)	Energy (J)	Remark
400	7.06	Indentation
500	8.8	Indentation
650	11.4	Indent with crack
700	12.3	Complete fracture

Using this method, matrix sheet of 3 mm thickness processed via compression molding was also tested and results were classified as fracture and no-fracture. At a particular energy, the matrix material broke into several pieces depending on the voids in the sheet. Some sheet broke into three parts whereas some broke into five parts. Here the energy absorbed by the matrix sample was only 1 J which was lesser than that of the composite (7 J for dry -11 J for wet). The matrix material had 24 kJ/m^2 impact strength when tested using izod impact test method, but that was injection molded notched specimen. Compared to this, compression molded specimen gave lower impact energy. This might be due to the processing effect. In injection molding, very high shear and instantaneous cooling is involved. During the shear through the single screw, the matrix components can react further and can form bonds during the process. When high pressure is applied to make the specimen, the molecules become ordered and no voids are generally found in the sample. Also, the instantaneous cooling leads to formation of γ-PA6, which also improves the ductility of the sample. Here in compression molding, the extruded pellets are directly compression molded, where the matrix components cannot mix with each other and the load applied for forming the sheet is also very small in comparison to the load applied in injection molding. The cooling time of molds in injection molding is 40 s whereas in compression molding it is around 25 min. Hence, slower cooling leads to better crystallization and hence brittle fracture could have occurred in the matrix specimen leading to low impact energy
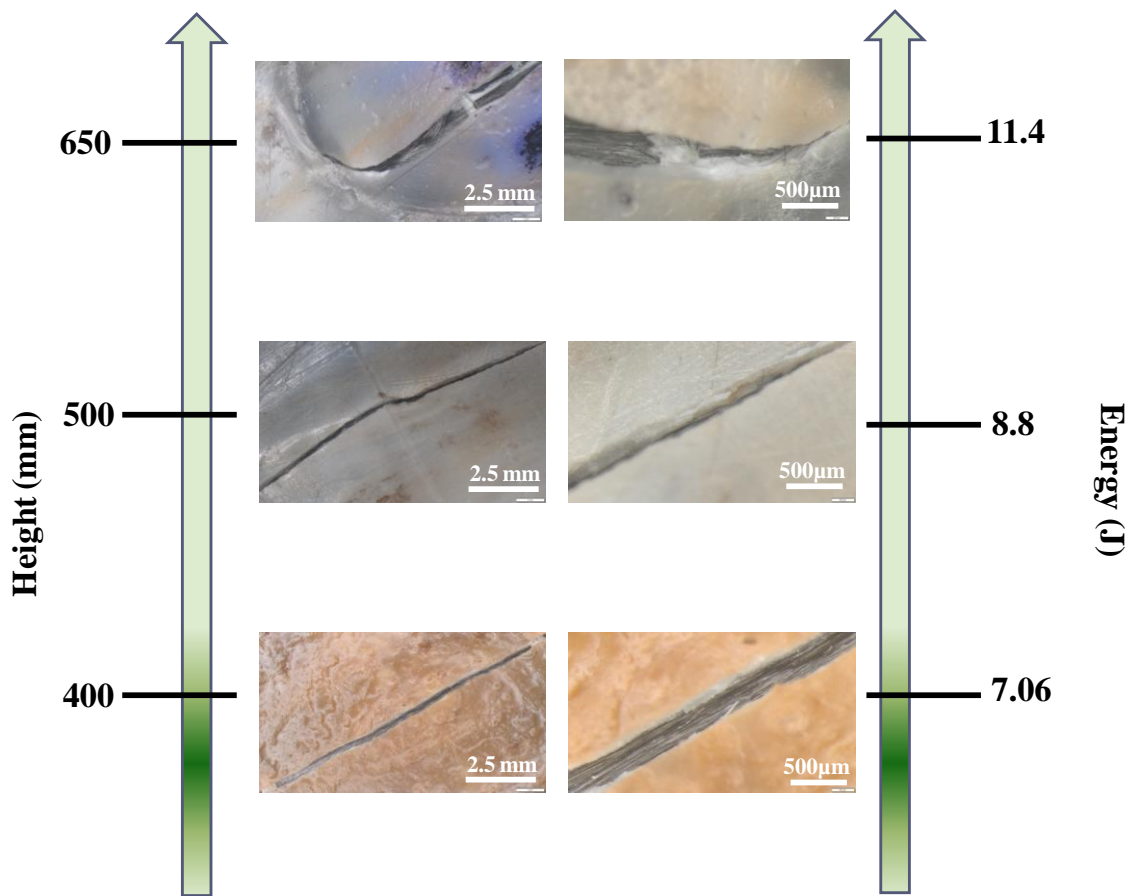
Figure 4.7: The expanding crack with increase in energy level as seen from optical microscopy of wet specimens at 0.8x (left) and 3.2x (right)

4.4. Thermal conductivity of PA6 blend based UDCF Composites

The thermal conductivity of the composite was found using hot disc method, where the transient heat source is used to calculate the thermal conductivity and thermal diffusivity. Here the thermal conductivity difference between the matrix and UDCF composite was found. The thermal conductivity was same in both directions of the surface (surface is rich in matrix and it is isotropic) as the thermal conductivity is calculated on the basis of temperature difference in the x-,y- and z-axis. Whichever direction has the highest temperature difference, that value is taken into consideration, and the extent of heat transfer is also considered. For conducting this test, the sensor is chosen on the basis of thickness of the samples, as all samples had thickness between 2-3 mm, sensor of 2.001 mm was used. "One-side" based analysis was done and on the "other-side" insulator was used to hold the sensor at place. The test

parameters are 40mW and 2.5 seconds. The resultant value for PA6, matrix blend, PA6 blend based UDCF composite and reference sample is shown in Figure 4.8.
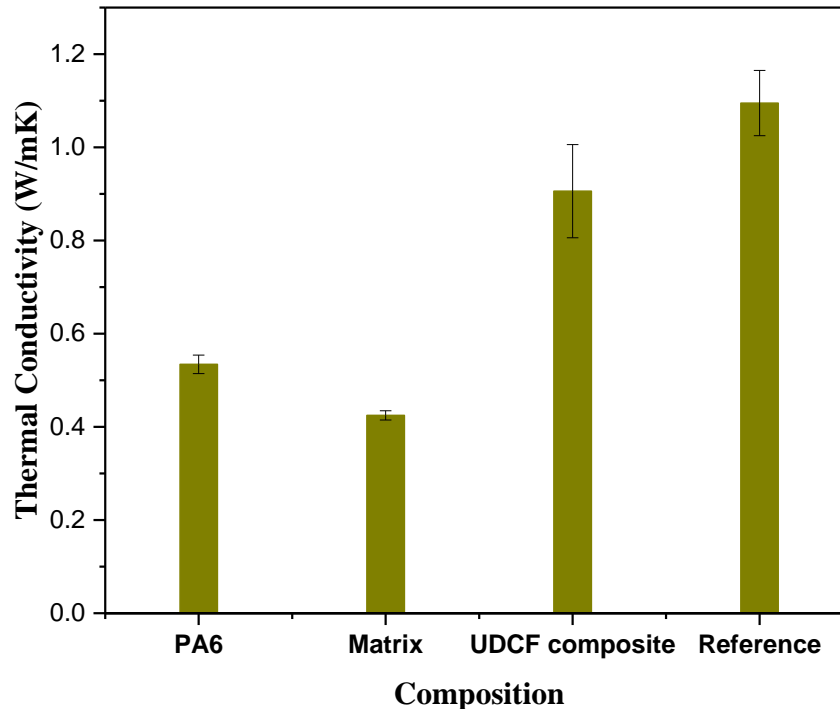
Figure 4.8: Thermal conductivity of compression molded PA6, matrix (PA6/PP/PP-g-MA), UDCF composite (PA6/PP/PP-g-MA/UDCF) and reference composite (BDCF/Epoxy) composite

From the Figure 4.8, it is evident that with addition of CF content, the thermal conductivity increases. It shows the effective transfer of heat from matrix to fibre, which also confirms the better interfacial adhesion between fibre and matrix. It is reported that the PAN based carbon fibre has very less thermal conductivity in comparison to pitch based carbon fibre (*Martins, 2018*). In this study all composite specimens are made using PAN based carbon fibres only. Also, in this method, the thermal conductivity of sample is tested through the transverse direction of the fibre. The longitudinal thermal conductivity (placing the sensor at cross section of the composite) of fibres is higher than the transverse direction as similar to that of the tensile strength (*Chawla, 1998*). Studies done by Rolfes et al. (*Rolfes, 1995*) reported similar values for CFRP composite when tested in transverse direction. Also, during the test, the sensor is placed over the matrix and not over the fibre as done by Dong et

al, (*Dong, 2016*), hence the value of thermal conductivity is lesser. Still, the addition of UDCF improved the thermal conductivity of the PA6 blend by 100 % showing the effect of reinforcement.

Matrix blend revealed slightly lower thermal conductivity compared to PA6, which could be due to the more number of voids in PA6/PP/PP-g-MA blend. The thermal conductivity of PA6 and matrix blend were lesser than the UDCF composite and the reference sample due to the inherent property of PA6 and PP which are acting as insulators to heat. Comparing UDCF composite with PA6, a two-fold increase can be observed which shows that the zones where the test was conducted had good wetting between carbon fibre and PA6/PP matrix leading to higher thermal conductivity. Reference sample which had ten layers of BDCF with epoxy as matrix, shown an increase of 20 % in its thermal conductivity compare to UDCF composite which might be due to the less numbers of voids in it. Epoxy, being a thermoset resin, has less viscosity and can wet all fibres in the composite leading to void-free composite after processing. The thermal conductivity of PA6 is 0.53 W/mK and that of epoxy is ~0.25 W/mK (literature data), hence it can be understood that the increase thermal conductivity for the composites (UDCF/PA6/PP composite: 0.93 W/mK; BDCF epoxy: 1.1 W/mK) was due to the reinforcement with PAN based carbon fabric only.

4.5. Short beam Shear Strength (ILSS) of PA6 blend based UDCF composite

The ILSS (Interlaminar Shear Strength) of the composite specimens were determined using short beam shear test. UTM (Zwick-Roell) having flexural test fixture was used for ILSS measurement (Figure 4.9). Here the specimen dimension of 100 x 12 x 2 mm^3 was used. Test fixture support roller had radius of 25 mm and indenting roller had the dimension of 10 mm. The span length should be around four times of composite sample thickness. Hence, the span length was fixed as 8 mm. Initially short beam test was considered as short beam shear test, where it was implied that the forces act in parabolic nature, with tensile and compressive stress becoming zero at the centre, leading to failure of sample by shearing only. But later it was understood that the failure mode is not always due to shear and the load is getting concentrated only on the centre, hence the standard ASTM D2344 was renamed as short beam strength test. However, it is stated in the standard that this test could be used for qualitative analysis

of comparison of properties between parallel (UD) fibre reinforced composites. The test becomes valid, when the failure mechanism is consistent in the samples. In this case, the samples after short beam test was analyzed using optical microscopy and it was found that the samples failed either at interface or at the compression point or due to fracture of sample away from the compression point.

Figure 4.9: ILSS (Inter Laminar Shear Strength) Test set-up used for UD composites

The samples showing failure at interface was taken into consideration. An average ILSS value of 22.7 MPa was observed. In this test, bending of samples was observed due to the ductile nature of the matrix. In all cases, crack was seen only at the interface and matrix crack was not observed. In this test, as the sample was compressed using the indenter roller, the samples tend to bend with giving some resistance to the compressive force. Initially matrix carries the load, and fibres tend to bend along with the matrix. At some point, saturation in strength was observed and on compressing the sample further, the strength drastically increased and then leading to a failure due to delamination. Here the fracture was due to the excessive force applied on the sample to delaminate from the matrix material. From literature it was found that the wetted PA6/UDCF composite has an ILSS of 40 MPa and dry spots in composite reduced ILSS value to 15 MPa which was measured using fibre pushin technique. Hence, the value obtained from this test lies in between these values and could be due to the dry spots (unwetted core rovings) present in the composite. ILSS value from this study (22.7 MPa) is around four times lesser than the value reported for UDCF/epoxy reinforced composite. Compared to thermoset resins, thermoplastics have high melt viscosity, so wetting is poor which always lead to lower ILSS value. As explained before, use of UDCF 12K rovings and the thick matrix sheet led to poor wetting and poor interfacial adhesion in the composites.

4.6. X-Ray CT-Scan and SEM analysis of PA6 blend based UDCF Composites

The following samples were studied using CT-Scan.
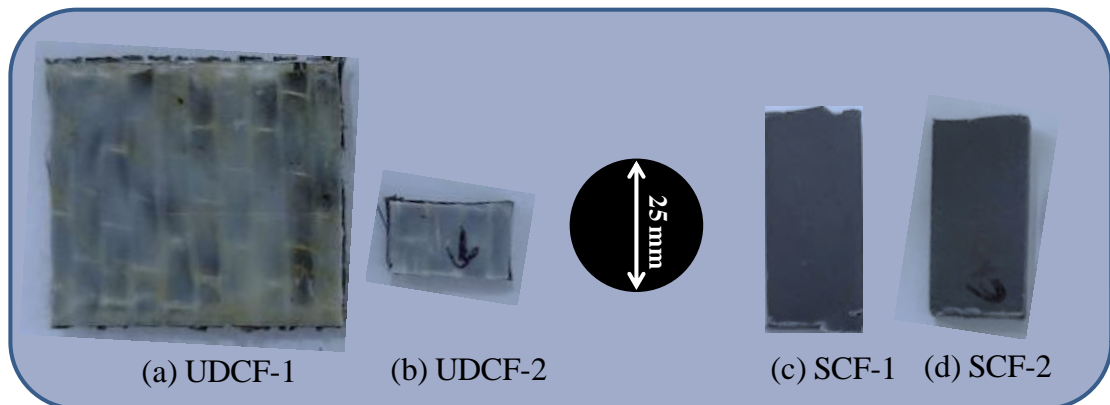
Figure 4.10: Two (a-b) UDCF specimens and (c-d) SCF specimens studied using X-Ray CT.

4.6.1. X-Ray CT-Scan of composites

CT (computer tomography) scan of two UDCF composite specimens was carried out at Carl Zeiss Pvt. ltd, Bangalore. The first sample (UDCF-1, Figure 4.10a) has the thickness of 3200 µm. Images were taken for every 110 µm thickness of the sample (around 30 images were captured in thickness direction). In the final composite, since the number of UD-fabric along with wetted matrix layers are 4 with each layer having thickness of 200-400 µm and matrix layers are 5 with each layer having thickness of 400-500 µm, the CT-Scan provides the images of matrix and fibre layers separately (Figure 4.11). The CT-Scan images of composite samples at three selected depths (top layer, middle layer and bottom layer) are shown in Figure 4.11 and the individual roving (12K carbon fibres) and the connective single glass fibres which are used to hold the UD carbon fabric are also visible. The slight misalignment of glass fibre i.e misaligned white threads in transverse direction are seen from Figure 4.11. The grey color in the images represent the matrix, the light grey color represent the fibre roving, and the dark grey colour within the roving represent the dry spots in the composite. To see the difference more significantly, a smaller sample of thickness 2500 µm was used for CT-Scan (UDCF-2).

| Top layer at 2.74 mm | Middle layer at 1.43mm | Bottom layer at 0.22 mm |
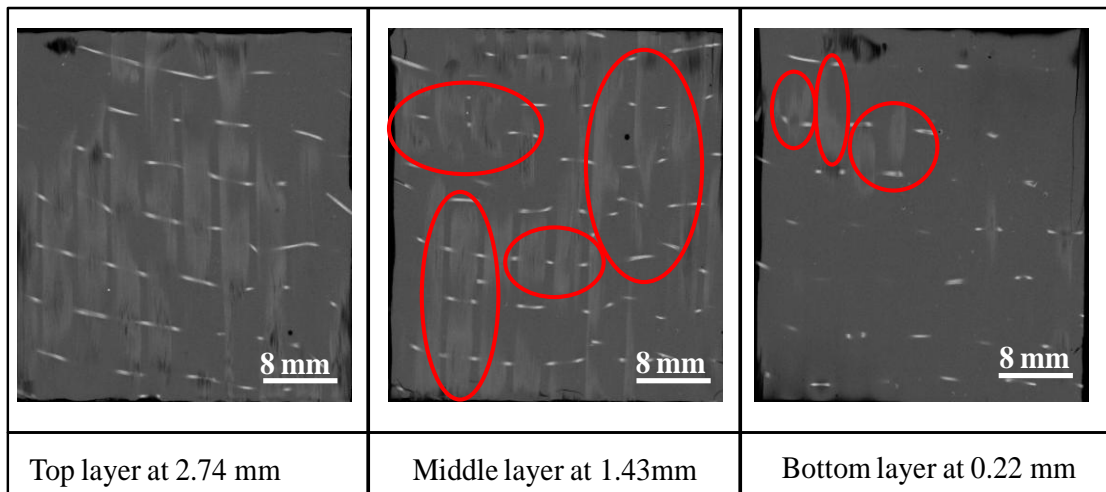
Figure 4.11: CT-Scan of the UDCF-1 composite specimen at three depths (white threads are glass fibres used to hold the UD carbon fibre rovings). The solid circle indicates poorly wetted regions, which are more in middle region.

In this sample, the images were taken at every 85µm thickness. From this image, the differences between wet and dry spot are more clearly visible (Figure 4.12). It is found that the matrix is wetting the composite from all four directions, but is unable to wet the roving throughout the thickness. Same conclusion was derived using optical microscopic studies. This is due to the usage of thick matrix sheet and thick reinforcement (12K roving). UD fabric with 3 K and 6 K rovings are not available in the market to use it as thin reinforcement in the current study.

| Top layer at 2.46 mm | Middle layer at 1.67mm | Bottom layer at 0.39 mm |
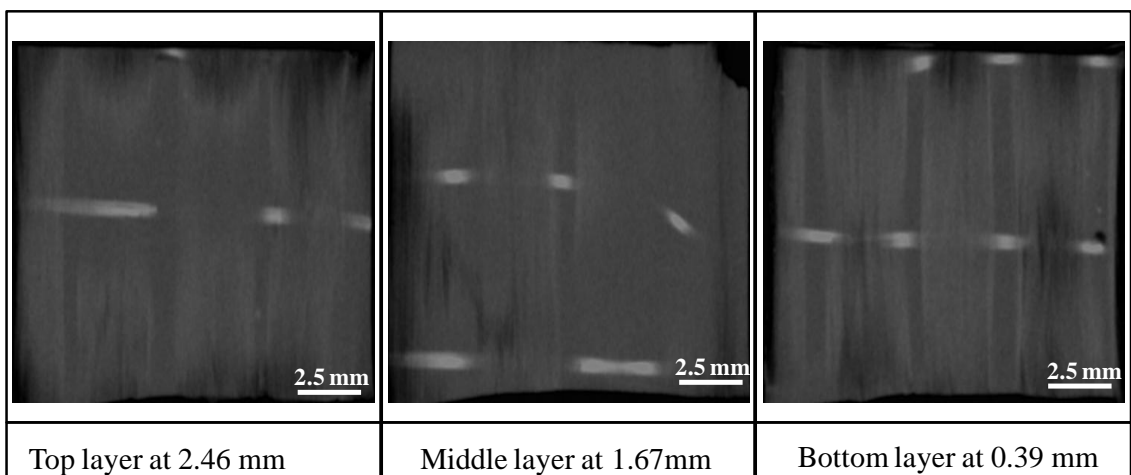
Figure 4.12: CT-Scan of the UDCF-2 composite specimen having thickness of 2.52mm.

4.6.2. SEM analysis

SEM (Scanning Electron Microscopy) analysis of UDCF laminate was done by cutting a small portion of sample cross-section and then smoothing the surface using rotary mictrotome. After surface sectioning, sample cross-section was checked through stereo microscope as shown in Figure 4.13a. It is clear that 4 layers of UDCF mat and 5 layers of matrix sheets are used to make the composite and it is also evident that selected matrix sheet thickness is too high. From the SEM images, it is visible that the fibres on the outer layer of rovings are wetted well with the matrix , whereas the core part of the roving remains not fully wetted (Figure 4.13 b-e). These unwetted zones or dry spots in thermoplastic composite are widely reported and most obvious reason could be the high melt viscosity of these thermoplastic matrices (*Botelho, 2010*)(*Y. Ma, Ueda, 2017*). Figure 4.13 b, d images show cross-section of fibre rovings, but slightly misaligned fibres is also seen, which eventually alters the properties of the composites. Even though the interfacial adhesion cannot be determined quantitatively using SEM images, qualitative conclusions can be drawn regarding the nature of the interface. As seen from SEM image 4.13c, the interfacial voids were not seen around the fibres (between matrix and fibre) which ensures compatibility between the fibre and the matrix phases. To improve the wettability of fibres in the core region of the rovings, plasticizer was introduced assuming that matrix viscosity will get reduced.
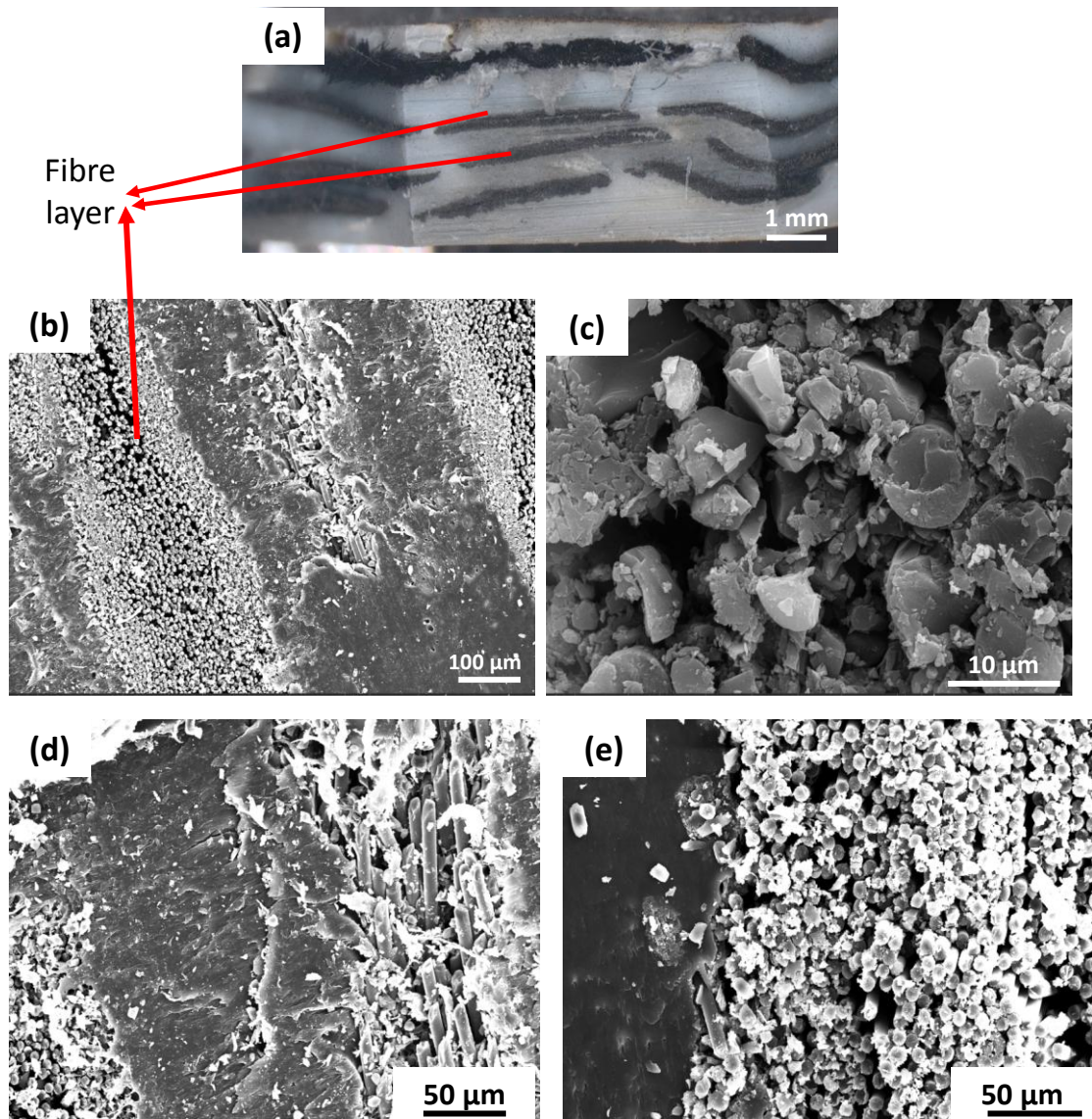
Figure 4.13: a) Stereo microscopic image of composite after surface smoothening with microtome, b)-e) SEM images of UDCF composite sample (cross-section)

4.7. Role of Plasticizer in matrix properties

n-butylbenzolsulphonamid (NBBSA) is widely used plasticizer for PA6, PA11, PA12 and copolyamides. In this study, Uniplex 214 from Lanxess was procured and used. It can also be used with polyacetals, polyacrylates, polycarbonates, polysulfones and cellulose derivatives. It aids in easy removal of material from mould, easier machining, better finish and better shape stability. Commercially, it is used in making nylon filaments, nylon-based hot melt adhesives, fuel lines, hoses and other high performance applications. Here, the matrix pellets were mixed with NBBSA liquid and then poured into the mould while making the matrix sheet. Since, the plasticizer

was liquid, it coated the matrix pellets thoroughly. Initially, 2.5 wt%, 7.5 wt% and 15 wt % of plasticizer was used and found that, with increase in plasticizer content, the flowability and flexibility of the matrix sheet improved, whereas the tensile strength and stiffness reduced. Hence, 2.5% plasticizer was fixed and used to make UDCF composite laminates, so that minimum compromise on tensile strength value is considered.
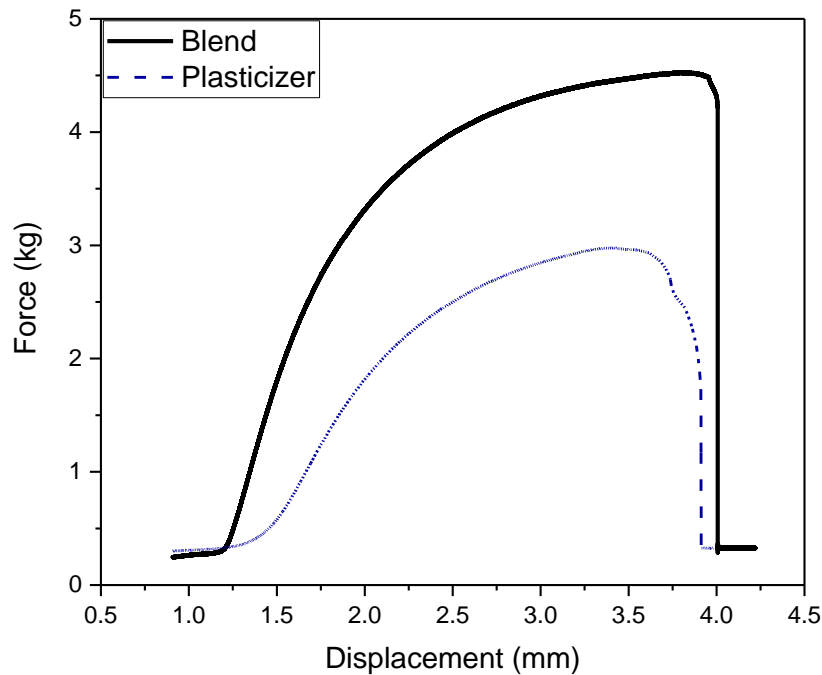
Figure 4.14: Representative Stress-strain plot for "matrix blend" sheet and "plasticized matrix blend" sheet

The tensile test was conducted using texture analyzer, with load cell of 500N and strain rate of 1.2 mm/s. The sample dimensions were 50 x 50 x (0.6-0.7) mm^3 and the gauge length was 20 mm. The matrix blend had higher strength and stiffness in comparison to the plasticized matrix blend sheet (2.5 wt %) (Figure 4.14). The reduction of strength was ~40%. The composite sample produced using plasticized matrix blend was found to be more brittle than the normal matrix blend. Hence, further processing and testing was not carried out because strength and stiffness increase of the matrix blend by reinforcing with the fibre is one of the objectives of this study.

4.8. Other attempts in processing of long carbon fibre composites

4.8.1. Processing of PA6 blend based BDCF composites using Compression molding

The processing of BDCF is similar to that of the UDCF composite. Here, BDCF made of 3K plain weave roving was used. Layers of matrix sheets and BDCF fabric sheets were stacked at room temperature. Matrix (7 layers) and fabric sheets (6 layers) of dimension 120 x 270 mm was used. Temperature of bottom plate was set at 260°C and top plate at 240°C. The composite was compressed at 240°C and held for 60 mins. Pressure of 80 bar was applied throughout the holding time and continued until the mold cools to 100°C using water as cooling agent. Composite was removed and allowed to cool at room temperature. Fibres rovings were misaligned and flowed along with the matrix during compression. Excess matrix seeped out of the mold which caused the fibre rovings to misalign from its weave pattern.

The misalignment of fibres was studied using CT-Scan of BDCF specimen. It can be clearly seen that the fibre rovings in different layers were misaligned. The thickness of sample was 1800µm and images were taken at every 60µm thickness and only three images are shown in Figure 4.15. Since the number of fabrics layers is more, the matrix is not seen separately as in the case of UDCF composite. Due to the high misalignment and the expected un-wetted zones at the cross-over of the fibre, further studies were not carried out. Here the thickness of fabric sheet is low due to usage of 3K rovings unlike 12K rovings used in UDCF composite which resulted better wetting and thinner matrix phase. But for any experimental analysis of composite, the fibre orientation is very critical in both warp and weft directions, because BDCF reinforcement is selected in order to make a composite with isotropic like properties. Since, the misalignment in all layers was different and not controllable, only UDCF samples were studied in detail.

| Top layer at 1.62 mm | Middle layer at 0.81mm | Bottom layer at 0.12 mm |
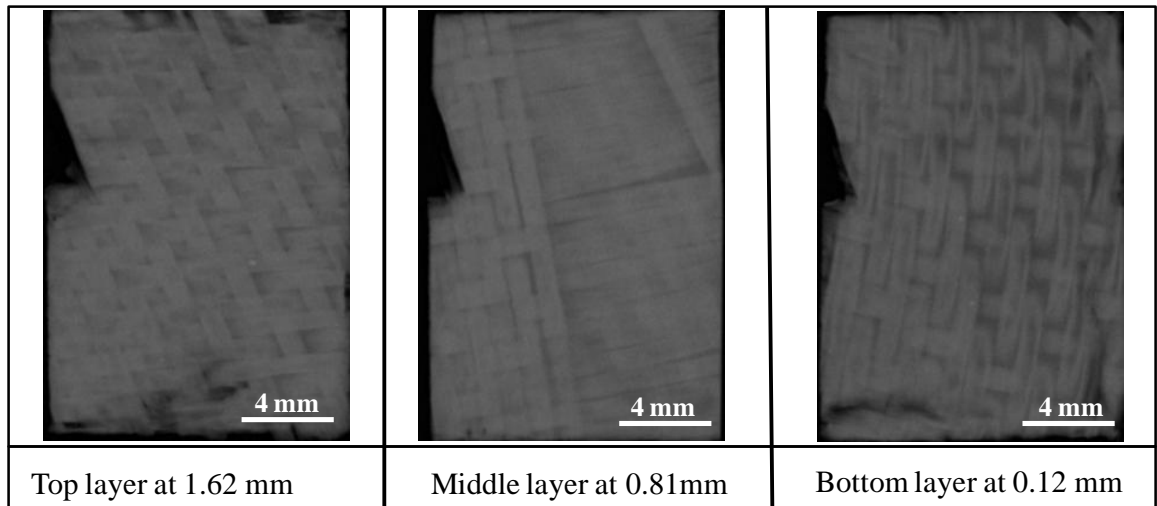
Figure 4.15: CT-Scan of the BDCF composite specimen. Note the misalignment of fibre rovings

4.8.2. *Processing difficulties in making UDCF / BDCF composites laminates using thermoplastic matrix*

Figure 4.16 shows the compression molding machine used for UDCF and BDCF composite laminate preparation. The optimization of processing of matrix sheet consists of two stages, macro-level optimization and micro-level optimization. While modifying the machine for composite preparation, the following changes were made.

- Mold dimension was increased to make both matrix blend sheet and composite
- Cooling facility for bottom mold was included
- Spacer plate to modify the thickness of the resulting sample was provided so that 1 mm, 2 mm and 4 mm thick sheets can be made
- Pressure gauge was installed to control the applied pressure
- Ejector pins were provided for easy removal of spacer plate
- Three pencil heaters with sensor in the middle region of the top and bottom molds were added
- Modified operating console was provided to set the temperature, pressure and operating the ejector pins and mold (moving the upper mold)
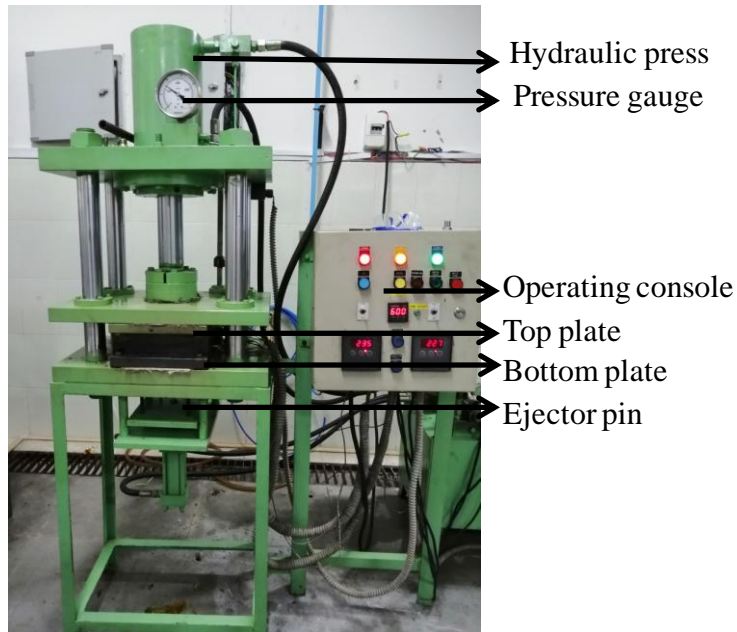
Figure 4.16: In-house modified compression molding machine

Major parameters optimized for matrix sheets processing are temperature of top and bottom mold, pressure to be applied, holding time, release agent and type of cooling to be used.

4.8.3. Trial for making blend sheet:

The compression molding equipment was used for making matrix sheet so as to confirm the working of the machine. The major issue faced during this stage was that the matrix material was sticking to the top mold and was very difficult to remove. Various release agents were used, among which kapton tape was found to be suitable. Moreover, there were no gaps in the mould for venting of air, so the grooves made in the spacer plate was useful to remove the trapped air and also to aid in removal of sample (Figure 4.17). Two types of cooling agents were used, water and air; wherein water was chosen for faster cooling of samples.
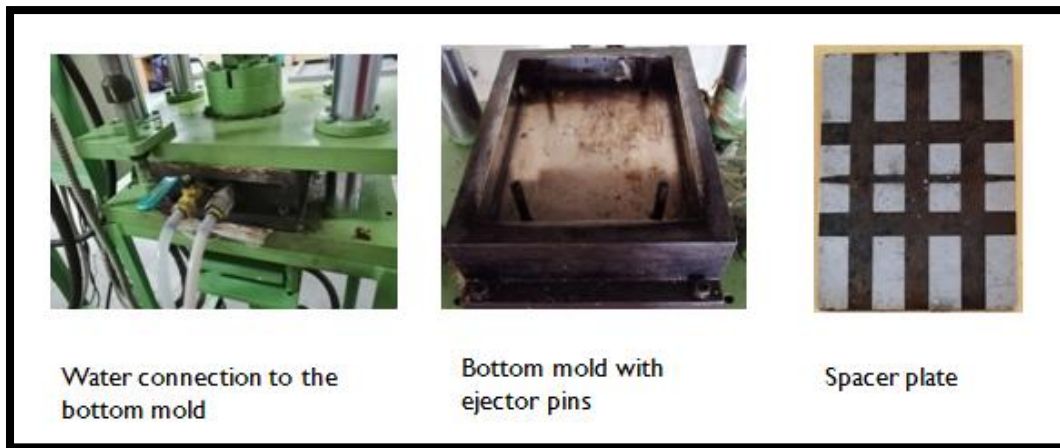
Figure 4.17: Major modified parts of compression molding machine

The crucial problem faced post initial trials, was that the mold took more than 4 hrs to reach 200°C. This issue was corrected by addition of two layer asbestos sheets in the bottom and top mold which acted as insulator and avoided the dissipation of heat through conduction/convection. Further, while using the kapton tape for longer time, this adhesive remained on the mold and also started to get stuck on to the matrix material, which lead to poor quality of matrix sheet. Hence the kapton tape was replaced with high viscous silicone oil as release agent. With application of silicone oil, the sample had brown spots on the top, which was due to the degradation of oil (prolonged exposure to heat). Hence, the release agent and the matrix material were added after reaching the mold temperature to >200 °C, to reduce the exposure time of the silicone oil. Since the bottom mold was thicker than the top mold due to the presence of spacer plate, the temperature increase was checked manually at all ports and then decided to have higher temperature for bottom mold and lower temperature for top mold to maintain the equilibrium. Pressure was varied from 70-100 bars initially. But with efficient temperature control system, the pressure was reduced to 80 bar. Holding time was varied from 15 to 45 minutes and finally it was concluded to hold for 30 minutes for the optimum sheet characteristics like uniform thickness with very few brown spots. The parameters that were optimized for making UD laminates with film stacking technique were pressure & temperature, number of matrix and fibre layers, number of cycles and holding time. Some key trials are explained here. Initially six layers of UDCF and seven layers of matrix was used to make the composites such that the weight fraction achieved would be 60 wt%.

(a)   (b)   (c)   (d)
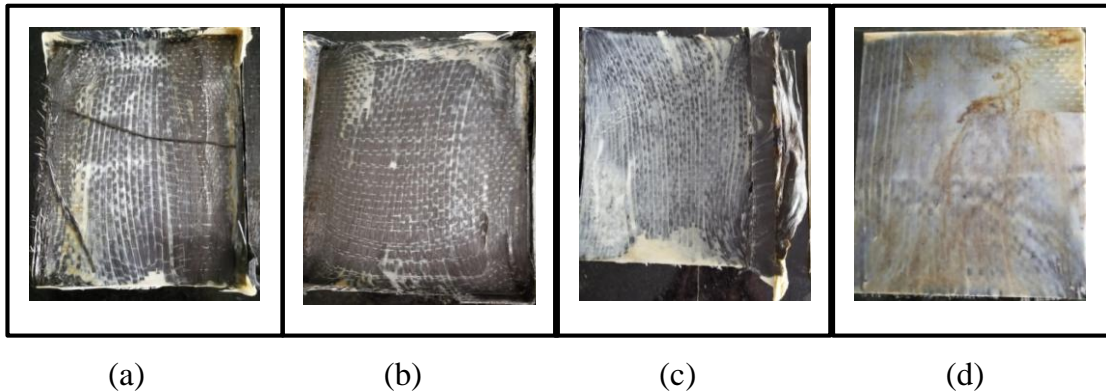
Figure 4.18: Resultant UDCF composite from trials a) Unwetted fibres at corner b) misaligned fibres c)fibre layer slipping along with matrix d) composite with aligned fibres

Since, the use of matrix as full sheet was causing misalignment, half of matrix sheet was used as alternate layers with UDCF fabric. Even though 90% of the fibres got wetted, the resin rich phase tends to have more misalignment in comparison to the empty place (Figure 4.18a). Hence, instead of this full matrix sheet was used and the layers were compressed to 50 bar from beginning of heating and pressure was applied at appropriate temperature. This led to the further misalignment of fibre which might be due to the excess pressure applied on the fibre-matrix (Figure 4.18b). Further, to reduce the fibre misalignment and to reduce the pressure, four layers of fibre along with five layers of matrix were used. Initially, thicker matrix of 4 mm was obtained, but the fibres held their position with very minimal misalignment in the corners of the mold. Hence, it was decided to re-mold the same composite to reduce the thickness of the composite as well as the matrix phase. During the initial trials with second cycle, it was found that at any pressure higher than 10 bar, the matrix tends to flow out along with the fibre fabric (Figure 4.18c). Hence, pressure not more than 5 bar was applied and the mold was monitored keenly, until the matrix tends to seep out, and the heater were turned off immediately. With this method as explained in the earlier section, composite with two step processing was done to evaluate the properties of blend based UDCF composites. (Figure 4.18d)

Conclusion:

Overall, the UDCF composite (PA6/PP/PP-g-MA with 30 wt % UDCF fabric of 12K rovings) was made using the in-house modified compression molding machine and its mechanical and thermal properties were tested. Composites were processed in three stages. I). Pellets of matrix blend were converted in to 0.9 mm thick sheets. II). Alternative layers of matrix sheet and UDCF fabric were subjected to compression molding at 260°C, 80 bar pressure to obtain 3-4 mm thick laminates. III). Composite laminates were repressed at 260°C, 5 bar pressure to obtain 2-3 mm thin composite laminates. The expected and theoretical results were higher than the experimental results due to the un-wetted core zones found in the composite despite samples being hot pressed twice. These un-wetted core zones were identified from X-ray CT scans. Same conclusions were derived using SEM and optical microscopic studies. The interfacial adhesion between the fibre and matrix was found good on sides (poor in core region) and does not decrease drastically after water absorption as seen from the impact test. The wet composites samples broke when the energy was increased to 12.3 J. Compared to dry samples, the impact strength of wet samples has increased by 64%. This is due to the plasticization of the matrix and corresponding influence on fibre-matrix adhesion. Due to water absorption, the interfacial adhesion became slightly weaker, which in turn resulted in 24.5% reduction in tensile strength compared to dry samples. To measure the interfacial adhesion quantitatively, ILSS value was measured and found to be low (23 MPa) compared to the value reported for epoxy based composite (~60 MPa), which is certainly due to the higher viscosity of PA6/PP matrix. The reinforcing effect of UDCF is seen from the increased tensile strength, modulus (353 MPa, 27.4 GPa) of the UDCF composite in comparison to the injection molded SCF reinforced composite (54 MPa, 5 GPa). Comparing UDCF composite with PA6, a two-fold increase in thermal conductivity can be observed which shows that the zones where the test was conducted had good wetting leading to higher thermal conductivity. UDCF composites revealed compressive strength of 42 MPa and compressive modulus of 4.5 GPa. With thinner matrix sheet (<0.4 mm) and 3K roving based UDCF fabrics, better composite can be made, but with the existing facility thin sheets of 0.9 mm are made and more over fabrics of 3 K rovings are not available currently in the market. However, the possibility of using blend based matrix system for UDCF composite has been proved.

CHAPTER 5:

Comparison of properties between PA6, matrix blend and composites

5.0.Introduction

In this chapter, the properties of PA6, Matrix blend-PA6B (PA6/PP/PP-g-MA 70/30/3 wt/wt/phr), SCF composite PA6B/15wt% SCF, and UDCF reinforced PA6B (PA6B/UDCF ~30 wt% UDCF) have been compared. Initially, water absorption of the blend and composites are compared to check the feasibility of these composites for high humidity applications. Tensile strength (dry and wet), impact strength (dry and wet), DSC thermogram (3 cycles) and thermal conductivity are compared among PA6, matrix blend and blend based SCF and UDCF reinforced composites.

5.1. Comparison of Water absorption

The overall water absorption of PA6, PA6B, PA6B/SCF and PA6B/UDCF laminate materials is shown in Figure 5.1. For all injection molded components, the tensile samples (dog bone specimens) were dipped in water. These samples were weighed every day until saturation, thereafter samples were used for conducting wet tensile test. The compression molded sample (PA6B/UDCF) was cut into dimension required for tensile test according to ASTM D3039 and then dipped in water as shown in Figure 5.1 (right).

Water absorption of pure PA6 was higher in comparison to matrix blend and SCF composite, while the water absorption of UDCF slightly became higher than PA6. This difference could be due to the different processing technique adopted for the SCF composite in comparison to UDCF composite as mentioned in Figure 5.1. Among the injection molded specimens, it could be seen that with inclusion of PP and SCF, the % of water absorption reduced drastically because PP and carbon fibre are hydrophobic in nature. It can be understood from X-ray CT of SCF composites (Figure 5.2), that the samples are having very few macro voids and macro-pores are absent at the fibre-matrix interface. The sudden increase in % of water absorption for UDCF composite laminate could be due to the presence of macro-pores present in the sample arising

from the un-wetted fibres in the central part of the roving and also due to the micro pores (air bubbles) in the matrix material arising from compression molding. Even though carbon fibres are hydrophobic in nature, the sizing agent present on carbon fibres might aid in accumulating the water between the fibres. Due to the above two reasons, the UDCF composite laminate had slightly higher water absorption than PA6. However, the water might not be chemically bonded to PA6 or carbon fibre as the resultant tensile strength of PA6/UDCF is higher than pure PA6 as shown in Figure 5.3.
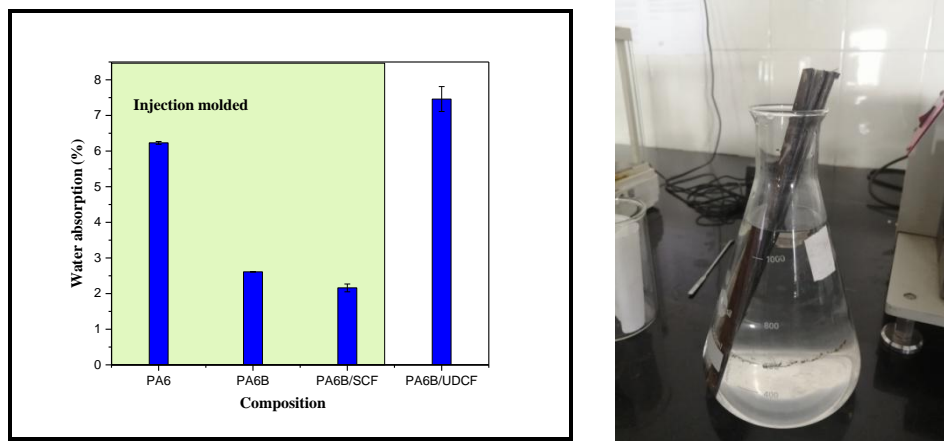
Figure 5.1: Left: Water absorption data of PA6, matrix blend -PA6B, PA6B/SCF composite (injection molding) and PA6B/UDCF composite laminate. (Compression molding). Right: Water absorption test set-up (note: sample is not fully immersed in water)

| Top layer at 3.06 mm | Middle layer at 1.64mm | Bottom layer at 0.11 mm |
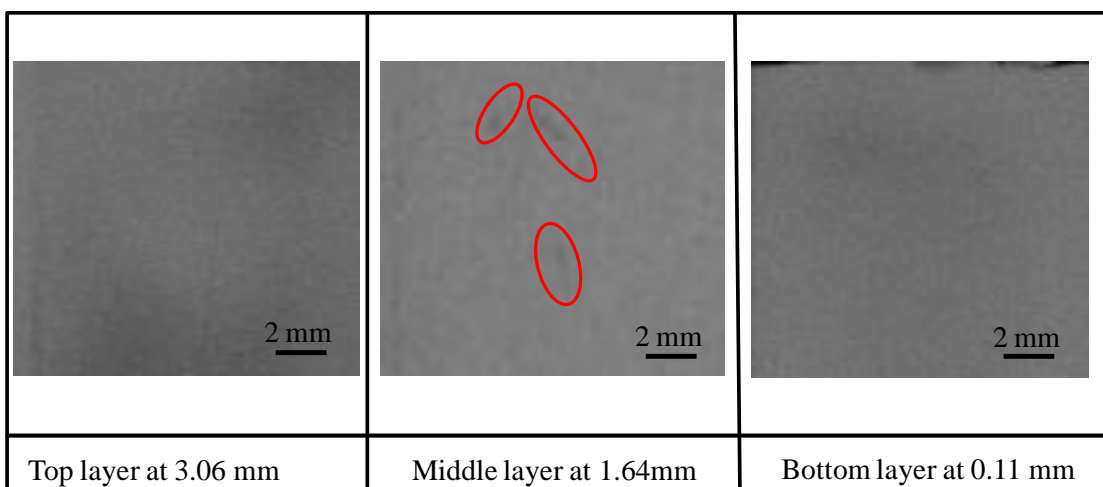
Figure 5.2: X-Ray CT-Scan of the SCF composite specimen of 3.12 mm thickness (oval indicates the micro voids)

Comparing the literature values of water absorption to the values from current study (Table 5.1), it can be definitely concluded that for injection molded specimens, the obtained blend and composite show lower water absorption which is considered to be important conclusion of this study. However, the compression molding technique adopted for UDCF laminate processing should be modified using thin fibre mats (3K or 6K rovings) to obtain composite laminates with good fibre-matrix wetting which should result in lower % of water absorption.

Table 5.1: Water absorption of PA6 based composites - comparison with literature data				
Composite	**Water absorption (%)**		**Test condition**	**Reference**
	Composition	**Value**		
• *PA6/PP/PP-g-MA /SCF*	*PA6* *PA6B* *PA6B/SCF(15wt %)*	*6.2±0.04* *2.6±0.01* *2.2±0.11*	*Room temperature*	*From this study*
• *PA6/PP/PP-g-MA/ UDCF*	*PA6B/UDCF (30 wt %)*	*7.5±0.35*		
PA6/nanoclay	PA6 PA6/10wt% nanoclay	3 1.8	70°C,65% RH	(*Vlasveld, 2005*)
PA6/PP/nanoclay	PA6 PA6/PP/8wt% nanoclay	7.3 5.4	Room temperature	(*Chow, Bakar, 2005*)
PA6/PP/PP-g-MA/SCF	PA6 PA6/PP/PP-g-MA/SCF	7.1 5.5	Room temperature	(*Do, 2016*)
PA6/UDCF	PA6/UDCF (60Vol%)	3.5	100°C	(*Pillay, 2007*)
PA6/UDCF	PA6 PA6/UDCF laminate (CF prepreg tape of 60 Vol %)	7.5 3.0	33°C, Sea water	(*Arhant, 2016*)

5.2. Comparison of tensile strength and tensile modulus (dry and wet)

The tensile strength of the PA6, matrix blend and composites are shown in Figure 5.3. Comparing the dry tensile strength data, the matrix blend has lower tensile strength than pure PA6 as explained in chapter 3. But as SCF fibres are added, the strength of the composite increased by 9.8% compared to pure PA6. With addition of UDCF

fibres, 6.5 fold increase in tensile strength is seen and it is due to the presence of unidirectional carbon fabric made by using rovings of 12000 individual long fibres. Compared to SCF (15 wt%) reinforced composite, 5.9 times increase in tensile strength has been observed for UDCF reinforced composite (30 wt%). Hence, the addition of UDCF provides its benefit by increasing the fibre-matrix interfacial area of interaction, thereby improving the strength. In composites, the key component determining the tensile strength of the composite is the fibre. The strength increases with the increase in fibre content as well as the fibre type. In SCF composite, the amount of fibre is 15 wt% and as stated earlier, the fibre length is only $50 \mu m$ post processing, due to which very low increase in tensile strength can be seen. However, in case of SCF, the dispersion of SCF in matrix is very uniform and the adhesion between the fibre and matrix was found to be good as the fibres are completely wetted by the matrix. In case of UDCF composite, compared to the literature data, the volume fraction used in this study is very low ~20 vol%, however owing to continuous fibres used in longitudinal direction, the tensile strength was improved by 650%. In case of UDCF composite, good bonding between fibre and matrix was seen, but limited to the top and bottom surface of the rovings. As the viscosity of the matrix blend is very high (compared to thermosets) and weight fraction of fibres (30 wt %) also increased compared to SCF composite, the wettability of fibre decreased leading to dry spots in core zone of the rovings which in turn leads to lower strength of the composite than expected. The obtained strength could also be low due to the usage of thick UDCF of 12 K roving and thick matrix sheets (> 900 µm).
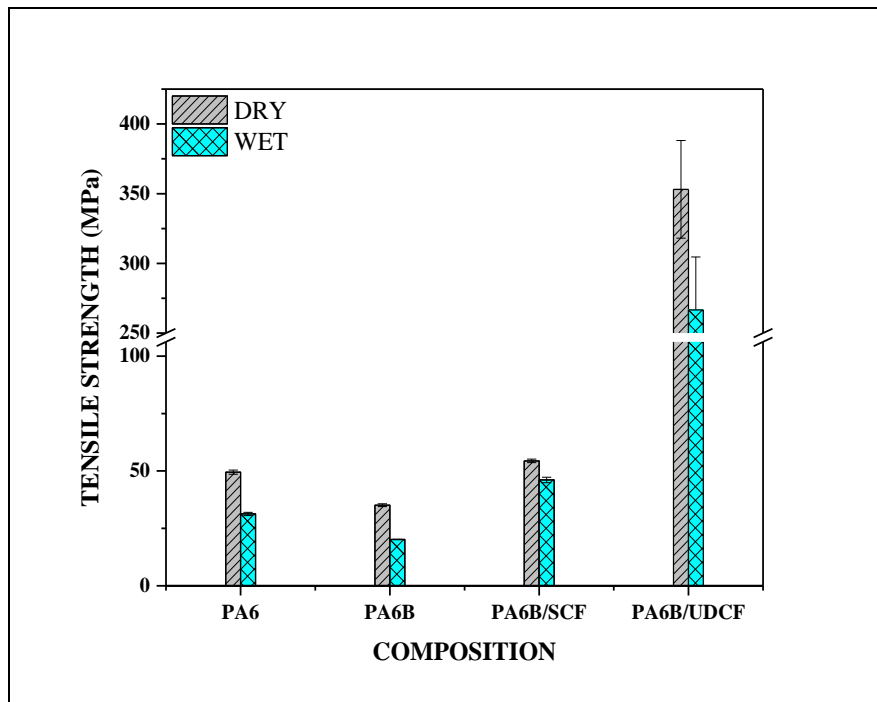
Figure 5.3: Tensile strength of PA6, matrix blend, SCF composite and UDCF composite in dry and wet condition

Among the wet samples, matrix blend has lower tensile strength than PA6, but as SCF is added, the wet strength of the composite increased by 47.2% compared to wet PA6. When compared between dry and wet tensile strengths, the % reduction is 37% for PA6, 42% for matrix blend (PA6/PP/PP-g-MA) and 15% for SCF composite and 24.5% for UDCF composite. The SCF composite has the combined advantage of lower water absorption and lower reduction in tensile strength post water absorption due to PP and SCF. The addition of compatibilizer was advantageous, as the interface between fibre-matrix did not get affected due to which better properties were observed. In wet UDCF composites, the voids formed due to the unwetted core zones are filled with water which in turn contributed 24.5% reduction in tensile strength which might be due to the poor interfacial adhesion due to unwetted zones, misalignment of fibres during processing and the change in load transfer from lamina to lamina. Yet, the observed 24.5% reduction in tensile strength is still on the lower side for a PA6 based composites due to addition of PP and PP-g-MA to PA6.

Table 5.2: Tensile strength of PA6 composites with comparison to literature data			
Composite	**Fibre fraction and processing technique**	**Tensile strength (MPa)**	**Reference**
PA6B/SCF (PA6/PP/PP-g-MA/SCF)	*15 wt%, twin screw extrusion followed by injection molding*	*Dry-54 ±0.8 Wet- 46 ± 1 (15% reduction)*	*This study*
PA6B/UDCF (PA6/PP/PP-g-MA/UDCF)	*30 wt% or 20 vol%, Film stacking technique*	*Dry- 353 ±35 Wet- 267±38 (24.5% reduction)*	*This study*
PA6/ SCF	15 wt%, twin screw extrusion followed by compression molding	Dry-170	(*Feng, 2013*)
PA6/SCF	20 wt%, 6mm fibre, twin screw extrusion followed by compression molding	Dry-80	(*Karsli, 2013*)
PA6/PP/PP-g-MA/SCF	20 wt%, 6mm fibre, single screw extrusion followed by injection molding	Dry- 142 Wet- 88 (38% reduction)	(*Do, 2016*)
PA6/UDCF	42 vol%, compression molding of PA6/UDCF prepregs	1308 (dry)	(*Y. Ma, Ueda, 2017*)
PA6/UDCF	60 vol%, compression molding of pre-impregnated PA6/UDCF tape	Dry- 1808 Wet- >1000 (~45% reduction)	(*Arhant, 2016*)

From the literature values shown in Table 5.2, it is clear that higher length of SCF has to be used in case of SCF reinforced composite and for UDCF composite, either prepregs/semipregs should be used to obtain higher strength in composites. However, considering the % reduction in strength after saturating with water, it can be seen that in current work, the reduction is only 15 % for SCF composites, whereas in literature it is greater than 35%. Hence, from current study, the existing matrix blend can be effectively used with long SCF fibres to obtain higher strength composites in both dry and wet conditions. As seen from the Table 5.2, the UDCF composites of PA6 is made using prepregs or tapes, which have better fibre-matrix bonding and better compaction after processing. In this study, since the matrix was of 900µm thickness and UDCF roving of 12K was used, the resultant ILSS value was also low because of which lower tensile strength was observed.
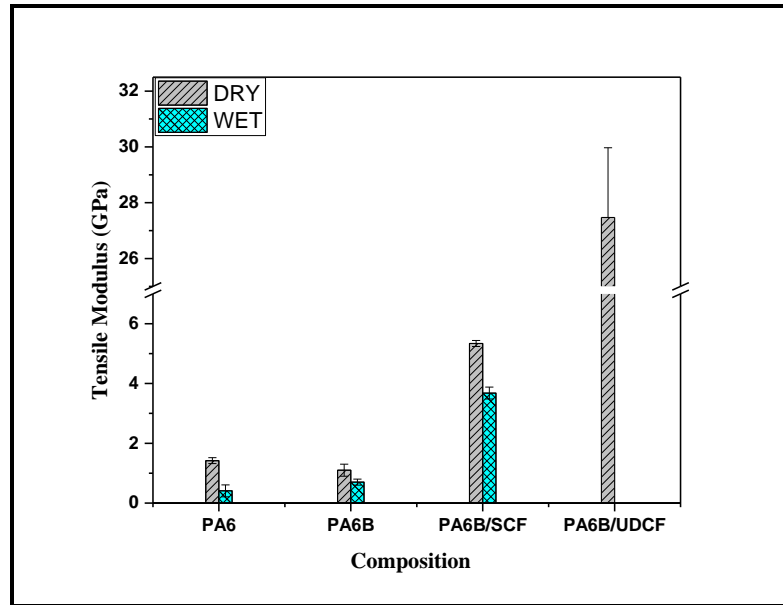
Figure 5.4: Tensile modulus of PA6, matrix blend, SCF composite in dry and wet condition and UDCF composite in dry condition

The tensile modulus (Figure 5.4) of PA6 in dry state was higher than PA6B. The presence of PP and PP-g-MA led to reduced tensile modulus in PA6B. Tensile modulus of PA6B/SCF and PA6B/UDCF increased due to the presence of carbon fibre (3.8 times and 23.9 times higher than PA6B respectively). This increase proves the reinforcing effect and the interfacial adhesion between the fibre and matrix of SCF and UDCF in blend matrix. Tensile modulus of PA6 decreases by 70% post water absorption whereas the blend matrix decreases by 36% compared to the dry counterpart. This is due to the decreased water absorption and the reaction between PA6-PP due to the addition of PP-g-MA. Tensile modulus of PA6B/UDCF in wet condition was not calculated as it is difficult to conduct the experiment. Comparing wet modulus, PA6B showed better modulus than PA6, which also proves the better interfacial adhesion in the matrix. Overall it was understood that with addition of PP and PP-g-MA, the retention in tensile modulus was higher in both blend matrix and SCF composite.

5.3. Comparison of Impact strength (dry and wet)

Figure 5.5: Izod-Impact test set-up used for blend and SCF composites

Two types of impact test were used in this study. The injection molded specimens were tested using Izod test (Figure 5.5) and compression molded specimen were tested using low velocity impact test. For comparison, all impact test results are converted to "Joules" as shown in Figure 5.6. The izod-dry impact strength of matrix blend was higher than PA6 and SCF composite. The compatibilization of blend and optimum size distribution of PP led to higher impact strength in blend. Whereas in SCF composites, the fibres act as stress concentrators and make the component brittle. The wet PA6B blend has increased impact strength by 66.7% (compared to dry) due to plasticization of PA6. The nullifying effect due to PP and SCF, led to no increase in impact strength of the SCF composite in the wet state compared to dry state.

Further, the low velocity impact of compression molded specimen gave different result in comparison to injection molded specimen. In LVI method, the PA6 had higher impact strength in comparison to matrix blend (Figure 5.6). This could be because of the variation in the processing technique as explained before and also due to the reduced amount of macro voids in the PA6 samples. However, in LVI method, the SCF reinforced composite had higher impact strength than matrix blend due to

retention of the fibre length during compression molding (15 wt % SCF content). Here the loss in fibre length was only due to extrusion and no further loss in fibre length occurred during compression molding unlike in injection molding.
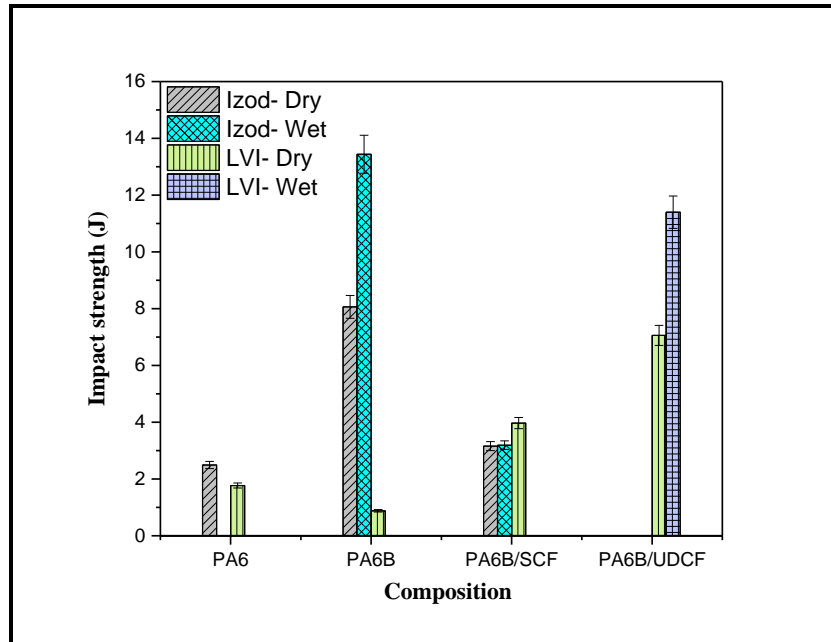
Figure 5.6: Impact strength of injection molded PA6, matrix blend (PA6/PP/PP-g-MA), SCF composite and compression molded UDCF composite in dry and wet condition. LVI denotes low velocity impact test

The UDCF samples had the highest impact strength in comparison to PA6 and SCF reinforced composite. The compression molded UDCF composite (LVI dry) had 7 fold increase in impact strength value compared to compression molded matrix (LVI dry). Wet impact strength was also studied for UDCF composite. On absorption of water, plasticization of matrix occurs, because of which higher impact strength than dry counterpart was observed. With this study, it can be concluded that the processing technique affects the properties of the material, and the UDCF reinforced PA6/PP matrix blend has led to higher tensile strength as well as higher impact strength. When compared between dry and wet UDCF composites, wet composites had less tensile strength (Table 5.2) and more impact strength than dry composites. Hence, the property variation in the blends and composite vary on water absorption. Synergistic effects of plasticization of matrix and presence of voids in samples is observed for the UDCF composite samples for improving the impact strength and reduction of tensile strength in wet condition as shown in Table 5.3.

Table 5.3: Impact strength of PA6 composites with comparison to literature data

Composite	Impact testing technique	Impact strength	Reference
PA6B/SCF (PA6/PP/PP-g-MA/SCF)	*Notched-Izod, (15wt% SCF)*	*Dry-9.5±0.1 kJ/m^2* *Wet- 9.4±0.1 kJ/m^2*	*This study*
	LVI (15wt% SCF)	*Dry- 3.75±0.01J*	*Reference*
	LVI (60 wt% BDCF/Epoxy)	*Dry- >7.95J*	
PA6B/UDCF (PA6/PP/PP-g-MA/UDCF)	LVI (30 wt% UDCF)	*Dry-7.06 J Wet-11.4 J*	*This study*
PA6/SCF	Notched-Izod (16 wt% SCF)	10.9 kJ/m^2 (dry)	(*Luo, 2014*)
PA6/PPS/SCF	Notched-Izod (15wt% SCF)	~ 11 kJ/m^2(dry)	(*S. Zhou, 2013*)
PA6/EVA/SCF PA6/EPDM/SCF PA6/SEBS/SCF	Notched-Izod (20 wt% SCF)	~0.5 kJ/m^2 ~1 kJ/m^2 ~0.75 kJ/m^2 (dry)	(*Y. Li, 2014*)
PA6/UDCF	Computerized LVI (60 vol% UDCF)	~ 60 J (dry)	(*Pillay, 2009*)

5.4. Comparison of Thermal properties

Thermal properties of PA6, matrix blend and composites were studied using DSC and thermal conductivity. From DSC, the cooling cycle representing crystallization and heating cycle representing melting of PA6, matrix blend and composite is shown in Figure 5.7. From heating cycle, it can be understood that PA6 phase in matrix blend is having higher %χ_c value in comparison to SCF composite (Table 5.4). In composite, the presence of SCF hindered the crystallization of PA6 due to the bonding between carbon fibre-PA6B matrix. Since the competition between compatibilization of blend and interaction of fibre-matrix in composite exists, the crystallization of PA6 becomes difficult in SCF Composites.
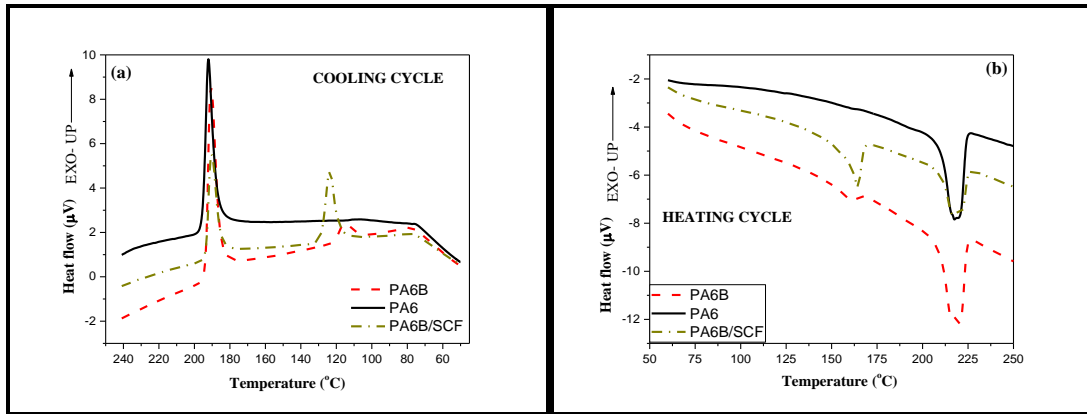
Figure 5.7: a) Cooling cycle b) Heating cycle thermograms of PA6, matrix blend (PA6B) and SCF composite (PA6B/SCF)

Table 5.4: %χ$_c$ and ΔH_M value of PA6 in blend and composites

	%χ$_c$	ΔH_M (J/g)
PA6	25.9	-56.21
PA6B	16.5	-42.27
PA6B/SCF	11.6	-23.95

From heating cycle, similar observation as that of cooling cycle can be observed. The ΔH_M of PA6 is higher for pure PA6 and matrix blend compared to the SCF composite. The existence of α-PA6 and γ-PA6 can be seen in both matrix blend as well as the composite. Thus the hindrance to crystallization of PA6 in SCF composites is also proved. PA6B/UDCF Composites was not considered in this comparison study.

Thermal conductivity of the compression molded PA6, matrix blend and composites were compared in Figure 5.8 and found using the gustaffson method as explained in Chapter 4. As reported in literature PA6 has thermal conductivity of 0.23 W/mK (*Minghui Li, 2013*), but in our study 0.53 W/mK was obtained, the difference could be due to the processing techniques adopted. Considering the 0.53 W/mK as the reference, it can be seen that the thermal conductivity of matrix blend was lesser than PA6 owing to the voids present in the PA6B (PA6/PP/PP-g-MA) (*Shahadat, 2017*). When voids are present, conductive heat transfer gets reduced; hence, the thermal conductivity is lesser in samples having more number of voids. With addition of SCF, minimal increase in thermal conductivity was observed. 0.3W/mK increase with

addition of 5 wt% SCF was reported by Li et al. (*Minghui Li, 2013*). Compared to this data, the observed increase of 0.18 W/mK is less which is due to the modified matrix in comparison to the metal hydride based composite used in the studies of Li et al. (*Minghui Li, 2013*).

In thermoplastics, the energy transfer is accomplished by the vibration and rotation due to polymer chains. Thermal conductivity depends on degree of crystallinity as in a crystalline phase of polymer there will be coordinated vibrations of the molecules due to the ordered crystalline structure (*William D. Callister, 2007*). Here the % crystallinity was calculated for injection molded specimen and not the compression molded specimen. Hence, it cannot be compared. The UDCF composite had the highest thermal conductivity which is 67% higher than the PA6 value. Hence, it can be understood that the UDCF composite lacked interfacial voids, and had increased thermal conductivity because of good fibre-matrix interaction at selected locations and also due to the higher fibre content (30 wt %). It can also be understood that the crystalline structure of PA6B in UDCF composite could be more, because of which it gives better strength, stiffness and thermal conductivity. The depth of penetration of heat in this case is 2 to 3mm, which covers the entire cross-section of the composite. Even with presence of voids, the increment in thermal conductivity proves the effective interfacial adhesion between the fibre and matrix in selected locations. Even though the rovings in core region did not wet completely, the interfacial adhesion between the fibre and matrix is sufficient enough to provide higher tensile strength, impact strength and thermal conductivity compared to PA6, but it requires improvement in processing using thin matrix sheets and 3K rovings, which are currently not available in the market.
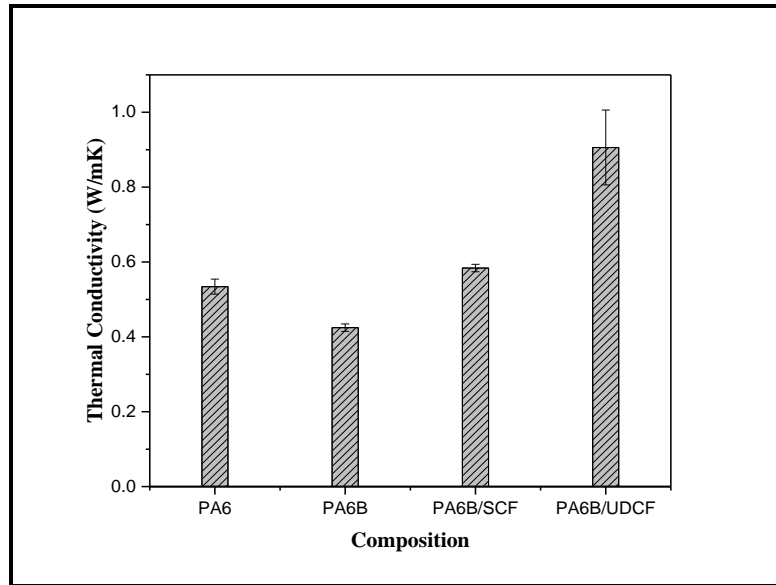
Figure 5.8: Thermal conductivity of PA6, matrix blend (PA6B), SCF composites (15 wt%) and UDCF composite laminate (30 wt%)

CHAPTER 6:

Conclusions

PA6 was modified using PP as dispersed phase in an attempt to decrease the moisture absorption. To improve the interfacial adhesion between PA6 and PP, the third polymer "PP-g-MA" was introduced as compatibilizer. The properties of blends were studied with increase in PP content before and after water absorption. From this study 30 wt% of PP was found to be optimum. Further, for optimizing the compatibilizer content in composites, 70/30 weight ratio of PA6/PP with 5wt% SCF was studied by varying the compatibilizer content between 3, 4 and 5 phr. From this study, 3phr PP-g-MA was found to be optimum. Hence, the matrix blend ratio was fixed as 70 wt/30wt/3phr of PA6/PP/PP-g-MA. This modified blend was used as matrix material for making the SCF composites (injection molding) and UDCF composites (compression molding). In case of SCF composites, SCF content was varied (3, 6, 9 and 15 wt%) and for UDCF composite, 30 wt% of UDCF was considered. For matrix blend and composites, tensile test and impact test was conducted in dry and wet states. Thermal conductivity test and morphology of the blends and composites were carried out in dry state only. The key conclusions from the above study is as follows:

- For the PA6/PP blend, at lower PP content (5 and 10 wt%), the yield strength and impact strength of the blend was higher, due to the homogeneous distribution of spherical PP domains in the PA6 phase.

- But for PA6/PP/PP-g-MA blend, PP domain size was in the range of 0.3 to 0.8 microns and was spherical in shape. The blends with higher PP content (30 and 50 wt%) gave comparative yield strength and higher tensile modulus in wet state compared to PA6 leading to cost effective blends with better properties.

- Maximum of 77.4% reduction in water absorption was observed for PA6/PP/PP-g-MA blend with **30 wt% PP content** in comparison to pure PA6. The composite with **3 phr compatibilizer** showed around 50 % increase in tensile strength in comparison to pure PA6 after water saturation.

- The composite containing 3 phr PP-g-MA had only 10 % reduction in tensile strength, 30 % reduction in modulus and 56 % increase in elongation due to

water absorption in comparison to the dry counterpart. Experimentally and statistically, **3 phr PP-g-MA** was found to be the optimum compatibilizer content for composites.

- With increase in SCF content (3-15 wt%), the tensile strength and tensile modulus increased, whereas the elongation at break and impact strength decreased in dry state for PA6/PP/PP-g-MA/SCF composites indicating the less number of micro voids as revealed by X-Ray CT of SCF composites.

- In wet state, about 15% reduction in tensile strength and 17% reduction in modulus was found for **15 wt% SCF content** in comparison to the dry counterpart indicating its use in humid conditions (not under water conditions). The water absorption in composite with **15 wt% SCF content** was 72% lesser than pure PA6 showing the synergistic effect of PP and SCF in the composite.

- For **UDCF composite (30 wt% carbon fibre)**, the tensile strength was six times and four times higher than pure PA6 in dry and wet state respectively indicating the reinforcing effect of carbon fibres.

- The water absorption was higher due to the micro voids in the sample especially in middle layers as revealed by X-Ray CT of UDCF composites (resulted due to the thick fibre mats / matrix sheets), but the reduction in tensile strength was only 24.5%. The impact strength of the UDCF composite was higher than PA6 in both dry and wet states due to the presence of micro voids.

Overall, it was understood that modifying PA6 with PP and PP-g-MA is advantageous as it restricts the water absorption, and the reduction in tensile strength in wet conditions is lowered as it curbs the plasticization of PA6 and also provides better interfacial adhesion between PA6 and PP at 3phr of PP-g-MA. Finally, it can be concluded that for SCF and UDCF composite, PA6/PP/PP-g-MA blend can be used as an effective matrix material to obtain composite with balanced tensile and impact properties in both dry and wet conditions. Extrusion and injection molding of SCF composites resulted dense composite with few micro voids in the middle layer, but UDCF composite made using compression molding resulted more number of voids in the middle layer due to thick UDCF mat, thick matrix sheet and its high viscosity.

CHAPTER 7:

Future Scope

- In literature it has been found that residual fibre length plays an important role in the final properties of fibre reinforced composites. Extrusion and injection molding processes are used for continuous production of the composites. So, studies can be done on optimizing process parameters and varying initial fibre length for obtaining higher residual fibre length in composites.

- Dynamic injection molding is a new emerging technique that can be investigated to obtain composites of considerable fibre length and the advantage is that the process is continuous and more practical for production of composites where carbon fibre reinforced composites need to be produced in bulk quantities.

- Another important area which is open for research is further improvement in the interfacial adhesion between the matrix and the fibre, both in case of SCF and UDCF based composites. Generally an epoxy coating is present on the carbon fibres, so this can be removed and other sizing agent or treatment methods can be investigated to improve the adhesion between the matrix and carbon fibre.

- In making the UDCF composite, the thickness of the matrix posed problems. Some work can be done in reducing the thickness of the matrix sheets. Various processing techniques can be investigated for making thin matrix sheet followed by the making of UDCF composites using film stacking technique.

- 3D printing of polymer material has already gained a lot of interest. However, all polymer filaments may not be 3D printed and properties of the polymers, blends and composites need to be modified for 3D printing. Rheology plays an important role in the use of the polymers for 3D printing. 3D printing of carbon fibre based composites would be an interesting area as specialized designs can be fabricated. So it would be good to investigate the rheology of the composites and design composite filament material suitable for 3D printing.

REFERENCES

Adusumalli, R., Reifferscheid, M., Weber, H. K., Roeder, T., Sixta, H., & Gindl, W. (2012). "Shear strength of the lyocell fibre/polymer matrix interface evaluated with the microbond technique." Journal of Composite Materials, 46(3), 359–367. https://doi.org/10.1177/0021998310382312

Agarwal, B. D., Broutman, L. J., & Chandrashekhara, K. (2006). Analysis and Performance of Fibre Composites Third Edition. John Wiley & Sons, Inc. Hoboken, NJ.

Agrawal, P., Rodrigues, A. W. B., Araújo, E. M., & Mélo, T. J. A. (2010). "Influence of reactive compatibilizers on the rheometrical and mechanical properties of PA6/LDPE and PA6/HDPE blends." Journal of Materials Science, 45(2), 496–502. https://doi.org/10.1007/s10853-009-3967-9

An, H. J., Kim, J. S., Kim, K. Y., Lim, D. Y., & Kim, D. H. (2014). "Mechanical and thermal properties of long carbon fibre-reinforced polyamide 6 composites." Fibres and Polymers, 15(11), 2355–2359. https://doi.org/10.1007/s12221-014-2355-5

Andreeva, M. B., Novotortzeva, T. N., Kalugina, E. V, Tochin, V. A., Gurinovich, L. N., Andreeva, T. I., … Zaikov, G. E. (2000). "Improvement of compatibility in glass-reinforced PA6/PP blends." Polymer-Plastics Technology and Engineering, 39(3), 513–528.

Anstey, A., Codou, A., Misra, M., & Mohanty, A. K. (2018). "Novel Compatibilized Nylon-Based Ternary Blends with Polypropylene and Poly(lactic acid): Fractionated Crystallization Phenomena and Mechanical Performance." ACS Omega, 3(3), 2845–2854. https://doi.org/10.1021/acsomega.7b01569

Arhant, M., Le Gac, P. Y., Le Gall, M., Burtin, C., Briançon, C., & Davies, P. (2016). "Effect of sea water and humidity on the tensile and compressive properties of carbon-polyamide 6 laminates." Composites Part A: Applied Science and Manufacturing, 91, 250–261. https://doi.org/10.1016/j.compositesa.2016.10.012

Arsad, A., Rahmat, A. R., Hassan, A., & Iskandar, S. N. (2010). "Mechanical and rheological properties of PA6/ABS blends - With and without short glass fibre." Journal of Reinforced Plastics and Composites, 29(18), 2808–2820. https://doi.org/10.1177/0731684409360076

Augustine, J. M., Maiti, S. N., & Gupta, A. K. (2012). "Mechanical properties and crystallization behavior of toughened polyamide-6/carbon nanotube composites." Journal of Applied Polymer Science, 125(S1), E478–E485. https://doi.org/10.1002/app.33975

Bahadur, S., Gong, D., & Anderegg, W. (1995). "Studies of worn surfaces and the transfer film formed in sliding by CuS-filled and carbon fibre-reinforced nylon against a steel surface," 181–183, 227–235.

Balamurugan, G. P., & Maiti, S. N. (2007). "Influence of microstructure and deformation behavior on toughening of reactively compatibilized polyamide 6 and poly(ethylene-co-butyl acrylate) blends." European Polymer Journal, 43(5), 1786–1805. https://doi.org/10.1016/j.eurpolymj.2007.02.035

Bengtsson, P. (2006). Rapid automated induction lamination (RAIL) of carbon fibre weave and thermoplastic film. Lulea University of Technology, Lulea. Retrieved from http://epubl.ltu.se/1402-1617/2006/093/LTU-EX-06093-SE.pdf

Bhattacharyya, A. R., Ghosh, A. K., & Misra, A. (2003). "Ionomer compatibilised PA6/EVA blends: Mechanical properties and morphological characterisation." Polymer, 44(5), 1725–1732. https://doi.org/10.1016/S0032-3861(02)00802-9

Bhattacharyya, A. R., Ghosh, A. K., Misra, A., & Eichhorn, K. J. (2005). "Reactively compatibilised polyamide6/ethylene-co-vinyl acetate blends: Mechanical properties and morphology." Polymer, 46(5), 1661–1674. https://doi.org/10.1016/j.polymer.2004.12.012

Bhattacharyya, A. R., Maiti, S. N., & Misra, A. (2002). "Mechanical properties and morphology of PA6/EVA blends." Journal of Applied Polymer Science, 85(8), 1593–1606. https://doi.org/10.1002/app.10686

Bliznakov, E. D., White, C. C., & Shaw, M. T. (2000). "Mechanical properties of blends of HDPE and recycled urea-formaldehyde resin." Journal of Applied Polymer Science, 77(14), 3220–3227. https://doi.org/10.1002/1097-4628(20000929)77:14<3220::AID-APP250>3.0.CO;2-4

Borggreve, R. J. M., Gaymans, R. J., & Schuijer, J. (1989). "Impact behaviour of nylon-rubber blends: 5. Influence of the mechanical properties of the elastomer." Polymer, 30(1), 71–77. https://doi.org/10.1016/0032-3861(89)90385-6

Botelho, E. C., Figiel, Rezende, M. C., & Lauke, B. (2003). "Mechanical behavior of carbon fibre reinforced polyamide composites." Composites Science and Technology, 63(13), 1843–1855. https://doi.org/10.1016/S0266-3538(03)00119-2

Botelho, E. C., & Rezende, M. C. (2010). "Evaluation by free vibration method of moisture absorption effects in polyamide/carbon fibre laminates." Journal of Thermoplastic Composite Materials, 23(2), 207–225. https://doi.org/10.1177/0892705709342614

Campbell, F. C. (2012). Lightweight Materials: Understanding the Basics. Retrieved fromhttps://www.asminternational.org/home/-/journal_content/56/10192/05355G/PUBLICATION

Chawla, K. K. (1998). Composite Materials: Science and Engineering (Third). New York: Springer. https://doi.org/10.1007/978-0-387-74365-3

Chen, J., Du, X. C., Zhang, W. Bin, Yang, J. H., Zhang, N., Huang, T., & Wang, Y. (2013). "Synergistic effect of carbon nanotubes and carbon black on electrical conductivity of PA6/ABS blend." Composites Science and Technology, 81, 1–8. https://doi.org/10.1016/j.compscitech.2013.03.014

Chen, Y., Wang, Q., Yan, W., & Tang, H. (2006). "Preparation of flame retardant polyamide 6 composite with melamine cyanurate nanoparticles in situ formed in extrusion process." Polymer Degradation and Stability, 91(11), 2632–2643. https://doi.org/10.1016/j.polymdegradstab.2006.05.002

Cheng, F., Li, H., Chen, D., & Jing, X. (2005). "Properties of compatibilized nylon 6/ABS polymter blends." "New Century, New Materials and New Life" - Proceedings of 2005 International Conference on Advanced Fibres and Polymer Materials, ICAFPM 2005, 1(December 2014), 553–556. https://doi.org/10.1080/00222340600770095

Cho, J. W., & Paul, D. R. (2001). "Glass fibre-reinforced polyamide composites toughened with ABS and EPR-g-MA." Journal of Applied Polymer Science, 80(3), 484–497. https://doi.org/10.1002/1097-4628(20010418)80:3<484::AID-APP1122>3.0.CO;2-5

Chow, W. S., Abu Bakar, A., Mohd Ishak, Z. A., Karger-Kocsis, J., & Ishiaku, U. S. (2005). "Effect of maleic anhydride-grafted ethylene-propylene rubber on the mechanical, rheological and morphological properties of organoclay reinforced polyamide 6/polypropylene nanocomposites." European Polymer Journal, 41(4), 687–696. https://doi.org/10.1016/j.eurpolymj.2004.10.041

Chow, W. S., Bakar, A. A., & Mohd Ishak, Z. A. (2005). "Water absorption and hygrothermal aging study on organomontmorillonite reinforced polyamide 6/polypropylene nanocomposites." Journal of Applied Polymer Science, 98(2), 780–790. https://doi.org/10.1002/app.22172

Chow, W. S., Ishak, Z. A. M., Ishiaku, U. S., Karger-Kocsis, J., & Apostolov, A. A. (2003). "The effect of organoclay on the mechanical properties and morphology of injection-molded polyamide 6/polypropylene nanocomposites." Journal of Applied Polymer Science, 91(1), 175–189. https://doi.org/10.1002/app.13244

Dayma, N., Jaggi, H. S., & Satapathy, B. K. (2013). "Post-yield crack toughness behavior of polyamide-6/polypropylene grafted maleic anhydride/nanoclay ternary nanocomposites." Materials and Design, 49, 303–310. https://doi.org/10.1016/j.matdes.2013.01.011

Do, V. T., Nguyen-Tran, H. D., & Chun, D. M. (2016). "Effect of polypropylene on the mechanical properties and water absorption of carbon-fibre-reinforced-polyamide-6/polypropylene composite." Composite Structures, 150, 240–245. https://doi.org/10.1016/j.compstruct.2016.05.011

Dong, K., Liu, K., Zhang, Q., Gu, B., & Sun, B. (2016). "International Journal of Heat and Mass Transfer Experimental and numerical analyses on the thermal conductive behaviors of carbon fibre / epoxy plain woven composites." International Journal of Heat and Mass Transfer, 102, 501–517. https://doi.org/10.1016/j.ijheatmasstransfer.2016.06.035

Feng, N., Wang, X., & Wu, D. (2013). "Surface modification of recycled carbon fibre and its reinforcement effect on nylon 6 composites: Mechanical properties, morphology and crystallization behaviors." Current Applied Physics, 13(9), 2038–2050. https://doi.org/10.1016/j.cap.2013.09.009

Fowler, M. W., & Baker, W. E. (1988). "Rubber toughening of polystyrene through reactive blending." Polymer Engineering & Science, 28(21), 1427–1433. https://doi.org/10.1002/pen.760282112

Frazier, G., & Martino, C. F. (1957). "Thermoplastic laminate." Google Patents.

Fu, D., Kuang, T., Chen, F., Lee, L. J., & Peng, X. (2015). "Fabrication of high strength PA6/PP blends with pressure-induced-flow processing." Materials Chemistry and Physics, 164, 1–5. https://doi.org/10.1016/j.matchemphys.2015.08.043

Fu, Y., Song, H., Zhou, C., Zhang, H., & Sun, S. (2013). "Modification of the grafting character to prepare PA6/ABS-g-MA blends with higher toughness and stiffness." Polymer Bulletin, 70(6), 1853–1862. https://doi.org/10.1007/s00289-

012-0879-7

Geier, S., & Bonten, C. (2013). "Mechanical and Morphological Properties of a Ternary Polyamide 6 Nanocomposite With Optimized Stiffness/ Toughness Performance." Polymer Engineering & Science, 54, 247–354. https://doi.org/10.1002/pen

Gilbert, M. (2016). Brydson's plastics materials. William Andrew.

González-Montiel, A., Keskkula, H., & Paul, D. R. (1995a). "Impact-modified nylon 6/polypropylene blends: 2. Effect of reactive functionality on morphology and mechanical properties." Polymer, 36(24), 4605–4620. https://doi.org/10.1016/0032-3861(95)96829-W

González-Montiel, A., Keskkula, H., & Paul, D. R. (1995b). "Impact-modified nylon 6/polypropylene blends: 3. Deformation mechanisms." Polymer, 36(24), 4621–4637. https://doi.org/10.1016/0032-3861(95)96830-2

Gowariker, V. R., Viswanathan, N. V, & Sreedhar, J. (1986). Polymer science. New Age International.

Guo, F., Yan, Y., Hong, Y., Li, X., & Ye, J. (2019). "Theoretical prediction for thermal expansion coefficients of unidirectional fibre-reinforced composites with variable elliptical cross-sections." Polymer Composites, 40(1), 187–201. https://doi.org/10.1002/pc.24627

Hamid, F., Akhbar, S., & Halim, K. H. K. (2013). "Mechanical and thermal properties of polyamide 6/HDPE-g-MAH/high density polyethylene." Procedia Engineering, 68, 418–424. https://doi.org/10.1016/j.proeng.2013.12.201

Hamid, F., Akhbar, S., & Ku, H. K. H. (2014). "Rubber toughened polyamide 6/high density polyethylene/HDPE-g-MAH nanocomposites with ethylene vinyl acetate." Key Engineering Materials, 594–595, 745–749. https://doi.org/10.4028/www.scientific.net/KEM.594-595.745

Hasegawa, A. (1974). "Studies on Polymer Blend of Nylon 6 and Polypropylene or Nylon 6 and Polystyrene Using the Reaction of Polymer," 18, 963–974.

Hemlata, & Maiti, S. N. (2012). "Nonisothermal crystallization kinetics of PA6 and PA6/SEBSg-MA blends." Journal of Polymer Research, 19(8). https://doi.org/10.1007/s10965-012-9926-1

Hollingsworth, B. L., & Sims, D. (1969). "New fibre-filled thermoplastics Part 2—Reinforcement by high modulus fibres." Composites, 1(2), 80–86.

Huber, T., Misra, M., & Mohanty, A. K. (2014). "Mechanical properties of compatibilized nylon 6/polypropylene blends; Studies of the interfacial behavior through an emulsion model." Journal of Applied Polymer Science, 131(18), 9455–9462. https://doi.org/10.1002/app.40792

Ishak, Z. A. M., & Berry, J. P. (1994). "Hygrothermal aging studies of short carbon fibre reinforced nylon 6.6." Journal of Applied Polymer Science, 51(13), 2145–2155. https://doi.org/10.1002/app.1994.070511306

Isik-Gulsac, I., Yilmazer, U., & Bayram, G. (2012). "Mechanical and Rheological Properties, and Morphology of Polyamide-6/Organoclay/Elastomer Nanocomposites." Journal of Applied Polymer Science, 125(5), 4060–4073. https://doi.org/10.1002/app

Iyer, S. R., & Drzal, L. T. (1990). "Manufacture of powder-impregnated thermoplastic composites." Journal of Thermoplastic Composite Materials, 3(4), 325–355.

Jime, E. J. (2011). "Viscoelasticity of Combined Thermally Insensitive Terpolyacrylamides," 2–8. https://doi.org/10.1002/pen

Jogi, B. F., Sawant, M., Brahmankar, P. K., Ratna, D., & Tarhekar, M. C. (2014). "Study of Mechanical and Crystalline Behavior of Polyamide 6/Hytrel/Carbon Nanotubes (CNT) based Polymer Composites." Procedia Materials Science, 6(Icmpc), 805–811. https://doi.org/10.1016/j.mspro.2014.07.097

Karsli, N. G., & Aytac, A. (2013). "Tensile and thermomechanical properties of short carbon fibre reinforced polyamide 6 composites." Composites Part B: Engineering, 51, 270–275. https://doi.org/10.1016/j.compositesb.2013.03.023

Kelnar, I., Rotrekl, J., Kotek, J., Kaprálková, L., & Hromádková, J. (2009). "Effect of montmorillonite on structure and properties of nanocomposite with PA6/PS/elastomer matrix." European Polymer Journal, 45(10), 2760–2766. https://doi.org/10.1016/j.eurpolymj.2009.06.024

Kim, K. J., Cho, H. W., & Yoon, K. J. (2003). "Effect of P(MMA-co-MAA) compatibilizer on the miscibility of nylon 6/PVDF blends." European Polymer Journal, 39(6), 1249–1265. https://doi.org/10.1016/S0014-3057(02)00366-X

Kirk, J. (1984). Fracture Behaviour of Polymers. Composite Structures (Vol. 2). https://doi.org/10.1016/0263-8223(84)90007-2

Kitayama, N., Keskkula, H., & Paul, D. R. (2001). "Reactive compatibilization of nylon 6/styrene - Acrylonitrile copolymer blends: Part 3. Tensile stress - Strain behavior." Polymer, 42(8), 3751–3759. https://doi.org/10.1016/S0032-3861(00)00695-9

Koning, C., Van Duin, M., Pagnoulle, C., & Jerome, R. (1998). "Strategies for compatibilization of polymer blends." Progress in Polymer Science (Oxford), 23(4), 707–757. https://doi.org/10.1016/S0079-6700(97)00054-3

Krishnaiah, K., & Shahabudeen, P. (2012). Applied design of experiments and Taguchi methods. PHI Learning Pvt. Ltd.

Kudva, R. A., Keskkula, H., & Paul, D. R. (1999). "Morphology and mechanical properties of compatibilized nylon 6/polyethylene blends." Polymer, 40(22), 6003–6021. https://doi.org/10.1016/S0032-3861(98)00829-5

Kudva, R. A., Keskkula, H., & Paul, D. R. (2000a). "Fracture behavior of nylon 6/ABS blends compatibilized with an imidized acrylic polymer." Polymer, 41(1), 335–349. https://doi.org/10.1016/S0032-3861(99)00244-X

Kudva, R. A., Keskkula, H., & Paul, D. R. (2000b). "Properties of compatibilized nylon 6/ABS blends: Part I. Effect of ABS type." Polymer, 41(1), 225–237. https://doi.org/10.1016/S0032-3861(99)00105-6

Kumar, S., Ramanaiah, B. V, & Maiti, S. N. (2007). "Effect of maleation on polyamide-6/EPDM-G-MAH blends." Soft Materials, 4(1), 85–100.

La Mantia, F. P., & Mongiovì, C. (1999). "Thermomechanical degradation of compatibilized and uncompatibilized nylon 6/polypropylene blends." Polymer Degradation and Stability, 66(3), 337–342. https://doi.org/10.1016/S0141-3910(99)00083-X

Lai, S. M., Li, H. C., & Liao, Y. C. (2007). "Properties and preparation of compatibilized nylon 6 nanocomposites/ABS blends: Part II - Physical and thermal properties." European Polymer Journal, 43(5), 1660–1671. https://doi.org/10.1016/j.eurpolymj.2007.02.009

Lee, L.-H. (1969). "Strength-Composition relationships of random short glass fibre-thermoplastics composites." Polymer Engineering & Science, 9(3), 213–224.

Li, B., Zhang, Y., Bai, X., Wang, S., & Ji, J. (2009). "Effect of PPO-g-MA on Structures and Properties of PPO/PA6/Short Glass Fibre Composites." Journal of Polymer Science Part B: Polymer Physics, 47, 2188–2197. https://doi.org/10.1002/polb

Li, D., Ou, B., & Jia, D. (2009). "Effects of polypropylene-g-dibutyl maleate on mechanical and rheological properties of PP/PA6 blends." E-Polymers, (143), 1–11. https://doi.org/10.1515/epoly.2009.9.1.1707

Li, H., Wang, J., Li, G., Lu, Y., Wang, N., Zhang, Q., & Qu, X. (2017). "Preparation of core-shell structured particle and its application in toughening PA6/PBT blends." Polymers for Advanced Technologies, 28(6), 699–707.

Li, L. P., Yin, B., Zhou, Y., Gong, L., Yang, M. B., Xie, B. H., & Chen, C. (2012). "Characterization of PA6/EPDM-g-MA/HDPE ternary blends: The role of core-shell structure." Polymer, 53(14), 3043–3051. https://doi.org/10.1016/j.polymer.2012.05.003

Li, Minggang, Wen, X., Liu, J., & Tang, T. (2014). "Synergetic effect of epoxy resin and maleic anhydride grafted polypropylene on improving mechanical properties of polypropylene/short carbon fibre composites." Composites Part A: Applied Science and Manufacturing, 67, 212–220. https://doi.org/10.1016/j.compositesa.2014.09.001

Li, Minghui, Wan, Y., Gao, Z., Xiong, G., Wang, X., Wan, C., & Luo, H. (2013). "Preparation and properties of polyamide 6 thermal conductive composites reinforced with fibres." Materials and Design, 51, 257–261. https://doi.org/10.1016/j.matdes.2013.03.076

Li, S., Wang, W., Yu, L., Xia, Z., & Li, X. (2018). "Influence of different compatibilizers on the morphology and properties of PA6/PET/glass fibre composites." Journal of Applied Polymer Science, 135(26), 1–7. https://doi.org/10.1002/app.46429

Li, Y., Xu, J., Wei, Z., Xu, Y., Song, P., Chen, G., … Liang, J. (2014). "Mechanical Properties and Nonisothermal Crystallization of Polyamide 6/Carbon Fibre Composites Toughened by Maleated Elastomers." Polymer Composites, 35, 2170–2179. https://doi.org/10.1002/pc

Liang, J. Z., & Li, R. K. Y. (2000). "Rubber toughening in polypropylene: A review." Journal of Applied Polymer Science, 77(2), 409–417. https://doi.org/10.1002/(SICI)1097-4628(20000711)77:2<409::AID-APP18>3.0.CO;2-N

Liao, C. Z., & Tjong, S. C. (2011). "Mechanical and thermal behaviour of polyamide 6/silicon carbide nanocomposites toughened with maleated styrene-ethylene-butylene-styrene elastomer." Fatigue and Fracture of Engineering Materials and Structures, 35(1), 56–63. https://doi.org/10.1111/j.1460-2695.2011.01561.x

Litmanovich, A. D., Platé, N. A., & Kudryavtsev, Y. V. (2002). "Reactions in polymer blends: interchain effects and theoretical problems." Progress in Polymer Science, 27(5), 915–970.

Luo, H., Xiong, G., Ma, C., Li, D., & Wan, Y. (2014). "Preparation and performance of long carbon fibre reinforced polyamide 6 composites injection-molded from core/shell structured pellets." Materials and Design, 64, 294–300. https://doi.org/10.1016/j.matdes.2014.07.054

Ma, L. F., Wei, X. F., Zhang, Q., Wang, W. K., Gu, L., Yang, W., Yang, M. B. (2012). "Toughening of polyamide 6 with β-nucleated thermoplastic vulcanizates based on polypropylene/ethylene-propylene-diene rubber grafted with maleic anhydride blends." Materials and Design, 33(1), 104–110. https://doi.org/10.1016/j.matdes.2011.07.017

Ma, Y., Jin, S., Ueda, M., Yokozeki, T., Yang, Y., Kobayashi, F., Hamada, H. (2018). "Higher performance carbon fibre reinforced thermoplastic composites from thermoplastic prepreg technique: Heat and moisture effect." Composites Part B: Engineering, 154(July), 90–98. https://doi.org/10.1016/j.compositesb.2018.07.060

Ma, Y., Ueda, M., Yokozeki, T., Sugahara, T., Yang, Y., & Hamada, H. (2017). "A comparative study of the mechanical properties and failure behavior of carbon fibre / epoxy and carbon fibre / polyamide 6 unidirectional composites." Composite Structures, 160, 89–99. https://doi.org/10.1016/j.compstruct.2016.10.037

Ma, Y., Yang, Y., Sugahara, T., & Hamada, H. (2016). "Review article A study on the failure behavior and mechanical properties of unidirectional fi ber reinforced thermosetting and thermoplastic composites." Composites Part B, 99, 162–172. https://doi.org/10.1016/j.compositesb.2016.06.005

Ma, Y., Yokozeki, T., Ueda, M., Sugahara, T., Yang, Y., & Hamada, H. (2017). "Effect of polyurethane dispersion as surface treatment for carbon fabrics on mechanical properties of carbon/Nylon composites." Composites Science and Technology, 151, 268–281. https://doi.org/10.1016/j.compscitech.2017.08.031

Malekzadeh, Y., Shelesh-Nezhad, K., & Adli, A. R. (2016). "The effects of surface treated carbon fibres and CaCO3 nanoparticles inclusions on the mechanical performances of PA6/ABS-based composites." Polymer Science - Series A, 58(6), 996–1003. https://doi.org/10.1134/S0965545X16060122

Martins, M., Gomes, R., Pina, L., Pereira, C., Reichmann, O., Teti, D., Rocha, N. (2018). "Highly conductive carbon fibre-reinforced polymer composite electronic box: Out-of-autoclave manufacturing for space applications." Fibres, 6(4), 1–23. https://doi.org/10.3390/fib6040092

Mehrabi Mazidi, M., Razavi Aghjeh, M. K., & Hasanpour, M. (2018). "Fracture resistance and micromechanical deformations in PP/PA6/EPDM ternary blends: Effect of rubber functionality, dispersion state and loading conditions." Engineering Fracture Mechanics, 191, 65–81. https://doi.org/10.1016/J.ENGFRACMECH.2018.01.021

Molnár, S., Rosenberger, S., Gulyás, J., & Pukánszky, B. (1999). "Structure and impact resistance of short carbon fibre reinforced polyamide 6 composites." Journal of Macromolecular Science - Physics, 38(June).

https://doi.org/10.1080/00222349908248134

Monetfe, L., Anderson, M. P., & Grest, G. S. (1993). "The Meaning of the Critical Length Concept in Composites : Study of Matrix Viscosity and Strain Rate on the Average Fibre Fragmentation Length in Short-Fibre Polymer Composites." Polymer Composites, 14(2), 101–115.

Navid, N., Mat, U. W., Azman, H., & Shaya, M. (2011). "Mechanical and thermal properties of polyamide 6 nanocomposite toughened with epoxidised natural rubber-25." Key Engineering Materials, 471–472, 518–523. https://doi.org/10.4028/www.scientific.net/KEM.471-472.518

Ogunsona, E. O., Misra, M., & Mohanty, A. K. (2017). "Accelerated hydrothermal aging of biocarbon reinforced nylon biocomposites." Polymer Degradation and Stability, 139(March), 76–88. https://doi.org/10.1016/j.polymdegradstab.2017.03.013

Ohlsson, B., Hassander, H., & Törnell, B. (1998). "Improved compatibility between polyamide and polypropylene by the use of maleic anhydride grafted SEBS." Polymer, 39(26), 6705–6714. https://doi.org/10.1016/S0032-3861(97)10290-7

Okada, O., Keskkula, H., & Paul, D. R. (2001). "blends of maleated EPR and nylon6.pdf," 42, 8715–8725.

Oromiehie, A., Ebadi-Dehaghani, H., & Mirbagheri, S. (2014). "Chemical Modification of Polypropylene by Maleic Anhydride: Melt Grafting, Characterization and Mechanism." International Journal of Chemical Engineering and Applications, 5(2), 117–122. https://doi.org/10.7763/ijcea.2014.v5.363

Oshinski, A. J., Keskkula, H., & Paul, D. R. (1992). "Rubber toughening of polyamides with functionalized block copolymers: 2. Nylon-6,6." Polymer, 33(2), 284–293. https://doi.org/10.1016/0032-3861(92)90985-6

Park, S., Kim, M. S., Choi, Y. S., Lee, E. S., Chon, J. S., & Yoo, H. W. (2015). "Properties of CF/PA6 Laminate Composites Prepared Using the Carbon Fibre Spreading Technology." Textile Science and Engineering, 52(6), 367–372.

Pillay, S., Vaidya, U. K., & Janowski, G. M. (2007). "The durability of liquid molded carbon nylon 6 composite laminates, exposed to an aggressive moisture environment." ICCM International Conferences on Composite Materials.

Pillay, S., Vaidya, U. K., & Janowski, G. M. (2009). "Effects of moisture and UV exposure on liquid molded carbon fabric reinforced nylon 6 composite laminates." Composites Science and Technology, 69(6), 839–846. https://doi.org/10.1016/j.compscitech.2008.03.021

Prasath Balamurugan, G., & Maiti, S. N. (2008). "The influence of reactive compatibilization on uniaxial large strain deformation and fracture behavior of polyamide 6 and poly (ethylene-co-butyl acrylate) blends." Polymer Testing, 27(6), 752–764. https://doi.org/10.1016/j.polymertesting.2008.05.010

Prasath Balamurugan, G., & Maiti, S. N. (2010). "Effects of Nanotalc Inclusion on Mechanical, Microstructural, Melt Shear Rheological, and Crystallization Behavior of Polyamide 6-Based Binary and Ternary Nanocomposites G." Polymer Engineering & Science, 50, 1978–1993. https://doi.org/10.1002/pen

Purnima, D., Maiti, S. N., & Gupta, A. K. (2006). "Interfacial Adhesion Through Maleic Anhydride Grafting of EPDM in PP / EPDM Blend," 102(October 2005), 5528–5532. https://doi.org/10.1002/app.24597

Ranganathan, S., Baker, W. E., Russell, K. E., & Whitney, R. A. (1999). "Peroxide-initiated grafting of maleic anhydride onto linear and branched hydrocarbons." Journal of Polymer Science, Part A: Polymer Chemistry, 37(20), 3817–3825. https://doi.org/10.1002/(SICI)1099-0518(19991015)37:20<3817::AID-POLA10>3.0.CO;2-V

Rashkovan, I. A., Kazakov, M. Y., Krasnov, A. P., & Kulachinskaya, O. B. (2014). "Investigation on short carbon fibre filled composites based on polyamide blend PA6 and PA6,6." In 16th European conference on composite material (pp. 1–7).

Ren, J., Wang, H., Jian, L., Zhang, J., & Yang, S. (2008). "Morphological, thermal and mechanical properties of compatibilized nylon 6/ABS blends." Journal of Macromolecular Science, Part B: Physics, 47(4), 712–722. https://doi.org/10.1080/00222340802119042

Rexford, B. (1959). "Glass-reinforced thermoplastic injection molding compound and injection-molding process employing it." Google Patents.

Rolfes, R., & Hammerschmidt, U. (1995). "Transverse thermal conductivity of CFRP laminates: A numerical and experimental validation of approximation formulae." Composites Science and Technology, 54(1), 45–54. https://doi.org/10.1016/0266-3538(95)00036-4

Scaffaro, R., Mistretta, M. C., & La Mantia, F. P. (2008). "Compatibilized polyamide 6/polyethylene blend-clay nanocomposites: Effect of the degradation and stabilization of the clay modifier." Polymer Degradation and Stability, 93(7), 1267–1274. https://doi.org/10.1016/j.polymdegradstab.2008.04.008

Shahadat, M. R. Bin, Masnoon, A. S., Ahmed, S., & Morshed, A. M. (2017). "Effect of surface roughness and void fraction on thermal transportation of a solid: A molecular dynamics study." AIP Conference Proceedings, 1919(December). https://doi.org/10.1063/1.5018555

Sharma, S. K., & Nayak, S. K. (2009). "Surface modified clay/polypropylene (PP) nanocomposites: Effect on physico-mechanical, thermal and morphological properties." Polymer Degradation and Stability, 94(1), 132–138. https://doi.org/10.1016/J.POLYMDEGRADSTAB.2008.09.004

Shashidhara, G. M., & Pradeepa, K. G. (2014). "Preparation and characterization of polyamide 6/liquid natural rubber blends." Journal of Applied Polymer Science, 131(2), 1–10. https://doi.org/10.1002/app.39750

Shen, C., Zhou, Y., Dou, R., Wang, W., Yin, B., & Yang, M. B. (2015). "Effect of the core-forming polymer on phase morphology and mechanical properties of PA6/EPDM-g-MA/HDPE ternary blends." Polymer, 56, 395–405. https://doi.org/10.1016/j.polymer.2014.11.027

Shen, Z., Bateman, S., Wu, D. Y., McMahon, P., Dell'Olio, M., & Gotama, J. (2009). "The effects of carbon nanotubes on mechanical and thermal properties of woven glass fibre reinforced polyamide-6 nanocomposites." Composites Science and Technology, 69(2), 239–244. https://doi.org/10.1016/j.compscitech.2008.10.017

Sun, S., Chen, Z., & Zhang, H. (2008). "Effect of reactive group types on the

properties of core-shell modifiers toughened PA6." Polymer Bulletin, 61(4), 443–452. https://doi.org/10.1007/s00289-008-0971-1

Taghizadeh, E., Naderi, G., & Razavi-Nouri, M. (2011). "Effects of organoclay on the mechanical properties and microstructure of PA6/ECO blend." Polymer Testing, 30(3), 327–334. https://doi.org/10.1016/j.polymertesting.2011.01.007

Tang, X. G., Yang, W., Shan, G. F., Yang, M. bo, Xie, B. hu, & Fu, Q. (2007). "Double yielding in PA6/TPV-MAH blends: Effect of dispersed phase with different content, modulus." Polymer, 48(25), 7404–7413. https://doi.org/10.1016/j.polymer.2007.09.052

Tjong, S. C. (1997). "The falling weight impact properties of maleic anhydride compatibilized polypropylene--polyamide blends." Journal of Materials Science, 32(17), 4613–4617.

Tjong, S. C., & Meng, Y. Z. (1999). "Microstructural and mechanical characteristics of compatibilized polypropylene hybrid composites containing potassium titanate whisker and liquid crystalline copolyester." Polymer, 40(26), 7275–7283. https://doi.org/10.1016/S0032-3861(99)00090-7

Tsenoglou, C. J., Pavlidou, S., & Papaspyrides, C. D. (2006). "Evaluation of interfacial relaxation due to water absorption in fibre-polymer composites." Composites Science and Technology, 66(15), 2855–2864. https://doi.org/10.1016/j.compscitech.2006.02.022

Viswanathan, A. (2010). "Wallace carothers: More than the inventor of Nylon and Neoprene." World Patent Information, 32(4), 300–305. https://doi.org/10.1016/j.wpi.2009.09.004

Vlasveld, D. P. N., Groenewold, J., Bersee, H. E. N., & Picken, S. J. (2005). "Moisture absorption in polyamide-6 silicate nanocomposites and its influence on the mechanical properties." Polymer, 46(26), 12567–12576. https://doi.org/10.1016/j.polymer.2005.10.096

Warlimont, H., & Martienssen, W. (2005). Springer Handbook of Condensed Matter and Materials Data. New York: Spinger Berlin Heidelberg.

William D. Callister, J. (2007). Materials Science and Engineering An Introduction. John Wiley & Sons, Inc. Hoboken, NJ (Vol. Seventh ed). https://doi.org/10.1007/BF01184995

Yan, X., Imai, Y., Shimamoto, D., & Hotta, Y. (2014). "Relationship study between crystal structure and thermal/mechanical properties of polyamide 6 reinforced and unreinforced by carbon fibre from macro and local view." Polymer, 55(23), 6186–6194. https://doi.org/10.1016/j.polymer.2014.09.052

Yin, B., Li, L. P., Zhou, Y., Gong, L., Yang, M. B., & Xie, B. H. (2013). "Largely improved impact toughness of PA6/EPDM-g-MA/HDPE ternary blends: The role of core-shell particles formed in melt processing on preventing micro-crack propagation." Polymer, 54(7), 1938–1947. https://doi.org/10.1016/j.polymer.2013.02.001

Zhang, S. shuang, Wang, X., & Wu, D. (2015). "Design and fabrication of Long-Carbon-Fibre-Reinforced Polyamide-6/Nickel Powder COmposites for Electromagnetic Interference Shielding and High Mechanical Performance." Polymer Composites, 37(9), 1–14. https://doi.org/10.1002/pc.23465

Zhao, D., Ma, Y., & Yang, Y. (2019). "Flexural damage behavior of CF/PA6 plain woven laminates with different layers." Composites Part B: Engineering, 162(January), 631–642. https://doi.org/10.1016/j.compositesb.2019.01.042

Zhou, H., Qian, Z., Meng, X., Ding, Y., Zhang, S., & Yang, M. (2007). "Fibre Breakage and Dispersion in Carbon-Fibre-Reinforced Nylon 6/Clay Nanocomposite." Journal of Applied Polymer Science, 106, 1751–1756. https://doi.org/10.1002/app.26818

Zhou, S., Zhang, Q., Wu, C., & Huang, J. (2013). "Effect of carbon fibre reinforcement on the mechanical and tribological properties of polyamide6/polyphenylene sulfide composites." Materials and Design, 44, 493–499. https://doi.org/10.1016/j.matdes.2012.08.029

Zo, H. J., Joo, S. H., Kim, T., Seo, P. S., Kim, J. H., & Park, J. S. (2014). "Enhanced mechanical and thermal properties of carbon fibre composites with polyamide and thermoplastic polyurethane blends." Fibres and Polymers, 15(5), 1071–1077. https://doi.org/10.1007/s12221-014-1071-5

LIST OF PUBLICATIONS

1. Influence of PP content on mechanical properties, water absorption and morphology in PA6/PP blend, **S. Aparna**, D. Purnima: *Journal of Applied Polymer Science,* 136, 47690, 1-13, 2019 (Scopus indexed, IF: 2.5; H Index: 159)

2. Effect of compatibilizer on the properties of Polyamide 6 blend based carbon fibre reinforced composite, **S. Aparna**, D. Purnima, R.B. Adusumalli: *Fibres and Polymers*, 19 (6), 1335-1346, 2018 (Scopus indexed, IF: 1.7; H Index: 47)

3. A Review on Various Compatibilizers and Its Effect on Mechanical Properties of Compatibilized Nylon Blends. **S. Aparna**, D. Purnima, R.B. Adusumalli: *Polymer-Plastic Technology and Engineering*, 2016, 56(6), 617-34 (Scopus indexed, IF: 1.6; H Index: 50)

4. Effect of carbon fibres and water absorption on mechanical properties and morphology of PA6/PP blend based composites. **S. Aparna**, D. Purnima, R.B. Adusumalli: *Polymer Composites, 2020,* https://doi.org/10.1002/pc.25784 (Scopus indexed, IF: 2.2; H Index: 78)

5. Surface Modified Carbon Fibre Reinforced PA6 and its Blend Based Composites. Anurag R. Patil, **S. Aparna**, D. Purnima: *Advances in Interdisciplinary Engineering: Proceedings of FLAME 2018, Lecture Notes in Mechanical Engineering, Springer, 2019* (Scopus indexed, H Index: 12)

6. PA6/PP blend based Short and Long Carbon fibre Composites for Humid applications: Processing and Characterization: **S.Aparna**, R.B. Adusumalli, D. Purnima, Karthik Chethan.V, *Submitted to "Journal of Composite Materials"* (Manuscript no: JCM-21-0437) in April 2021.

LIST OF CONFERENCES

1. Study of Thermoplastic Blend as Matrix for Fibre Reinforced Composites. **S. Aparna**, Anurag R. Patil, and D.Purnima. EEC-2018, BITS-Pilani, Hyderabad Campus, Hyderabad, 16th February, 2018.

2. Carbon fibre reinforced thermoplastic composites for under water applications. **S. Aparna**, D.Purnima and Ramesh Babu Adusumalli. ICCMA-2018, Hyderabad, 19th-20th January, 2018.

3. Effect of PP and PP-g-MA on mechanical properties of PA6/PP blends. **S. Aparna**, D.Purnima and Ramesh Babu Adusumalli. APA-2017, New Delhi, 23-25th November, 2017.

4. Effect of Temperature on Mechanical Properties of (Nylon 6) PA6 / Talc Composite. Namrata Verma, **S. Aparna** and D. Purnima. The 3rd Indo-Austrian Symposium on Advances in Materials Engineering, Mumbai, 19th and 20th December 2016.

5. Comparison of Mechanical Properties of Organic and Inorganic Filler Reinforced Nylon Composites, Avasarala Satya Teja**, S. Aparna** and D. Purnima, Proceedings of SCHEMCON-2016, Hyderabad, September 10-11, 2016.

Biography of Aparna S

Aparna S has completed her B.Tech (Chemical Engineering) and M.Tech (Polymer Science and Engineering) from Anna University. She joined as Ph.D. student in the Department of Chemical Engineering in BITS- Pilani, Hyderabad Campus, under the supervision of Dr. D.Purnima and Prof. Ramesh Babu Adusumalli. Her research interest includes developing polymer blends for making fibre reinforced composites, surface treatment of fibres and hybrid composites. She has authored/co-authored five publications in international peer-reviewed journals and presented six papers at national/international conferences.

Biography of Dr. D. Purnima

Dr. D.Purnima is working as an assistant professor in the Department of Chemical Engineering in Birla Institute of Technology and Science, Pilani, Hyderabad Campus, India. Her research interest encompasses polymer blends and composites focusing towards the processing and characterization of various fibre and particulate reinforced hybrid composites. Fibre surface treatment, extraction of nano-cellulose from natural fibre and use of natural fibre in commercial applications are a part of her research areas. She has published many articles in international peer-reviewed journals. Currently her group is working on polymer composite films and membranes for heavy metal removal, packaging and bio-medical applications.

Biography of Prof. Ramesh Babu Adusumalli

Prof. Ramesh Babu Adusumalli is working as an associate professor in the Department of Chemical Engineering in Birla Institute of Technology and Science, Pilani, Hyderabad Campus, India. His research area includes mechanical characterization, micro and nano- characterization of fibres, wood based composite materials and fibre reinforced composites. Extraction of nano-cellulosic fibres from wood and natural fibre is also a part of his research area. He has completed two projects for DRDO and a project for DST and he has two ongoing projects for DRDO. Two students have completed Ph.D. under his supervision. He has published 25 articles in international/national peer-reviewed journals. Currently his group is working on environmental conditioning and testing of thermoset composite used in defence applications.